

The Source of Uranium for the Lac Cinquante Uranium Deposit, Nunavut, Canada

By
Gracie Avery

A Thesis Submitted to
Saint Mary's University, Halifax, Nova Scotia
in Partial Fulfillment of the Requirements for
the Degree of Honours in Geology

April 27th, 2024, Halifax, Nova Scotia

Copyright Gracie Avery, 2024

Approved: Dr. Erin Adlakha
Supervisor
Department of Geology

Approved: Dr. Jeremy Powell
Second Reader
Geological Survey of Canada

Date: April 27th, 2024

The Source of Uranium for the Lac Cinquante Uranium Deposit, Nunavut, Canada

by Gracie Avery

Abstract

The Lac Cinquante uranium deposit is hosted in an Archean greenstone belt below the Paleoproterozoic Baker Lake Basin, Nunavut, and is currently characterized as a vein-type uranium deposit. Vein-type uranium deposits are usually spatially associated with source granitoids and consist of uranium mineralization concentrated in fractures, shear zones, and stockworks. The source of uranium in the Lac Cinquante is unknown and is determined in this study through petrographic work and trace element analysis of uranium minerals. We hypothesize that the uranium was sourced in one of two ways: either uranium was leached from apatite, zircon, or monazite, or sourced from exsolved fluids, from nearby c. 1.84 Ga Hudsonian granites or the uranium was sourced from glass, or fluids related to, the c. 1.83 – 1.81 Ga potassic volcanic rocks (Christopher Island Formation; CIF) of the Baker Lake Group. Petrographic work including micro-XRF mapping and scanning electron microscopy confirm the complete paragenetic history of the Lac Cinquante uranium deposit: i) primary minerals of the host rock including plagioclase and quartz, ii) albitization of plagioclase, iii) formation of uraninite, brannerite, hydrothermal zircon, apatite, (\pm barite, pyrite, chalcopyrite, molybdenite, sphalerite, and galena) in calcite and albite veins, and iv) hematite, carbonate, and chlorite alteration. Pervasive albitization of the host rocks, the complex mineralogy (brannerite, hydrothermal zircon, apatite), and the distinct geochemistry (high Ti, Ba, Zr) indicate reclassification of this deposit as Na-metasomatic uranium deposit is warranted. Furthermore, trace element data of uraninite and brannerite reveals four distinct chondrite normalized REE

patterns with flat (i.e. none) to positive Eu anomalies and enrichments in LREE/HREE. These profiles are inconsistent with a granite source but are similar to the CIF. The ore minerals are also high in Ti, Ba, Zr, and Sr, consistent with CIF geochemistry that is more enriched in these components than the Hudson granites.

April 27th, 2024

Acknowledgments

I would like to thank Kivalliq Energy Corporation for providing the samples used in this research. Additionally, I would like to extend my gratitude to TGI-6 for funding this project and making this research possible. Thank you to Dr. Xiang Yang for assistance with SEM analysis at Saint Mary's University and Mr. Brandon Boucher at the University of New Brunswick for analysis and help in processing LA-ICP-MS data. Additionally, I would like to thank my external reviewer Dr. Jeremy Powell (Geological Survey of Canada) for his comments as second reader. Finally, thanks to my supervisor Dr. Erin Adlakha for all of the support and guidance throughout this thesis.

Table of Contents

The Source of Uranium for the Lac Cinquante Uranium Deposit, Nunavut, Canada.....	1
Acknowledgments	4
Table of Contents	5
List of Figures.....	6
Chapter 1 – Introduction and Purpose	8
1.1. Introduction	8
1.2. Purpose.....	11
Chapter 2 - Background.....	12
2.1. Vein-hosted uranium deposits	12
2.2. Uranium geochemistry	13
2.3. Rare Earth Element and Trace Element Abundances in Uranium Oxides and Implications for Source Discrimination of Uranium	14
2.4. Past Research of uranium occurrences in the Baker Lake basin and the Lac Cinquante uranium Deposit.....	15
Chapter 3 – Geological Setting	21
3.1. Regional Geology	21
3.2. Local Geology	24
Chapter 4 – Methods	30
Chapter 5 – Results.....	33
5.1. Petrography and Paragenesis	33
5.2. Uranium Mineral Chemistry	48
5.3. Laser Ablation Inductively Coupled Plasma Mass Spectrometry	50
Chapter 6 – Discussion	58
6.1. Paragenesis	58
6.2. Classification of deposit type.....	60
6.3. Uranium source.....	71
6.4. Genetic model and implications for future exploration and research.....	76
Chapter 7 – Conclusion	78
Chapter 8 – References.....	79
Appendix.....	87
Appendix A – List of samples and techniques	87
Appendix B – Petrographic Descriptions.....	91

Appendix C – XRF Descriptions	103
Appendix D – Sample List and Descriptions	142
Appendix E – SEM data	152
Appendix F – LA-ICP-MS data	152
Appendix G – Comparison of REE profiles of various uranium deposits to REE profiles of LC uranium minerals	152

List of Figures

Figure 1: Regional geological map of the Western Churchill Province with location of study area and distribution of Proterozoic intracontinental basins	9
Figure 2: Local and property geological maps of the Western Churchill Province with location of study area.....	10
Figure 3: Spider diagram of the Archean volcanic rocks at the LC deposit showing trace element abundances.....	18
Figure 4: Stratigraphic section of the Dubawnt Supergroup.....	27
Figure 5: Trace element and REE abundances of the Hudson granites and the Christopher Island Formation ultrapotassic minettes	29
Figure 6: Paragenetic sequence of the Lac Cinquante Deposit.....	34
Figure 7: False colour micro-XRF elemental distribution maps and photomicrographs of host tuff	35
Figure 8: False colour micro-XRF elemental distribution maps of albitized host tuff	36
Figure 9: False colour micro-XRF elemental distribution maps of albitized host tuff	37
Figure 10: False colour micro-XRF elemental distribution maps and photomicrographs of host tuff with simple vein-hosted uranium.....	39
Figure 11: False colour micro-XRF elemental distribution maps of host tuff with simple vein-hosted uranium	40
Figure 12: False colour micro-XRF elemental distribution maps and BSE images of complex vein-hosted uranium	43
Figure 13: False colour micro-XRF elemental distribution maps of host rock with disseminated uranium	44
Figure 14: False colour micro-XRF elemental distribution maps and photomicrographs of LC alteration.	46
Figure 15: False colour micro-XRF elemental distribution maps of a conglomerate with minor uranium mineralization	47
Figure 16: U-Ti-Si & U-Si-Ca ternary plots of uranium phases and BSE image of uranium phases	49
Figure 17: REE abundances in uraninite, normalized to chondrite.....	53
Figure 18: REE abundances in brannerite.....	54
Figure 19: Trace element abundances (ppm) in uraninite.....	56
Figure 20: Trace element abundances (ppm) in brannerite.....	57
Figure 21: REE abundances of various uranium deposits	65
Figure 22: REE abundances and trace element abundances in uraninite, brannerite, Hudson granites, and Christopher Island Formation ultrapotassic minettes.....	75

List of Tables

Table 1: Comparison of Lac Cinquante deposit to various uranium deposits. 66

Chapter 1 – Introduction and Purpose

1.1. Introduction

The Lac Cinquante (LC) uranium deposit is currently characterized as a vein-hosted uranium deposit hosted within basement rocks of the Archean Angikuni greenstone belt, located in the Western Churchill Province, Nunavut, Canada (Figure 1, Figure 2). The basement was unconformably overlain by 1.833 – pre 1.720 Ga Paleoproterozoic sediments and volcanic units of the Baker Lake Group in the Baker Lake Basin (Rainbird et al., 2003, Aspler et al., 2004). Volcanic units consist of a series of ultrapotassic minettes of the 1.833 – 1.811 Ga Christopher Island Formation (van Breeman et al., 2005). In the region surrounding the LC are numerous granitic intrusions including the 1.85-1.79 Ga Hudson granites and 1.76-1.75 Ga Nueltin granites (Peterson et al., 2002). Uraninite is the main ore mineral at the Lac Cinquante deposit and primary mineralization of uraninite has been calculated to have formed at minimum temperatures of 230°C to 350°C (obtained using chlorite geothermometry) at a minimum age of 1828 ± 29 Ma (calculated using $^{206}\text{Pb}/^{238}\text{U}$ and $^{207}\text{Pb}/^{235}\text{U}$ SIMS) (Bridge et al., 2013).

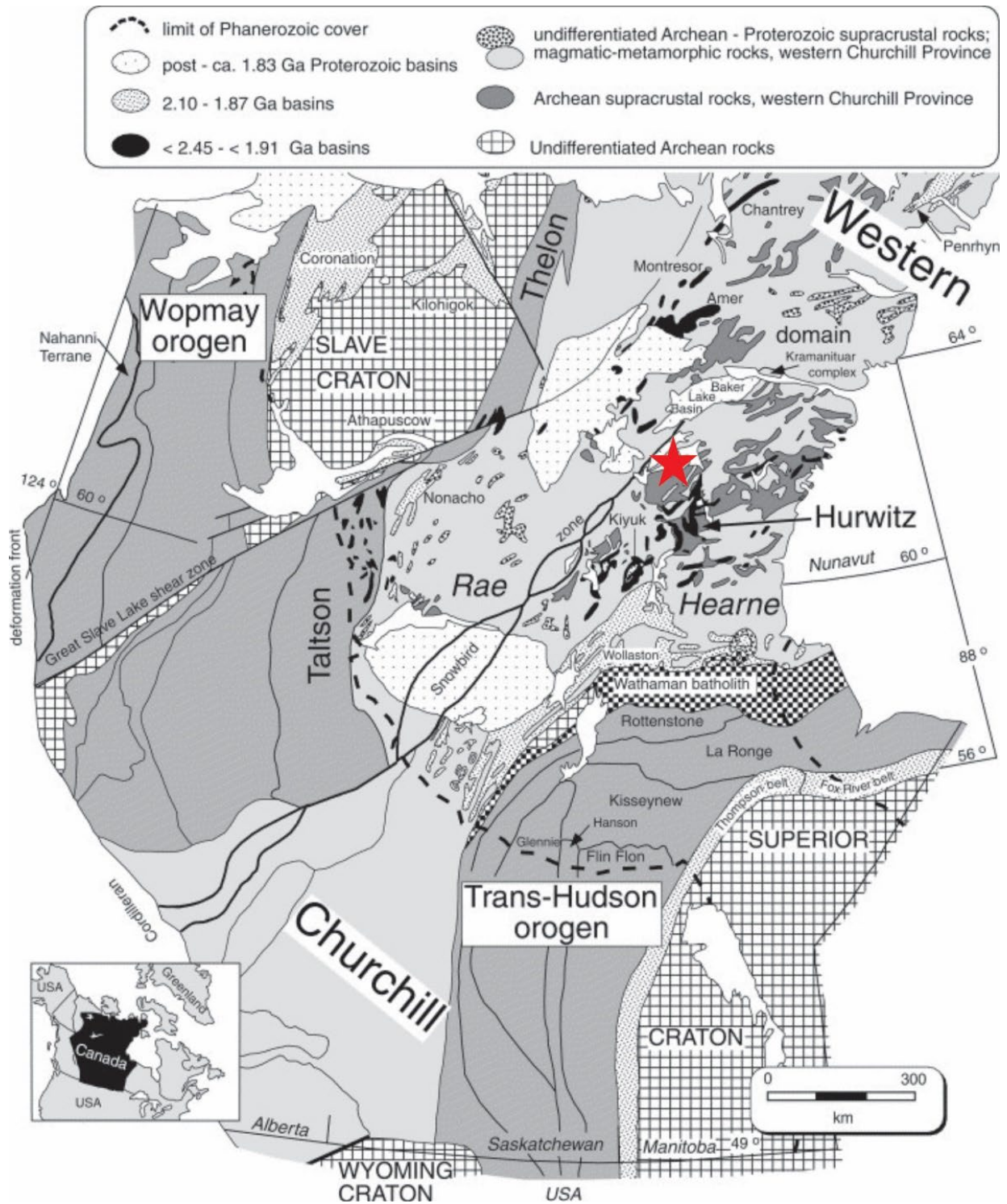


Figure 1: Regional geological map of the Western Churchill Province with location of study area and distribution of Proterozoic intracontinental basins. Study area indicated by red star (modified from Aspler et al., 2001).

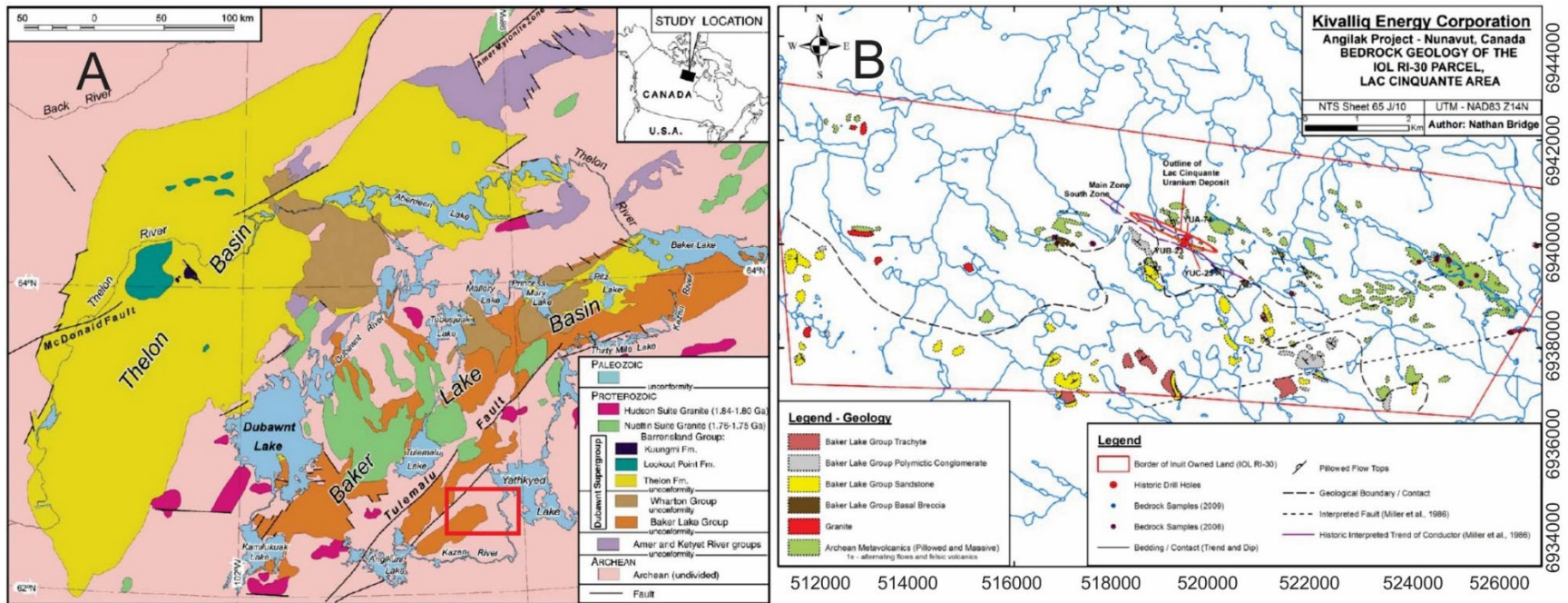


Figure 2: Local and property geological maps of the Western Churchill Province with location of study area. A) Geological map of the Baker Lake basin and Thelon basin. Approximate study area is shown by the red box (modified from Rainbird et al., 2003) B) Property geology of the Lac Cinquante area (modified from Bridge et al., 2013).

1.2. Purpose

The objectives of this study are: i) produce a complete paragenetic sequence for the deposit through petrographic methods, micro-XRF, and SEM analysis, ii) assess the characterization of this deposit as vein-type, and iii) determine the source of uranium for the Lac Cinquante uranium deposit through trace element analysis of uranium minerals. Uranium for this deposit is suspected to be sourced from one of two ways: i) apatite, zircon, or monazite, or exsolved fluids, of the 1.85 – 1.79 Ga Hudson granites, or ii) volcanic glass of, or fluids related to, the ultrapotassic volcanic rocks of the 1.83-1.81 Ga Christopher Island Formation (CIF).

Since U^{4+} is held in the structure of minerals such as apatite, zircon, monazite, titanite, and xenotime in the average granitoid (Cuney et al., 2014), uranium may have originated from fluids that leached uranium from these minerals within the Hudson granites, or from fluids exsolved during crystallization of the Hudson granites. Comparison to rare earth element (REE) profiles and trace element abundances of these rocks as a whole will be used to evaluate whether the Hudson granites are a likely source. Ideally, the comparison would be made between the minerals (apatite, monazite, zircon) potentially sourcing the uranium, however, this data is unavailable in published literature, therefore whole rock trace element data will be used instead. On the other hand, ultrapotassic volcanic rocks enriched in incompatible elements also represent a good potential source of uranium for deposits because they can host uranium in volcanic glass. Following devitrification of this volcanic glass during alteration, the uranium is then easily leached by fluids (Cuney, 2008, Cuney, 2014). With that in mind, the volcanic glass of the CIF or fluids exsolved during crystallization of the CIF, may be the source of uranium for this deposit. The REE profile and trace elements of the CIF will be compared to the uraninite at the Lac Cinquante to determine whether the uranium is originating from the CIF.

Chapter 2 - Background

2.1. Vein-hosted uranium deposits

For the purpose of the International Atomic Energy Agency (IAEA) (2009) publication, the classification of vein deposits and granite-related deposits have been combined in an effort to relate geological settings or lithology to deposit type. However, according to the classification by the IAEA (2009), uranium-bearing veins can occur in a broad range of lithologies and geologic environments, such as felsic intrusives (granites), volcanic rocks, metasedimentary rocks, and sedimentary rocks. The classification of vein-type is rather broad, and the term simply conveys a description of the mineral occurrence geometry without a geological context.

Despite the poorly constrained definition, vein-hosted deposits have been subdivided into two types of granite-related deposits (IAEA, 2009). This is due to a recognition of a spatial relationship between granitic plutons and surrounding host rocks of some vein-type deposits (Margnac, France, Jáchymov, Czech Republic) (IAEA, 2009, René et al., 2017, René et al., 2019). These deposits have been subdivided into two categories: i) “Endo (or intra-) granitic deposits and related contact-granitic deposits”, ii) “perigranitic deposits in meta-sediments and in contact-metamorphic rocks” (IAEA, 2009). Uranium mineralization in granite-related vein-type deposits occurs either as i) veins and stockworks consisting of ore and gangue minerals in granite, contact metamorphic rocks and meta-sediments, and ii) uranium mineralization that is disseminated in episyenite bodies. The typical ore minerals include pitchblende (low temperature uraninite), which is commonly associated with Fe-sulfides (pyrite, marcasite), Ag, Co, Ni ± Cu, Pb, Zn, and Mo sulfides. Gangue minerals are typically comprised of fluorite, quartz ± barite, calcite (IAEA, 2009).

2.2. Uranium geochemistry

Uranium in VIII coordination has a high ionic charge (4+ or 6+) and a small ionic radius (1.14Å or 1.00Å, respectively) (Hoshino et al., 2016) making it a high field strength element (HFSE). As a result, it behaves incompatibly with most rock forming silicates during crystallization of a melt (Cuney, 2014). Consequently, it is preferentially fractionated into felsic silicate melts throughout Earth's evolution through tectono-magmatic processes, where it may be held in the structure of accessory minerals in granites (i.e. Hudson granites) such as zircon, monazite, titanite, apatite (Cuney, 2014). This has led to a concentration of uranium, and other incompatible elements into the crust (> 2.7 ppm of U) in comparison to the Earth's mantle (21 ppb of U) (Cuney, 2014). Uranium can also be held in the structure of uraninite in peralkaline and peraluminous granites that have undergone extreme fractionation to saturate UO_2 (Cuney, 2014).

Uranium can also be concentrated in metasomatized subcontinental lithospheric mantle, which tends to be enriched in incompatible elements (Cousens et al., 2001). The enrichment of uranium along with other HFSE in the metasomatized lithospheric mantle occurs during subduction when uranium and HFSE are transferred from sediments of the subducting slab into the subcontinental lithospheric mantle by hydrothermal fluids. Subsequent low degrees of partial melting of the subcontinental lithospheric mantle can derive potassic magmas enriched in uranium like the CIF of this study (Cuney, 2014).

The geochemical behaviour of uranium is governed by the two ionic species in which it exists: reduced U^{4+} and oxidized U^{6+} . In its oxidized state, U^{6+} is very mobile as the UO_2^{2+} ion, as opposed to its reduced state, U^{4+} , where it is relatively immobile and insoluble as uraninite (Burns 1999, Cuney, 2009). Thus, precipitation of uranium in most hydrothermal uranium

deposits is controlled by an interaction of the oxidized, uranium-bearing fluids, with a reductant, such as carbonaceous matter like graphite, or other reductants like magnetite, H₂S, sulfides, among others (Cuney, 2009). Many hydrothermal uranium deposits (roll-front deposits, unconformity type uranium deposits) form from the leaching of uranium from U-rich granite source rocks by oxidizing fluids that deposit uraninite in reducing sedimentary or metasedimentary rocks (Cuney, 2009).

Most uranium deposits around the world are comprised of U⁴⁺ minerals. Uraninite is the most common U⁴⁺ mineral species and the U⁴⁺ cation in uraninite is coordinated by eight oxygen atoms in a cubic arrangement. Each of the oxygen atoms will bond to four U⁴⁺ cations. Other minerals with uranium in its reduced state are coffinite (U(SiO₄)_{1-x}(OH)_{4x}), an orthosilicate mineral with U⁴⁺ coordinate by eight oxygen atoms in a distorted cube-like polyhedral, and brannerite ((U, Ca, Ce)(Ti, Fe)₂O₆), that contains both U⁴⁺ and Ti⁴⁺ in octahedral coordination with eight oxygen atoms (Burns, 1999).

2.3. Rare Earth Element and Trace Element Abundances in Uranium Oxides and Implications for Source Discrimination of Uranium

Trivalent REEs in VIII coordination have similar ionic radii to U⁴⁺, ranging from 0.98 Å to 1.16 Å (Hoshino et al., 2016), therefore they can be incorporated into the structure of uraninite during crystallization (Mercadier et al., 2011). In fact, the substitution of elements, such as REES, for U⁴⁺ is common (Burns, 1999). Consequently, analysis of the abundance of these elements in uraninite can provide insight into the composition of the mineralizing fluids and can therefore help determine the origin of the uranium (Mercadier et al., 2011). According to Mercadier et al. (2011), different styles of uranium mineralization can be characterized by their

chondrite normalized REE patterns since this profile is related to the source of uranium; for example, the geological setting and the characteristic of the mineralizing fluids at each deposit.

In vein-hosted uranium deposits, the REE patterns within the uranium oxides will be highly fractionated, with an enrichment in light REEs (LREE) with respect to heavy REEs (HREE) by two to three orders of magnitude, regardless of their formation temperature (Mercadier et al., 2011). They also tend to have profiles that exhibit negative Eu anomalies. Correspondingly, they will have REE profiles that will imitate the profile of the uranium source i.e. granites. In sum, the REE abundances in vein-type deposits are source-controlled, and therefore can be used in this study to determine the source of uranium for the Lac Cinquante deposit (Mercadier et al., 2011).

2.4. Past Research of uranium occurrences in the Baker Lake basin and the Lac Cinquante uranium Deposit

An extensive study of the LC region was done by Miller et al. (1986), with a focus on deposit geology of the LC. This study reported uranium mineralization following two northeast-trending zones that are known as the Main zone and the South zone (Figure 2B). The Main Zone contains approximately 400 m of mineralization along strike.

Miller et al. (1986) also described the deposit geology in depth. The basement rocks consist of Archean metavolcanics and metasediments. Note from here on out the prefix meta- is omitted for brevity, however, all rocks discussed have undergone greenschist metamorphism in the LC area. The main lithology of these volcanic units are basaltic flows and pillows with a primary mineralogical assemblage of relict plagioclase (An_{30-35}), clinopyroxene, and clinoamphibole. The metamorphic assemblage consists of chlorite, epidote, carbonate, albite, and sericite. Metasedimentary units are interlayered with the mafic volcanics and consist of chert-sulfide-chlorite bearing tuffs. The tuff zone that hosts the U-mineralization at the LC deposit is

comprised of fine-grained quartz, chlorite, graphite, sericite-muscovite, sulfides, and minor carbonate. Pyrite is framboidal and makes up the majority of the sulfides, however, minor occurrences of chalcopyrite and sphalerite are also noted. Dacitic to rhyolitic felsic pyroclastic rocks are also interlayered with the mafic volcanics and tuffs and have a mineral assemblage comprising of quartz, sericite, carbonate with albite and pyrite. The pyroclastic rocks are interpreted as having an exhalative origin (Miller et al., 1986). Finally, the basement rocks in the deposit area are intersected by phlogopite-rich lamprophyres of the Christopher Island Formation (Miller et al., 1986).

Shearing in the deposit area has led to a foliation in the mafic volcanic outcrops and the extreme stretching of pillows. In drill core, foliation is reported in the felsic lapilli tuffs and have caused laminations in the tuffaceous and exhalative metasediments (Miller et al., 1986). Miller et al. (1986) also noted that the metasedimentary units underwent recrystallization due to dynamic metamorphism and resulted in cataclastic textures and mineralogically diverse units: quartz-mica-graphite schist, pyrite-sericite-carbonate-feldspar-chlorite schist, graphite-chlorite quartzose metasediment and laminated pyritic tuffaceous metasediment.

Miller et al. (1986) characterized the deposit as hydrothermal vein-hosted and divided the uranium mineralization into three groups: i) disseminated pitchblende with base metals in fractured carbonaceous-sulfide-chert exhalative tuff, ii) discrete pitchblende veins that cut across the exhalative-tuff and iii) quartz, carbonate, sulfide, pitchblende gash veins (small veins that open perpendicular to extensional forces) (Bons et al., 2012). The ore metal assemblage of the LC deposit is $U + Pb + Mo + Ag + Cu \pm Zn$. The mineralization contains a complex alteration assemblage of hematization, chloritization, carbonization, silicification, and albitization that seems to be spatially constrained to the ore zones (Miller et al., 1986).

Uraninite is the main ore forming mineral at the LC and commonly occurs i) as colloform texture (spherical growth of uraninite) infilling veins, ii) along volcanic fragments in breccia, and iii) disseminated throughout pervasively hematized and chloritized wall rocks. Galena is associated with uraninite mineralization and is thought to form as a result of Pb released through radiogenic decay of uranium (Miller et al., 1986). Lead is geochemically incompatible in the uraninite structure owing to its larger ionic radius and different charge (Alexandre & Kyser, 2005). Therefore, Pb is easily removed from uraninite during the decay of uranium and can subsequently form galena (Alexandre & Kyser, 2005). Felted aggregates (randomly oriented grains) of molybdenite are also commonly associated with uraninite. Chalcopyrite is most common with pitchblende, suggesting in part remobilization of copper from the exhalative metasediments (Miller et al., 1986).

Geochemical data suggests that the ore deposit resulted from two mineralization processes. First, primary low-grade Cu, Zn, Pb mineralization was associated with exhalative sediments. Then deformation occurred, concentrated within the exhalative unit, and created an increase in permeability and porosity to allow for penetration of CO₂-rich fluids throughout the rock. These fluids deposited uranium, molybdenum ± silver from the reactions with mafic volcanic rocks and carbonaceous sulfide-bearing metasediments. Subsequent reactivation probably allowed for the remobilization of uranium and copper to develop in open fracture filling veins. In sum, Miller et al. (1986) has characterized the LC deposit as a vein-type hydrothermal U + Mo ± Ag deposit.

Another study within the LC deposit was conducted by Bridge et al. (2013) to characterize ore mineralogy, date uranium mineralization events, and compare the LC deposit to other deposits. The authors concluded the uranium mineralization at LC was “a mineralogically simple, vein-hosted deposit” (Bridge et al., 2013).

Bridge et al. (2013) performed bulk rock chemistry analyses on the volcanic rocks in the area. The results show the dominant rock type in the region is a high-Fe tholeiitic basaltic andesite transitional to tholeiitic basaltic-andesite, which suggests a back-arc depositional environment of the Archean basement rocks. Trace element geochemistry provides further evidence and demonstrates the signature of these volcanics transitions from normal mid-ocean ridge basalt (N-MORB) to ocean island basalt (OIB) (Figure 3). Furthermore, the results show that the samples contain high content of large ion lithophile elements (LILE) and HFSE compared to N-MORB, which may suggest an evolved N-MORB protolith (Bridge et al., 2013).

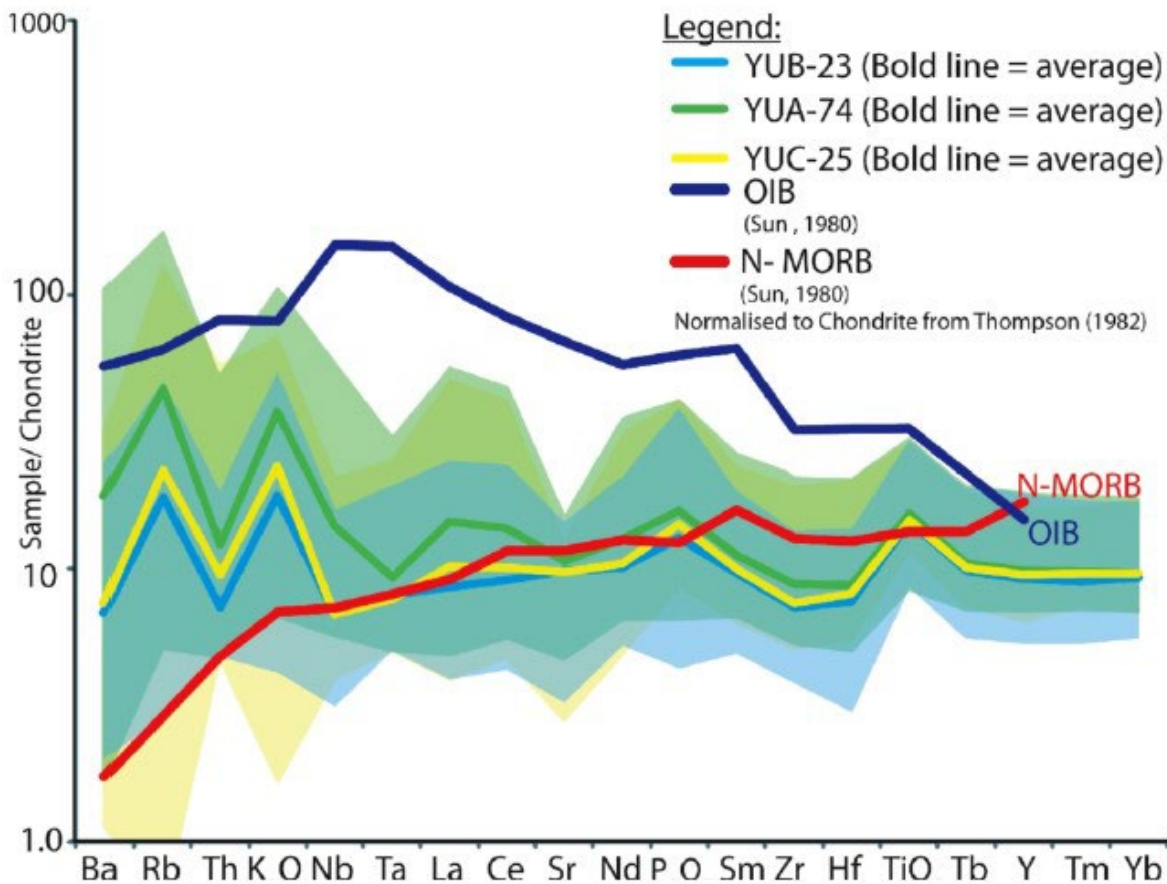


Figure 3: Spider diagram of the Archean volcanic rocks at the LC deposit showing trace element abundances normalized to chondrite (Bridge et al. 2013.)

Bridge et al. (2013) gave detailed descriptions of the alteration systematics at the LC deposit. All rocks studied in the region have undergone some degree of hydrothermal alteration resulting in carbonate and chlorite alteration that is concentrated in fractures and veins as well as greenschist facies metamorphism. In addition to the background alteration and metamorphism, rocks in the area have been exposed to hanging wall alteration, porphyry alteration, and vein alteration. The hanging wall alteration consists of a mineral assemblage of carbonate, chlorite, albite, and hematite with albite and chlorite defining a schistosity. The porphyry alteration occurs where porphyry dikes intersect the tuff units of the Main zone of uranium mineralization. The alteration assemblage is comprised of carbonate \pm pitchblende (low temperature colloform uraninite), albite, and quartz and are rimmed by hematite, and chlorite. The veins are described as gash veins that crosscut the country rock. The alteration mineral assemblage consists of hematite-carbonate-chlorite alteration that penetrates 0.5 to 0.1 m into the basaltic host rock surrounding associated quartz-pitchblende gash veins. The paragenetic sequence in these veins appears to be from earliest to latest chlorite, pitchblende, and hematite. Carbonate is a post-ore open space filling in the veins (Bridge et al., 2013).

The research by Bridge et al. (2013) yielded geochronology for the LC deposit. The U-Pb isotopic ages from pitchblende of hematite-chlorite-calcite gash veins reveal two clusters of ages: 1828 ± 29 Ma and 1437 ± 31 Ma. The least altered pitchblende at 1828 ± 29 Ma is interpreted to represent the age of primary mineralization and is similar in age to the emplacement of the 1.85 to 1.79 Ga Hudson granite suite (Peterson et al., 2002) as well as the 1.833 to 1.811 Ga Christopher Island Formation (van Breemen et al., 2005), making these two magmatic units plausible sources of uranium for the LC deposit. Furthermore, the emplacement of these magmas could have produced the heat required to drive the hydrothermal circulation of uranium-bearing

fluids. Altered pitchblende that yielded an age of 1437 ± 31 Ma is interpreted to represent resetting by a later fluid event (Bridge et al., 2013). Chemical ages of pitchblende using Pb/Pb isotopes were also calculated in research by Bridge et al. (2013) and reveal four periods of resetting at 1260 – 1321 Ma, 895 Ma, 741 – 813 Ma, and 660 – 706 Ma. The Pb/Pb chemical ages provide less accurate dates than U/Pb dating due to the loss of lead in uraninite because of its geochemical incompatibility within the uraninite structure (Alexandre & Kyser, 2005). However, this dating method is sensitive to tectonic events, and therefore these ages are interpreted to reflect resetting due to tectonic events. The first age has been interpreted to correspond to the emplacement of the 1267 ± 2 Ma MacKenzie Dike swarm. The other resetting ages calculated using Pb/Pb chemical ages are thought to be related to the assembly and break up of the supercontinent Rodinia (Bridge et al., 2013).

Finally, chlorite geothermometry was conducted by Bridge et al. (2013) and the resulting temperatures, related to retrograde chlorite formation, were constrained to 230° C to 350° C.

Chapter 3 – Geological Setting

3.1. Regional Geology

The Canadian Shield comprises a number of agglomerated Archean provinces (Slave, Rae, Hearne, Wyoming, Superior, Nain) consisting of Archean granite to greenstone basement rocks and Early Proterozoic sedimentary cover (Figure 1). Along the boundaries of these Archean provinces are many orogenic belts that correspond to a series of Early Proterozoic collisional events that resulted in cratonic amalgamation. For the purpose of this study, the collisional events (New Quebec, Torngat, Rinkian-Nagssugtoqidian orogens) that make up the east of modern-day Canadian Shield will be omitted from this discussion (Hoffman, 1988). The focus instead will be on the Archean provinces that make up the Western Churchill province, where the Lac Cinquante uranium deposit in Nunavut, Canada is located (Figure 1, Figure 2).

The Western Churchill province is comprised of Archean basement rocks that were unconformably overlain by various intracontinental Paleoproterozoic basins (Rainbird et al., 2003). It is split in two by the Snowbird Tectonic Zone (STZ) and divides the Hearne and Rae provinces (Figure 1). The provinces that make up the Western Churchill province were brought together by a series of Proterozoic collisional events (Hoffman, 1988). Some of which, the Thelon, Taltson, and Trans-Hudson orogenies, outline the Western Churchill province to the northwest and southeast (Hanmer et al., 2004). The Thelon and Taltson orogenies were first interpreted by Hoffman (1988) as a combined orogeny that occurred between 2.02 – 1.91 Ga (van Breeman et al., 1987a, b, Bostock et al., 1987) and brought together the Archean Slave and Rae provinces in a dextral-oblique system (Hoffman, 1988). A study by Card et al. (2024) concluded that the most likely model for the accretion of the Slave and the Rae provinces, although similar to the proposed model by Hoffman (1988), involved two separate subduction

zones, resulting in the differences in ages of magmatism and metamorphism seen in the Thelon tectonic zone and the Taltson tectonic zone. This implies that the (2.02 – 1.98 Ga) (Card et al., 2024) Thelon orogeny occurred slightly before the (1.986 – 1.959 Ga) (Card et al., 2024) Taltson orogeny and the two orogenies should be considered distinct from each other (Card et al., 2024). Following the Thelon and Taltson orogenies, the Wopmay orogeny took place between 1.95 – 1.84 Ga (Bowring, 1985) and evolved as an active margin setting off the western margin of the Slave province (Hoffman, 1988). Subsequently, the Snowbird orogen of 1.92 – 1.85 Ga (Cutts et al., 2024) is thought to have brought together the Rae and Hearne provinces and resulted in the formation of the Snowbird Tectonic Zone (Berman et al., 2007, Cutts et al., 2024, Hoffman, 1988). This structure is comprised of mylonitic rocks that span from Alberta to Nunavut and separates the Rae and Hearne provinces (Hoffman 1988). The STZ has previously been a topic of debate (Flowers et al., 2006, Hanmer et al., 1995, Regan et al., 2017), however, many recent studies support the idea that this cryptic structure represents the ca. 1.9 Ga collisional boundary between the Rae and Hearne cratons (Berman et al., 2007, Card et al., 2021, Cutts et al., 2024, Gibb & Walcott, 1971, Hoffman, 1988, Pehrsson et al., 2013b). Immediately following the collision of the Hearne and the Rae, the Trans-Hudson orogeny peaked at 1.81 Ga (Kraus & Menard, 1997, White, 2005), and brought together the Superior and the Hearne provinces, reworking the Western Churchill Province (Berman et al., 2007).

Several Paleoproterozoic intracontinental basins unconformably overlie the Archean basement rocks in the Western Churchill Province (Rainbird et al., 2003). A number of these basins are uraniferous and host of variety of different deposit types, a few are listed here. The Athabasca Basin is a major economic source of uranium in Canada, with unconformity-related uranium deposits dominant across the basin (Jefferson et al., 2007). The basement rocks consist

of Archean and Paleoproterozoic granitoids, gneisses, metasedimentary rocks, and minor gabbro (Alexandre et al., 2007, Card et al., 2007). The Athabasca Basin formed 1740 – 1730 Ma and is comprised of thick fill of clastic Paleoproterozoic sequences (Ramaekers, 1990, Rainbird et al., 2007). The uranium deposits hosted in this basin record two primary ages of hydrothermal ore-forming events: 1600 to 1500 Ma (Alexandre et al., 2003) and 1460 to 1350 Ma (Fayek et al., 2002). Major Athabasca basin uranium deposits include McArthur River, Rabbit Lake, Eagle Point, and Cigar Lake deposits (Jefferson et al., 2007). The Beaverlodge uranium district in Saskatchewan within the Paleoproterozoic Martin Lake Basin commonly hosts vein-type and Na-metasomatic uranium deposits (Dieng et al., 2015). The basement rocks within the Beaverlodge district consist of a suite of Archean granitoids and orthogneisses (Dieng et al., 2013). Unconformably overlying the basement is 2.33 to 2.17 Ga Murmac Bay Group, a package of metamorphic sedimentary rocks and mafic volcanics and intrusives (Liang et al., 2017). The Martin Group unconformably overlies the Murmac Bay Group and is a thick unit of continental red beds and mafic volcanics (Liang et al., 2017). The age of uranium mineralization within this uranium district are variable, however the dates for the major deposits are concentrated within 2300 – 1820 Ma (Dieng et al., 2013). Major deposits within this basin include the Gunnar deposit (Na-metasomatic) and Fay, Ace, and Verna deposits (vein-type) (Dieng et al., 2015). The Thelon Basin (Figure 2A) also contains a variety of uranium deposits, mainly within the Kiggavik area, that are not as well studied as the Athabasca basin. They are poorly understood, however a few deposits are considered basement-hosted unconformity-type uranium deposits (Shabaga et al., 2020). The basement underlying the Thelon basin is comprised of crystalline and metasedimentary rocks (Pehrsson et al., 2013a). Basin fill is unconformably overlying the basement rocks and consists primarily of the (< 1720 – 1540 Ma) Barrenland Group (Rainbird

et al., 2003). The reported U-Pb ages of uraninite of various deposits within the Thelon basin range from ~1400 – 1000 Ma (Chi et al., 2017, Riegler, 2013, Shabaga et al., 2017, Shabaga et al., 2020, Sharpe et al., 2015). Major deposits within the Kiggavik area of the Thelon Basin are the Bong, End, Andrew Lake, and Kiggavik deposits (Shabaga et al., 2017, Sharpe et al., 2015). This study focuses on the uranium mineralization within the Baker Lake Basin (Figure 1, Figure 2).

3.2. Local Geology

The LC area is located within the Angikuni subbasin of the Baker Lake Basin (Figure 2A, B) and is composed of three major rock types: Archean basement rocks, Proterozoic Dubawnt Supergroup, and Proterozoic Nueltin and Hudson granites (Aspler & Chiarenzelli, 1996, Rainbird et al., 2003, Peterson et al., 2002), that are described in detail below. The 2.68 Ga (MacLachlan et al., 2005) Archean basement rocks of the Ennadai-Rankin Greenstone Belt are primarily composed of mafic lavas, interlayered with tuff and a mixed volcanic unit (Bridge et al., 2013). The mafic lavas are predominantly tholeiitic basalts that are massive to pillowed and basaltic andesite in composition. The basalts are interpreted to have undergone metamorphism to a greenschist facies due to a current mineral assemblage of albite, chlorite, epidote, actinolite, hornblende, and secondary quartz. The interlayered tuff units host the uranium mineralization at the LC deposit and the dominant mineral assemblage for these rocks is plagioclase, diopside, hornblende, and chlorite, with sulfides, minor graphite, biotite, carbonate, and hematite (Bridge et al., 2013).

The central Ennadai-Rankin greenstone belt is interpreted to be the product of a prograding submarine volcanic plateau-slope-basin depositional system (Aspler & Chiarenzelli, 1996). This system is thought to have formed in transitional to oceanic crust in a back arc basin

setting. The back arc basin model involves the growth of a volcanic arc due to the subduction of oceanic crust beneath oceanic crust at 2.78 – 2.70 Ga (Aspler & Chiarenzelli, 1996). Rollback of the subducting slab is thought to have caused back-arc extension, forming the volcanic and sedimentary units of the Ennadai-Rankin greenstone belt. Finally, a change in the arc system, interpreted as a response to a decrease in the rate of slab rollback, shifted the extensional forces to compressional forces and caused the collapse of the back-arc basin (Aspler & Chiarenzelli, 1996). This model is consistent with the interpretations made by Bridge et al. (2013), who performed geochemical analyses of basement rocks that resulted in a tholeiitic character. The geochemical signature and bimodal volcanism observed by Bridge et al. (2013) is typical of a back-arc setting.

The basement rocks in the Angikuni subbasin are crosscut by a network of shear zones consisting of mylonites and cataclasites. Two of which had important control on the sedimentation and deposition of the Baker Lake Group: the eastern shear zone and the Tulemalu fault. The eastern shear zone shows evidence of dextral movement in the Archean (~2.62 – 2.61 Ga), however brittle Paleoproterozoic reactivation (~ 1.85 Ga) has been interpreted (Aspler et al., 2004). Activity along the Tulemalu fault has a complex history but has been dated to a series of Paleoproterozoic ages (Aspler et al., 2000).

The Archean rocks are unconformably overlain by mixed volcanics and siliciclastics of the 1845 – <1720 Ma Proterozoic Dubawnt Supergroup (Rainbird & Davis, 2007). The Dubawnt Supergroup is subdivided into a series of groups (Figure 4). The 1845 – 1785 Ma (Rainbird et al., 2003) Baker Lake Group marks the base of the Dubawnt Supergroup and is comprised of coarse alluvial red beds that make up the 1845 Ma (Rainbird et al., 2003) South Channel Formation. Overlying the South Channel Formation is the 1813 Ma (Roddick & Miller, 1994) Kazan

Formation, consisting of finer-grained distal equivalents (Rainbird et al., 2003). The South Channel Formation and the Kazan Formation are intruded by the ultrapotassic mafic lava flows and volcanoclastics of the Christopher Island Formation (CIF) (Rainbird et al., 2003). Within the Baker Lake Basin, this unit is dominated by a mineralogical assemblage composed of K-feldspar, alkali-rich amphibole, magnetite, titanite, and primary carbonate minerals (Peterson et al., 2002). In terms of trace elements (Figure 5), this volcanic unit has a strong enrichment in LILE (Rb, Ba, and K), LREEs, and some HFSE (Zr, Th, and U) (Cousens et al., 2001, Peterson et al., 2002). However, the CIF exhibits a very strong depletion in other HFSE, particularly Ti, Nb, and Ta, relative to primitive mantle, due to the occurrence of refractory rutile in subcontinental lithospheric mantle (Cousens et al., 2001, Peterson et al., 2002). The trace element pattern is similar to the Hudson granites, except for the depletion in Ba and P seen in the Hudson granites (Peterson et al., 2002). This geochemical pattern is characteristic of subduction-zone lamprophyres, and therefore is suggestive that the CIF magmas were modified by subduction fluids. The ultrapotassic rocks were likely derived from melts of metasomatized subcontinental lithospheric mantle. This metasomatism is proposed to have occurred in the Archean and was followed by long-term storage in the enriched lithospheric mantle until 1.83 Ga extension led to decompression melting, and resulting magmatism of the CIF (Cousens et al., 2001).

Finally, the Baker Lake Group is topped by the 1785 Ma (Rainbird et al., 2003) Kunwak Formation that is not interfingering with the Christopher Island Formation. The Baker Lake Group is interpreted to have formed during the opening of an intracontinental rift basin; therefore, it is interpreted as being a record of the initial stages of development of the Baker Lake Basin (Rainbird et al. 2003, Mercadier et al., 2013). Fault-induced subsidence to accommodate sedimentation in the Angikuni subbasin was most-likely a result of regional uplift and extension

within the Western Churchill province due to the terminal collision and post collisional convergence of the Trans-Hudson orogeny in the southern flank of the Western Churchill Province (Aspler et al., 2004).

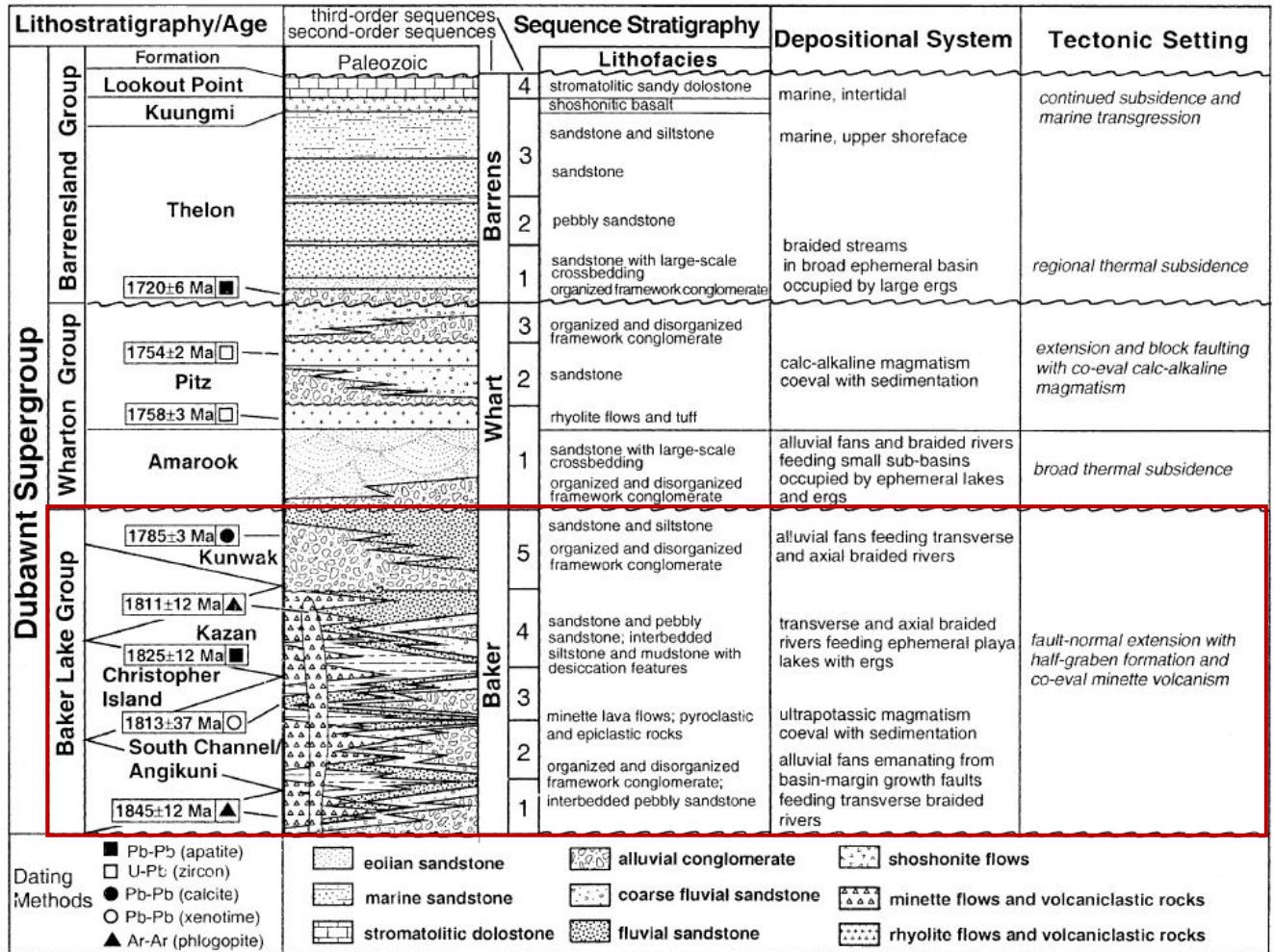


Figure 4: Stratigraphic section of the Dubawnt Supergroup. Baker Lake Group outlined in red box with the South Channel formation, Christopher Island Formation volcanics, Kazan sedimentary succession, and Kunwak formation (modified from Rainbird et al., 2003).

Within the area, there are also a number of granitic intrusions, the Hudson and the Nuelin granites. The Paleoproterozoic Hudson granites are dated to 1.85 to 1.79 Ga (Peterson et al., 2002) and are typically characterized as non-foliated, slightly peraluminous granodiorite

(Peterson et al., 2002). They also represent a good source of uranium (Cuney 2014) and are one of the hypothesized sources of uranium for the LC deposit. The trace element pattern of the Hudson granites are similar to the trace element abundances of the CIF, except for the depletion in Ba and P seen in the Hudson granites (Peterson et al., 2002). Furthermore, they have very low Y contents. These rocks are interpreted as evidence of early post-orogenic intrusions because of their depletion in Y and high ratios of LREE/HREE. Also of note is their feldspar composition between An₁₀₋₂₀, broad range in Or and the negative Eu anomaly in their REE profile (Figure 5) (Peterson et al., 2002).

The Nueltin granites are also Paleoproterozoic in age, however, are a bit younger than the Hudson granites and have been dated to 1.76 to 1.75 Ga. These granites are strongly porphyritic with phenocrysts of quartz, potassium feldspar, and anorthite. They exhibit myrmekitic and rapakivi textures. Unlike the Hudson granites, the Nueltin granites do not have a depletion in Y, however they do share the prominent negative Eu anomaly (Figure 5). They also have a much lower Ce/Yb than the Hudson granites with the mean sitting at Ce/Yb = 47 (Peterson et al., 2002).

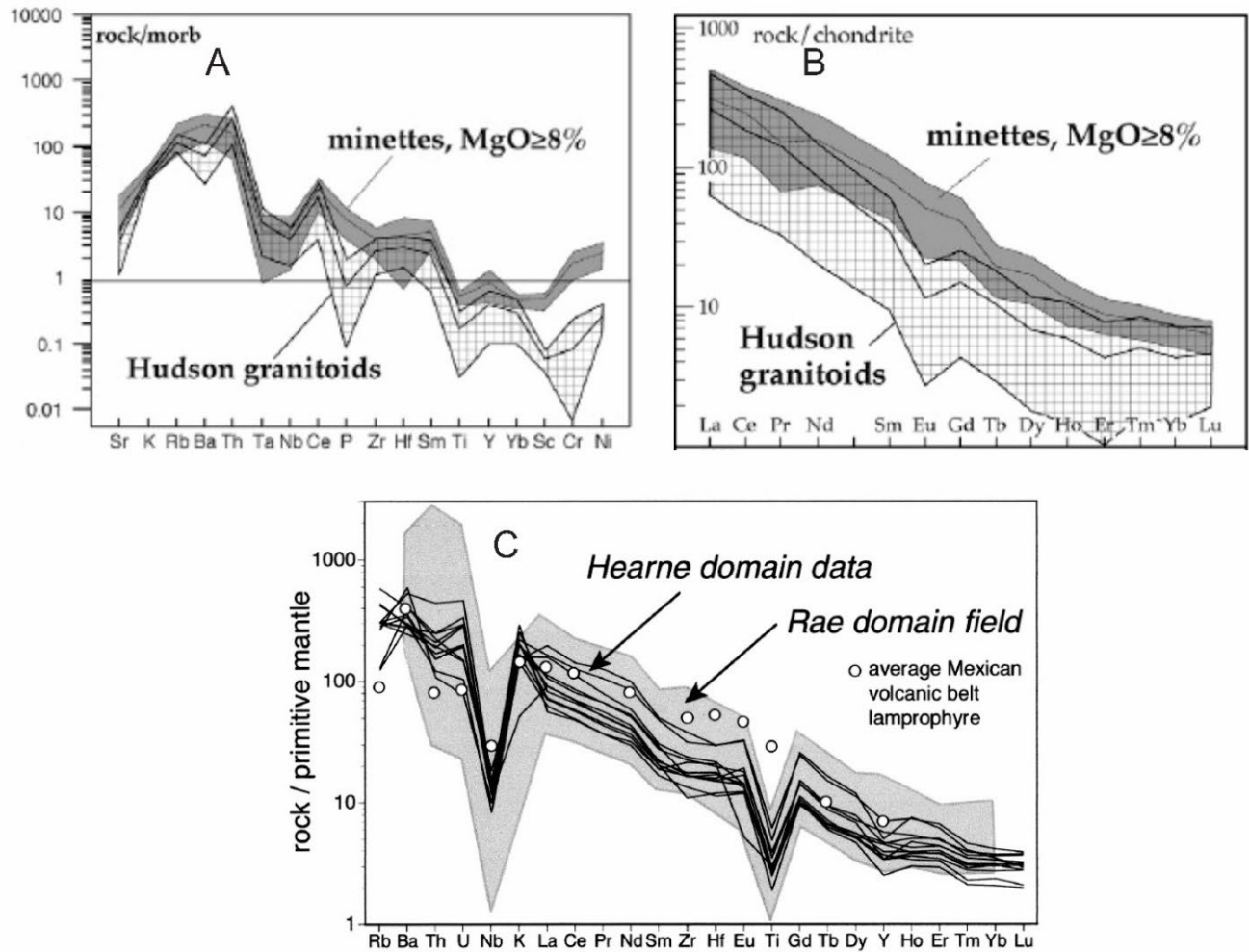


Figure 5: Trace element and REE abundances of the Hudson granites and the Christopher Island Formation ultrapotassic minettes. A) Spider diagram of the trace elements abundances normalized to MORB within the Hudson granitoids and ultrapotassic minettes of the Dubawnt Supergroup, from Peterson et al., 2002. B) REE abundances normalized to chondrite of the Hudson granitoids and ultrapotassic minettes of the CIF, from Peterson et al., 2002. C) Spider diagram of trace element abundances of the CIF, normalized to primitive mantle, from Cousens et al., 2001.

Chapter 4 – Methods

Fifty-three thick sections provided by Kivalliq Energy Corporation by way of the Geological Survey of Canada were analysed using a polarizing microscope in both reflected light and transmitted light at Saint Mary's University, Halifax, Nova Scotia.

Petrographic descriptions and interpretation of paragenetic relationships were aided by the false-colour elemental distribution maps produced for thirty-nine of the thick sections (Appendix C) using a Bruker M4^{tomadoplus} Super Light Element Micro-XRF at Saint Mary's University. Analyses were conducted under vacuum (2 mbar) with a Rh source at a voltage of 50 kv, beam current of 600 μ A and focused to 20 μ m. Each pixel was measured for 10 ms with 30 μ m between pixels. Two silicon drift detectors capture characteristic X-rays between 0 – 30 keV, and the spectra (keV vs. intensity) were resolved for every pixel using the M4 software. In-depth petrographic reports were created for 18 of the thick sections that were selected based on their XRF data as good representatives of their specific rock types. The reports contain detailed textural descriptions, paragenetic relationships, and modal abundance (Appendix B).

A TESCAN MIRA 3LMU Variable-Pressure Schottky Field-Emission Scanning Electron Microscope (SEM) was used for detailed textural analysis and collection of chemical data at Saint Mary's University, Halifax, Nova Scotia. Fourteen thin sections were carbon-coated and analysed using back scattered electron (BSE) imaging to aid detailed textural analysis. Energy dispersive X-ray spectroscopy (EDS) was done to determine mineral chemistry, classify U-phases, and measure internal standards of calcium (Ca) for use in laser ablation-inductively coupled plasma-mass spectrometry (LA-ICP-MS). The working distance used was 17.10 mm with a 20.0 kV voltage and a collection time of 40 s/spot. Mineralogy was resolved from spectra collected during EDS analyses using the INCA and AZtec software.

Trace element abundance was assessed via laser ablation-inductively coupled plasma-mass spectrometry (LA-ICP-MS) that targeted uraninite in thirteen thin sections and brannerite in three thin sections. Data were collected using the Agilent 8900QQQ (triple Quad) at the University of New Brunswick with a 193 μm excimer laser ablation system, which houses a Laurin Technic S-155 cell. Ablated material was transported to the mass spectrometer via nylon tubing using a mix of carrier gasses of 300 ml/min ultra-pure nitrogen and a 900 ml/min of argon. Prior to analysis, samples were targeted using the polarizing microscope in both transmitted and reflected light to focus on areas devoid of fractures and inclusions. Following data collection, signal-time intensity graphs were inspected for possible contamination by inclusions. Spot analyses were conducted with a beam size of 26 μm , laser rep rate of 4 Hz and an on-sample fluence of 2 J/cm^2 on uraninite (n=157) and brannerite (n=17) grains. National Institute of Standard and Technology glass standard (NIST610) was used to correct for instrumental drift. Integration times for all elements were 15 ms, except for Pb, Bi, Th, and S which were 10 ms. ^{235}U was collected at a dwell time of 50 ms. Total sweep time was 0.605 seconds. Each sample was ablated for 30 seconds and was bracketed by a 30 second gas background. Washout time was ~ 2.5 seconds with both squids attached. Data reduction was completed using the IOLITE 4 software and the SEM-derived Ca-content internal calibration standards. General Specification for the Environment (GSE-1G) glass was used as a secondary standard. Most of the values reported high accuracy (^{42}Ca , ^{49}Ti , ^{45}Sc , ^{51}V , ^{55}Mn , ^{57}Fe , ^{88}Sr , ^{89}Y , ^{90}Zr , ^{93}Nb , ^{133}Cs , ^{137}Ba , ^{139}La , ^{140}Ce , ^{141}Pr , ^{146}Nd , ^{147}Sm , ^{151}Eu , ^{157}Gd , ^{159}Tb , ^{163}Dy , ^{165}Ho , ^{167}Er , ^{169}Tm , ^{173}Yb , ^{175}Lu , ^{177}Hf , ^{181}Ta , ^{207}Pb are within 5 % accuracy) based on the GSEG-1G. Some elements reported between 5% and 10% accuracy (^{25}Mg , ^{29}Si , ^{59}Co , ^{208}Pb are within 10% accuracy) based on GSE-1G. Total Pb, ^{27}Al , ^{206}Pb , ^{209}Bi are within 20% accuracy. Only ^{232}Th

and ^{235}U were over 20% accuracy, reporting at 28% accuracy and 55.05% accuracy, respectively. Additionally, most elements reported high precision, based on GSE-1G, calculated to one standard deviation. Many elements reported variation below 5 % (total Pb, ^{25}Mg , ^{29}Si , ^{42}Ca , ^{49}Ti , ^{51}V , ^{57}Fe , ^{59}Co , ^{88}Sr , ^{90}Zr , ^{133}Cs , ^{137}Ba , ^{139}La , ^{157}Gd , ^{163}Dy , ^{177}Hf , ^{206}Pb , ^{207}Pb , ^{208}Pb). Some elements were reported within a variation between 5% and 10% (^{27}Al , ^{45}Sc , ^{55}Mn , ^{89}Y , ^{93}Nb , ^{140}Ce , ^{141}Pr , ^{146}Nd , ^{147}Sm , ^{151}Eu , ^{159}Tb , ^{165}Ho , ^{169}Tm , ^{173}Yb , ^{175}Lu , ^{181}Ta , ^{209}Bi , ^{235}U). Two elements recorded much higher variation with ^{167}Er within 20 % and ^{232}Th reporting as 100.72 %. The high variation of ^{232}Th was expected due to the very small abundances commonly reported in uranium minerals.

In addition to LA-ICP-MS data collected for this project, thirteen point analyses between two thin sections were analysed using Laser Ablation-Inductively Coupled Plasma-Mass Spectrometry (LA-ICP-MS) at the Geological Survey of Canada to determine trace-element chemistry of uraninite and were provided for this study.

Chapter 5 – Results

5.1. Petrography and Paragenesis

Based on the petrographic descriptions (Appendix B), coupled with the micro-XRF elemental maps (Appendix C), a four-stage paragenetic sequence was interpreted (Figure 6) and uranium mineralization was characterized for the LC deposit. The first stage is the formation of the foliated, metamorphic volcanic tuff host rock (Figure 7A). It should be noted that all the samples in this study have undergone varying degrees of alteration, however petrographic and micro-XRF study of the least altered samples show plagioclase (~ 50%) and quartz (~30 %) with relict microcline (<5%), and muscovite (<5%) (Figure 7C). Plagioclase forms fine-grained anhedral grains that have been albitized (Figure 7C). Quartz commonly occurs as fine-grained anhedral grains (Figure 7C). The microcline occurs as subhedral to euhedral mineral grains exhibiting microcline twinning within the host rock (Figure 7E). The muscovite occurs as laths that are defining a weakly-aligned fabric and are also in low abundance (Figure 7C, F). Within some samples are minor amounts of anhedral ilmenite, titanite, rutile, and apatite (Figure 7B, D). The age relationships of these minerals are unclear, they may represent part of the initial mineral assemblage, or may have been disseminated throughout the host rock following albitization. The least altered samples typically show a low degree of alteration to hematite (Figure 7D) and calcite (Figure 7B); however they are albitized, shown by the high Na-content in Figure 7C.

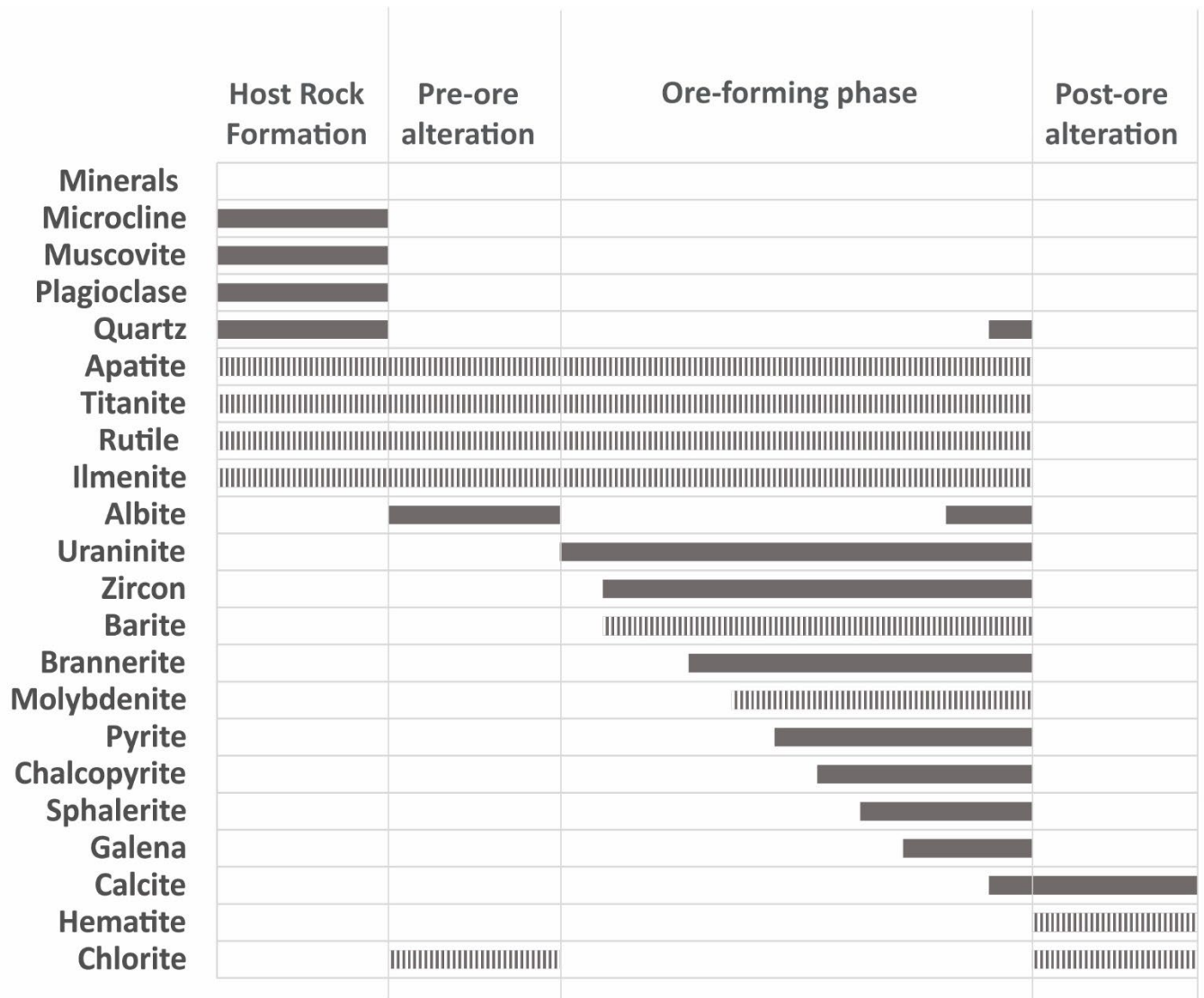


Figure 6: Paragenetic sequence of the Lac Cinquante Deposit. Four stages include: host rock formation, pre-ore alteration, ore-forming phase, and post-ore alteration. Dashed lines indicate uncertain age relationships.

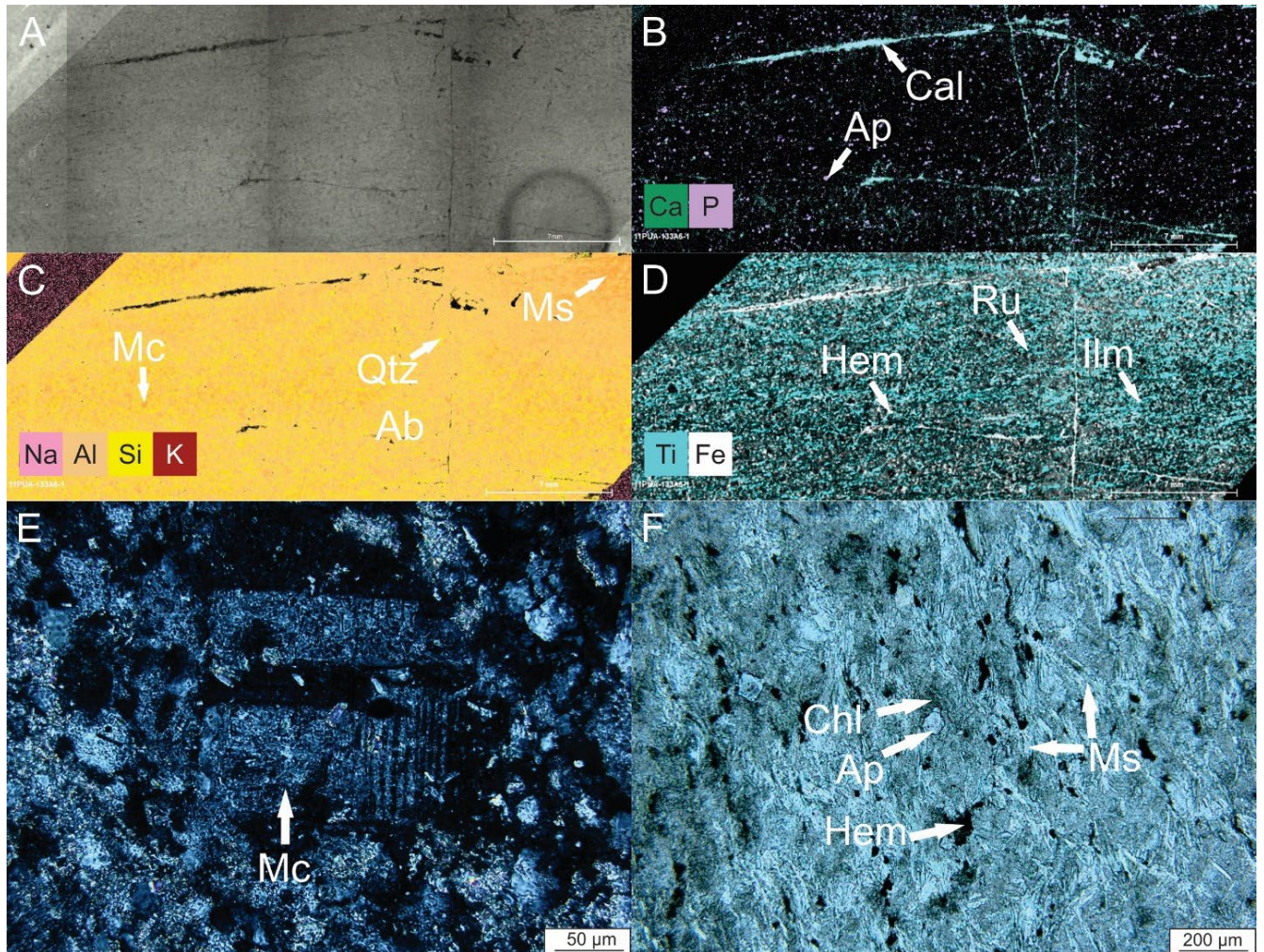


Figure 7: False colour micro-XRF elemental distribution maps and photomicrographs of host tuff (sample 11PUA-133A6-1). A) Image of least altered host tuff. B) High Ca & P indicate Ap grains within host rock. High Ca also shows Cal vein cross cutting sample. C) Albitized host rock shown by high Na content in the sample. High K indicates Mc grains and concentration of Ms in host rock. Si distribution shows Qtz in sample. D) Ti-oxides (Ru) and Ti-Fe oxides (Ilm) in sample. Disseminated Hem as shown by high Fe. E) XPL photomicrograph showing twinning in microcline. F) PPL photomicrograph with Chl, Hem, Ap, Ms, throughout sample. Mineral abbreviations are as follows: Ab = albite, Ap = apatite, Cal = calcite, Chl = chlorite, Hem = hematite, Ilm = ilmenite, Mc = microcline, Ms = muscovite, Ru = rutile, Qtz = quartz. Other abbreviations: PPL = plane-polarized light, XPL = cross-polarized light, RL = reflected light.

The second stage in the paragenetic sequence is the complete replacement of the host rock by albite. Samples from the Lac Cinquante deposit have undergone albitization and are characterized by pervasive replacement of all initial textures by fine-grained albite. This is shown by micro-XRF maps showing compositions of plagioclase as sodium-rich (Figure 8C &

Figure 9C). Cross-cutting relationships of calcite, uraninite, and the albitized host rock indicate the albitization of the host rock was early and pre-dates the ore-forming phase. The calcite replacement post dates the albitization (Figure 8E and Figure 9E) and the uraninite also post dates the albitization (Figure 8F, Figure 9F).

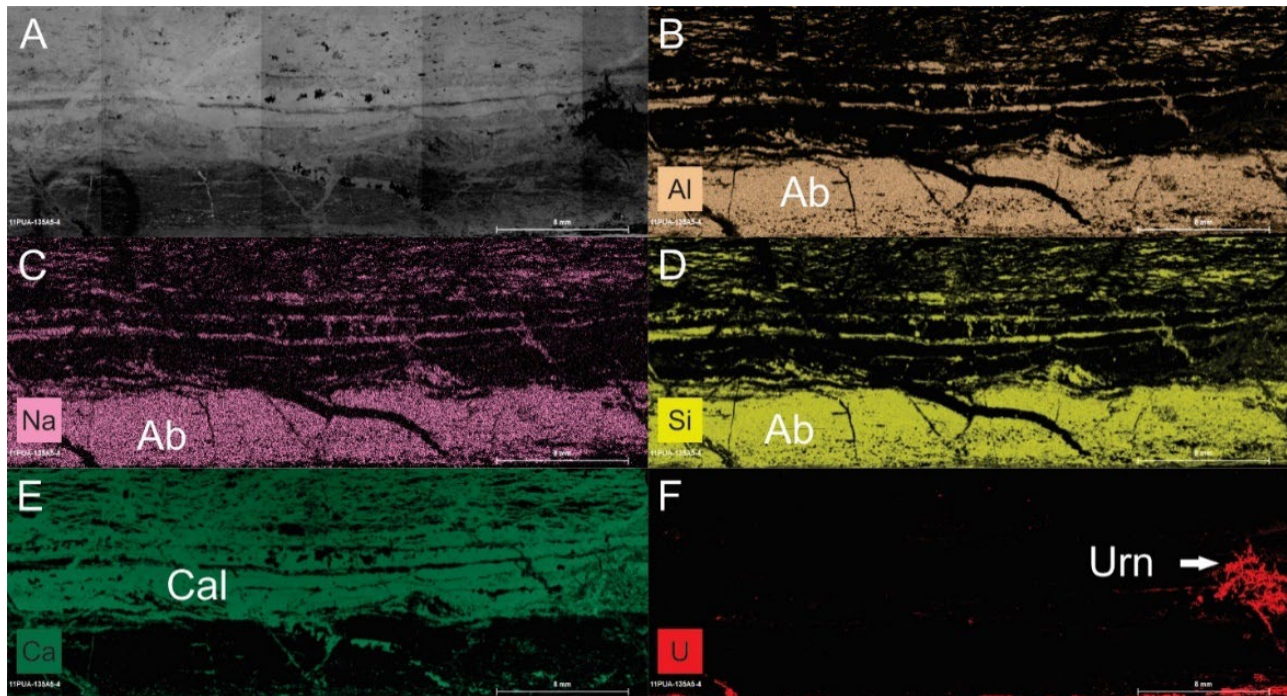


Figure 8: False colour micro-XRF elemental distribution maps of albitized host tuff (sample 11PUA-135A5-4). A) Image of host tuff. B), C), D) Al, Na, Si distribution showing Na-rich composition of the host rock (Ab). Ab has pervasively replaced host rock. E) Calcite replacement of host rock, indicated by high Ca distribution. Calcite replacement crosscuts early Ab replacement. F) U-mineralization shown by U concentration in the sample. Mineral abbreviations are as follows: Ab = albite, Cal = calcite, Urn = uraninite.

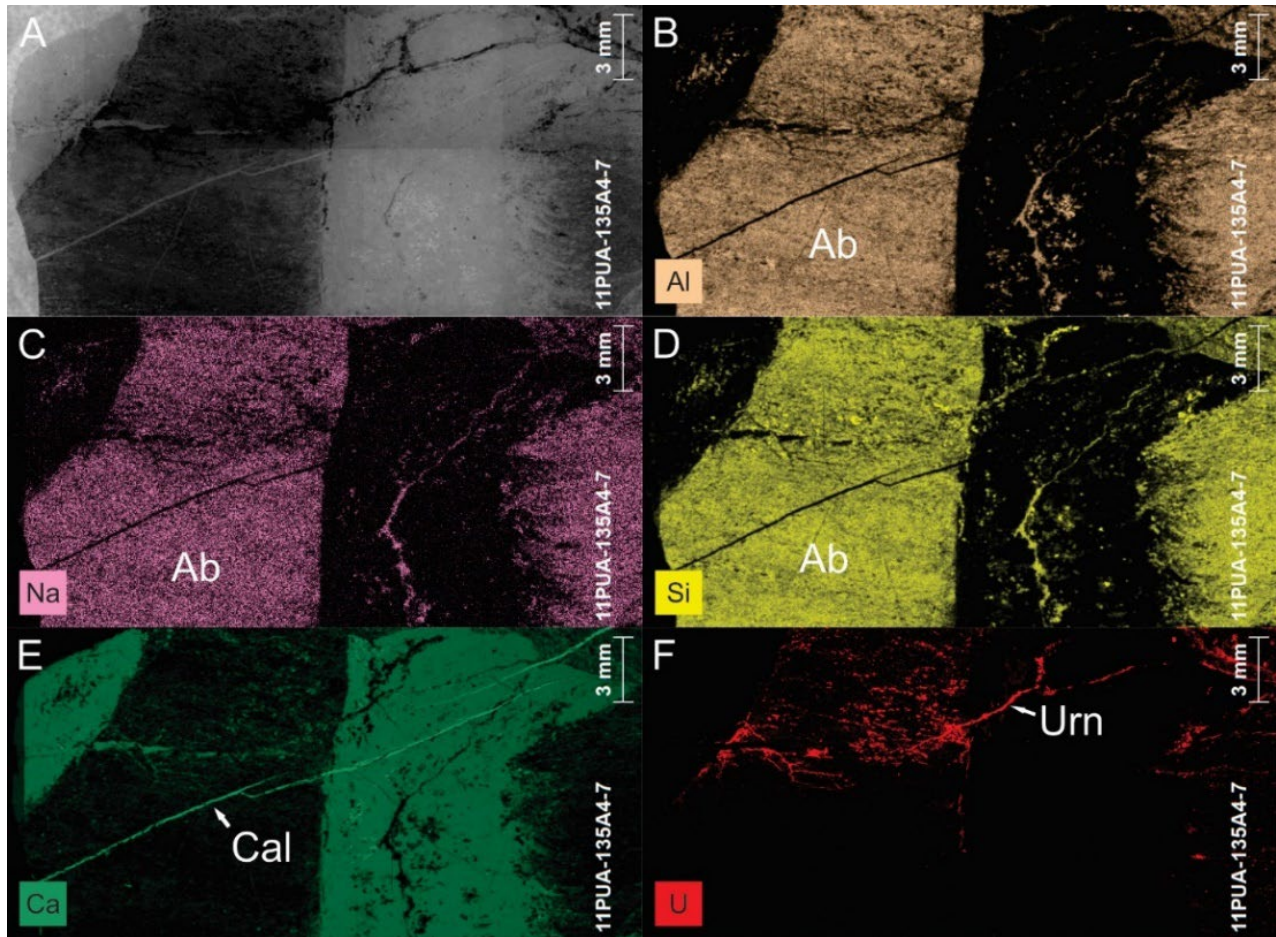


Figure 9: False colour micro-XRF elemental distribution maps of albitized host tuff for sample (11PUA-135A4-7). A) Image of host tuff. B), C), D) Al, Na, Si elemental distribution indicating high Na (Ab) of the albitized host rock. E) Calcite replacement of host rock shown by high Ca content. F) Simple vein-hosted U-mineralization (uraninite) shown by the high content of U. Mineral abbreviations are as follows: Ab = albite, Cal = calcite, Urn = uraninite.

The ore-forming stage follows the albite alteration of the host rock. Three styles of uranium mineralization characterize this deposit: i) mineralogically simple vein-hosted uranium \pm pyrite, chalcocopyrite, molybdenite, sphalerite, galena within calcite and/or albite veins (Figure 10, Figure 11), ii) mineralogically complex vein-hosted uranium brannerite, zircon, \pm fluorapatite, barite, pyrite, chalcocopyrite, molybdenite, sphalerite, galena within calcite and albite veins (Figure 12), iii) disseminated uranium \pm pyrite, chalcocopyrite, sphalerite, hematite within the albitized host rock (Figure 13).

Simple vein-hosted uranium with associations of pyrite, chalcopyrite, molybdenite, sphalerite, and galena are hosted within calcite and albite veins. Calcite is found as subhedral, blocky grains within the veins (Figure 11E) or occurs as the main vein mineral (Figure 10B). These veins host the mineralization of uraninite (Figure 10B, D) with associations of pyrite (Figure 10C, D), chalcopyrite (Figure 10D), and galena. Uraninite predominantly exhibits a botryoidal texture surrounding, or within, the veins (Figure 10E, F). Pyrite often forms euhedral to subhedral grains concentrated in veinlets (Figure 10H) or as euhedral to subhedral grains disseminated within the albitized host rock. Chalcopyrite occurs as subhedral to anhedral grains centered in veins (Figure 11G, H) or disseminated as anhedral grains throughout the sample (Figure 10G). Molybdenite is commonly spatially associated with uraninite and is mineralized throughout the host rock as anhedral grains. Sphalerite is disseminated throughout the host rock as anhedral grains (Figure 10C). Finally, galena is spatially associated with uraninite as very fine-grained anhedral grains or infilling uraninite grains (Figure 10F).

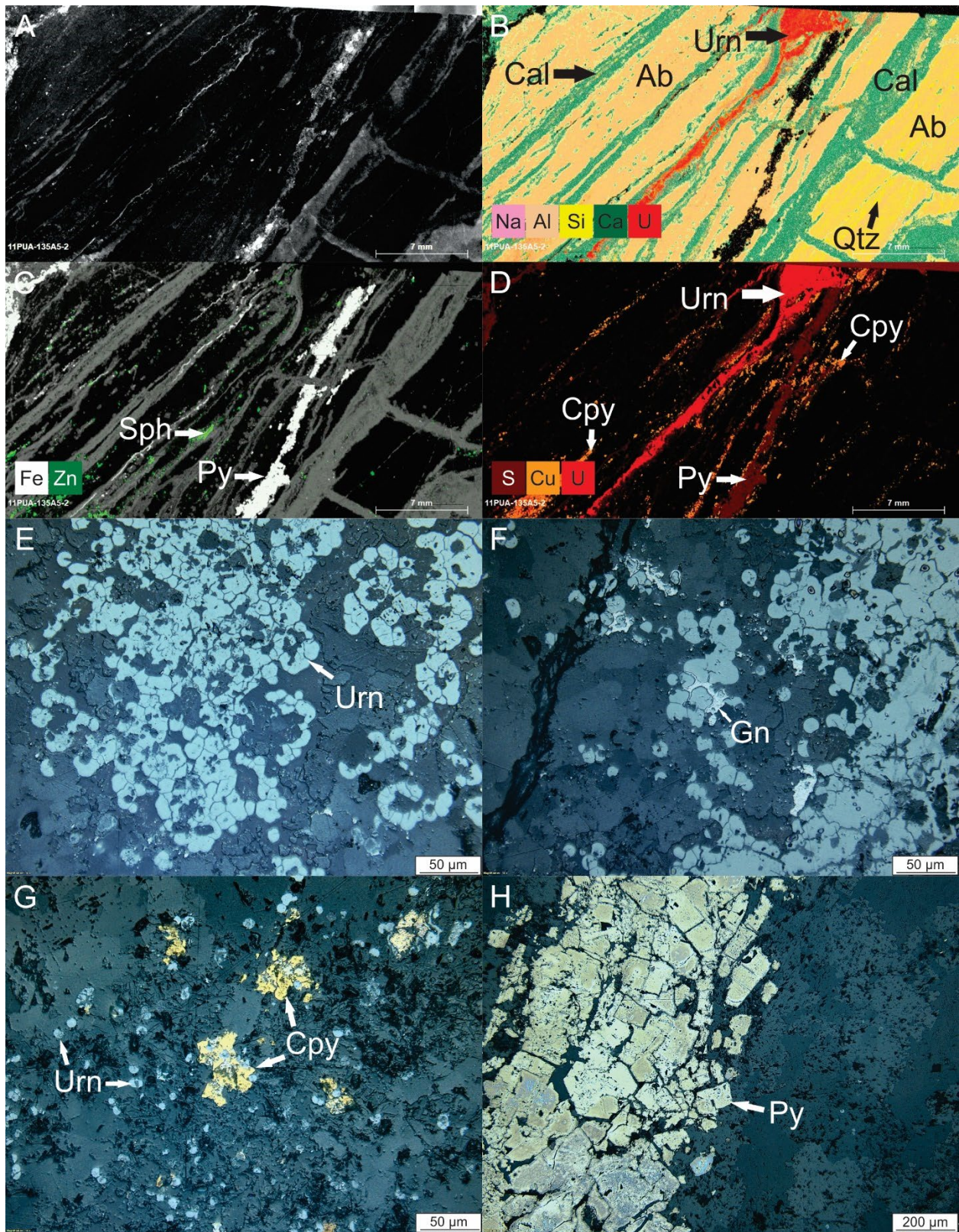


Figure 10: False colour micro-XRF elemental distribution maps and photomicrographs of host tuff with simple vein-hosted uranium (sample 11PUA-135A5-2). A) Image of host tuff. B) High

Na distribution shows albitized host rock. Some quartz in host rock, shown by high Si content. Calcite cross-cutting albitized host rock, shown by high Ca content. High U content indicates vein-hosted uraninite mineralization. C) Pyrite mineralization in vein indicated by high Fe content. Zn distribution shows location of sphalerite grains. D) Cu & S distribution shows location of chalcopyrite mineralization. S content displays pyrite mineralization in vein. U distribution (in red) shows vein-hosted U-mineralization (Uraninite). E) RL photomicrograph showing botryoidal texture of uraninite. F) RL photomicrograph with botryoidal uraninite and infilling galena. G) RL photomicrograph with anhedral chalcopyrite and grains of uraninite. H) RL photomicrograph showing pyrite mineralization concentrated along vein. Mineral abbreviations are as follows: Ab = albite, Cal = calcite, Cpy = chalcopyrite, Gn = galena, Py = pyrite, Qtz = quartz, Sph = sphalerite, Urn = uraninite. Other abbreviations: PPL = plane-polarized light, XPL = cross-polarized light, RL = reflected light.

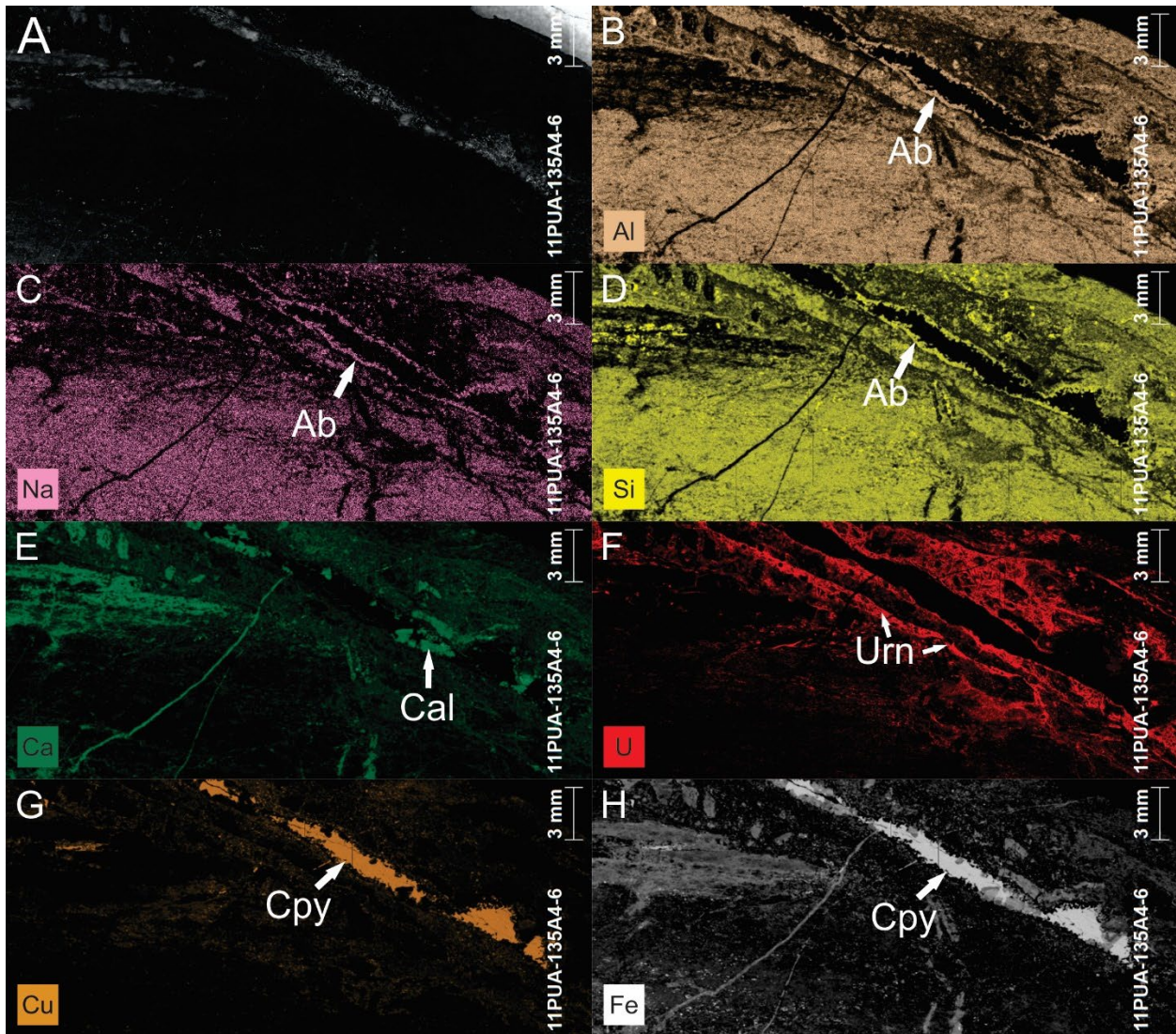


Figure 11: False colour micro-XRF elemental distribution maps of host tuff with simple vein-hosted uranium (sample 11PUA-135A4-6). A) Image of host rock, tuff. B), C), D) Al, Na, Si

distribution. High Na content from albitized host rock and albitized mineralization rimming chalcopyrite vein. E) Calcite within veins and as alteration replacement, shown by high Ca content. F) U-mineralization (uraninite) surrounding chalcopyrite vein, indicated by high U content. G), H) Chalcopyrite mineralization concentrated within vein, shown by high Cu & Fe. Mineral abbreviations are as follows: Ab = albite, Cal = calcite, Cpy = chalcopyrite, Urn = uraninite.

The most mineralogically complex type of uranium mineralization in this system is vein-hosted uraninite associated with brannerite, zircon, fluorapatite, barite, pyrite, chalcopyrite, molybdenite, sphalerite, and galena and occurs in calcite and albite veins (Figure 12). Uraninite commonly exhibits a botryoidal texture (Figure 12I) within or rimming the edge of the calcite (Figure 12G) or albite veins (Figure 12G). Brannerite is often euhedral, forming large, blocky grains within calcite (Figure 12F, Figure 12I) or albite veins. Back scattered electron images and EDS analyses also revealed hydrothermal zircon associated with uranium mineralization (Figure 12I, J). Back scattered electron images were used to aid in determining the paragenetic relationship of zircon and it can be seen infilling the older uraninite (Figure 12J). Zircon mineralization is spatially associated with uraninite (Figure 12E) commonly exhibiting a similar botryoidal texture to uraninite (Figure 12I). Vein-hosted pyrite is usually subhedral to euhedral, forming along the center of the vein (Figure 12H), whereas chalcopyrite commonly forms anhedral grains throughout the vein (Figure 12G). Molybdenite occurs in some samples as anhedral grains disseminated within host rock (Figure 12B). Fine-grained sphalerite is present in some samples as anhedral grains hosted within calcite and albite veins (Figure 12C). Finally, barite (Figure 12H) and fluorapatite (Figure 12C) are present as grains throughout the complex veins.

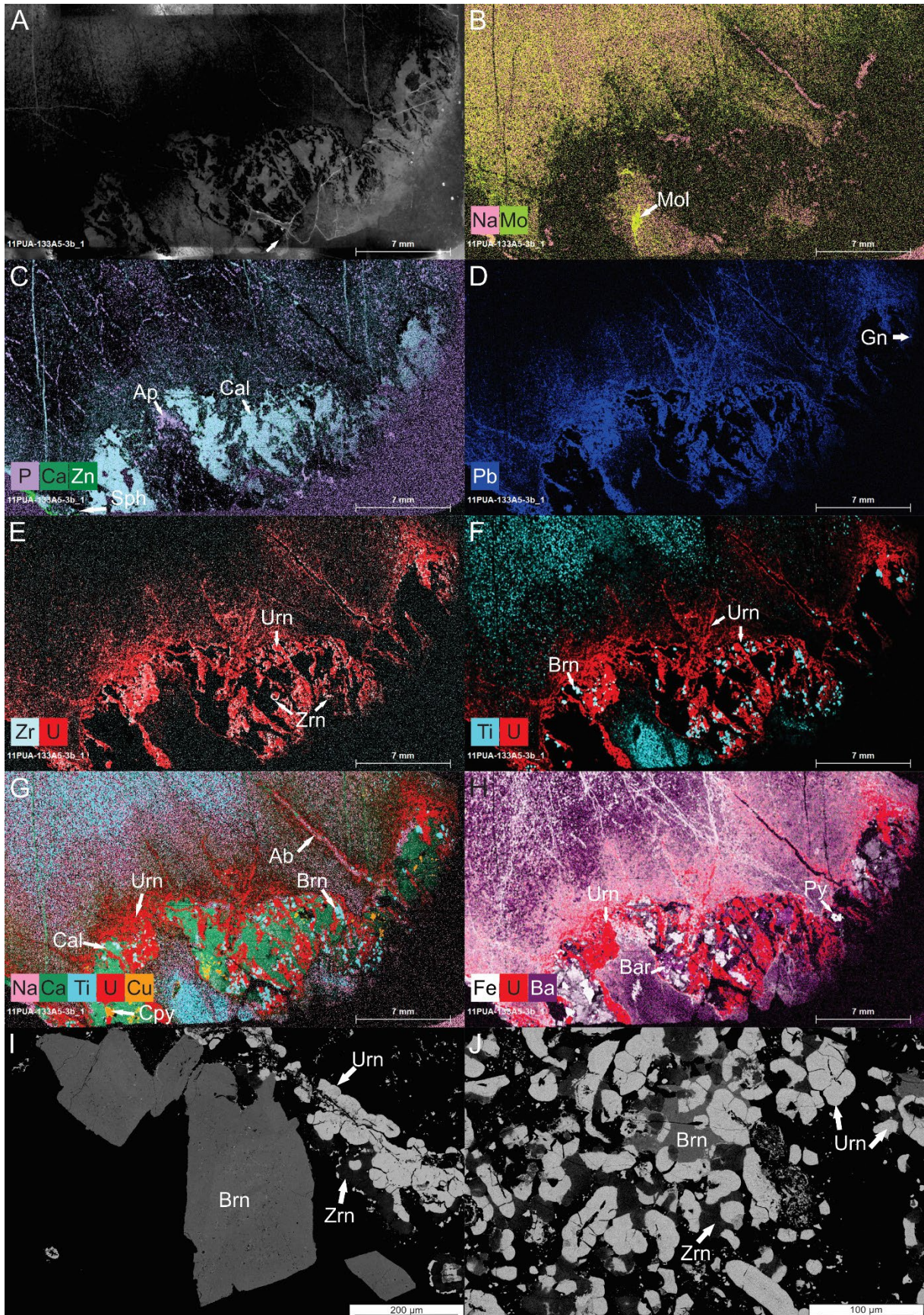


Figure 12: False colour micro-XRF elemental distribution maps and BSE images of complex vein-hosted uranium for sample 11PUA-133A5-3b of tuff. A) Image of host rock, tuff. B) High Na indicates albitized host rock. Molybdenite grain shown by high Mo distribution. C) Calcite vein (high Ca content) and sphalerite mineralization indicated by high Zn content. D) Galena grains shown by high Pb content with high Zn indicating sphalerite. Apatite mineralization shown by high Ca and P. E) Zircon and uraninite mineralization shown by high Zr and U, respectively. F) Brannerite grains indicated by high Ti & U. G) Uraninite, brannerite mineralization with chalcopyrite, shown by high Cu. H) Pyrite mineralization (indicated by high Fe). Barite within the vein shown by high Ba. I) BSE image showing textures of large, blocky grains of brannerite, botryoidal uraninite mineralization, and hydrothermal zircon. J) BSE image showing age relationships between brannerite, zircon, and uraninite. Brannerite is infilling earlier zircon. Zircon is infilling earlier uraninite. Mineral abbreviations are as follows: Ab = albite, Ap = apatite, Bar = barite, Brn = brannerite, Cal = calcite, Cpy = chalcopyrite, Gn = galena, Py = pyrite, Sph = sphalerite, Urn = uraninite, Zrn = zircon.

The final type of uranium mineralization at the LC deposit is disseminated uraninite with pyrite, chalcopyrite, and hematite throughout the host rock. These minerals are typically fine-grained and anhedral within the host rock (Figure 13), this is shown by micro-XRF elemental maps showing uranium mineralization, disseminated throughout sodium-rich host rock (Figure 13C&F).

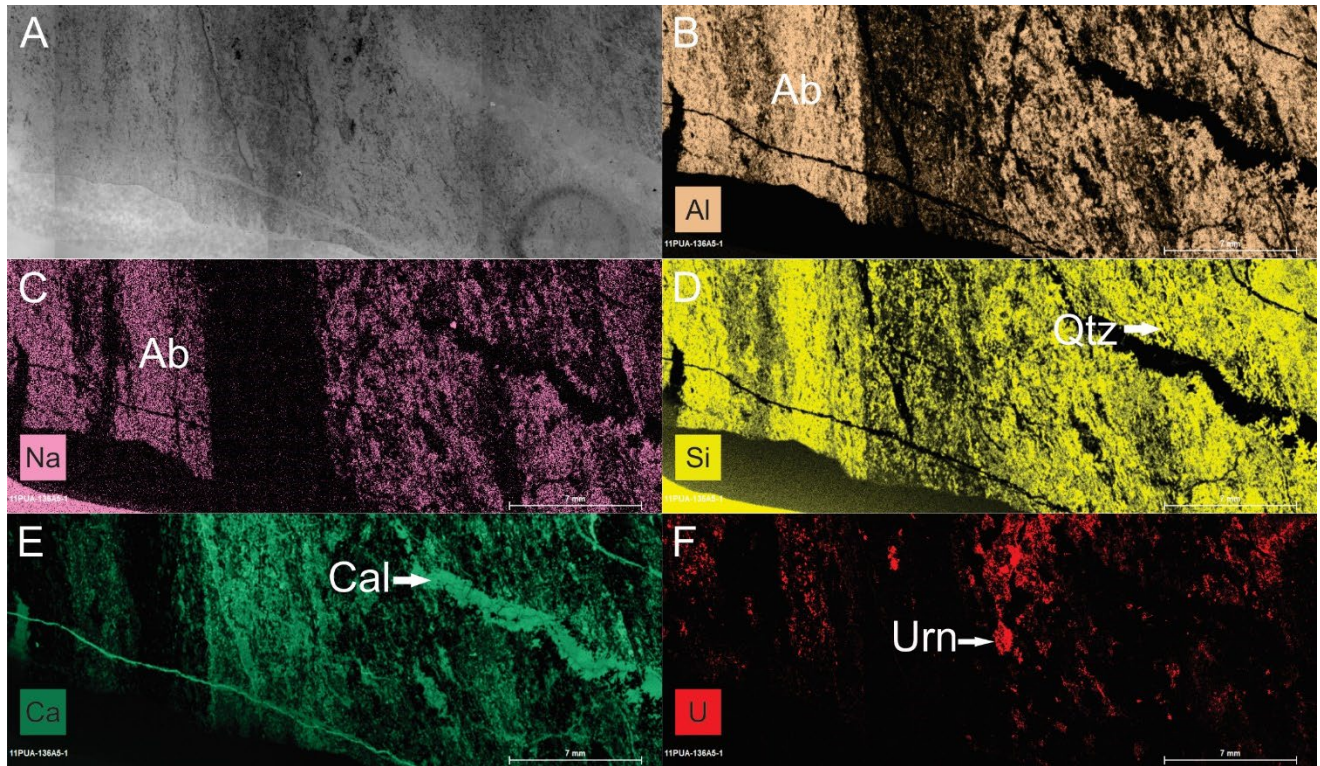


Figure 13: False colour micro-XRF elemental distribution maps of host rock with disseminated uranium for sample 11PUA-136A5-1 of tuff. A) Image of host rock, tuff. B) Al, Na, and Si distribution within sample. High Na content shows albitized host rock. Quartz grains within calcite vein, indicated by high Si. E) Calcite replacement and calcite veins crosscutting sample, shown by high Ca content. F) Uranium mineralization disseminated throughout albitized host rock, shown by high U content. Mineral abbreviations are as follows: Ab = albite, Cal = calcite, Qtz = quartz, Urn = uraninite.

The final stage in the paragenetic sequence at the Lac Cinquante deposit is post-ore alteration. All samples experienced varying degrees of hematite, chlorite, and carbonate alteration. Hematite replacement is shown by the high-Fe content in Figure 14B, where the host rock is being replaced by anhedral grains of hematite (Figure 14E). Chlorite replacement is pervasive throughout some samples (Figure 14D) and can be seen by the high concentrations of Fe and Mg in Figure 14A. Chlorite is present as either acicular, radial aggregates or laths defining a weak foliation within samples, or completely replacing all preexisting minerals to form an anhedral mass of chlorite. Lastly, the calcite replacement is very pervasive (Figure 14F) and occurs throughout most samples. The calcite replaces the host rock to form fine-grained

anhedral masses preserving no initial textures. This replacement is crosscutting the earlier albitized host rock (Figure 14C), implying calcite replacement was younger than albitization.

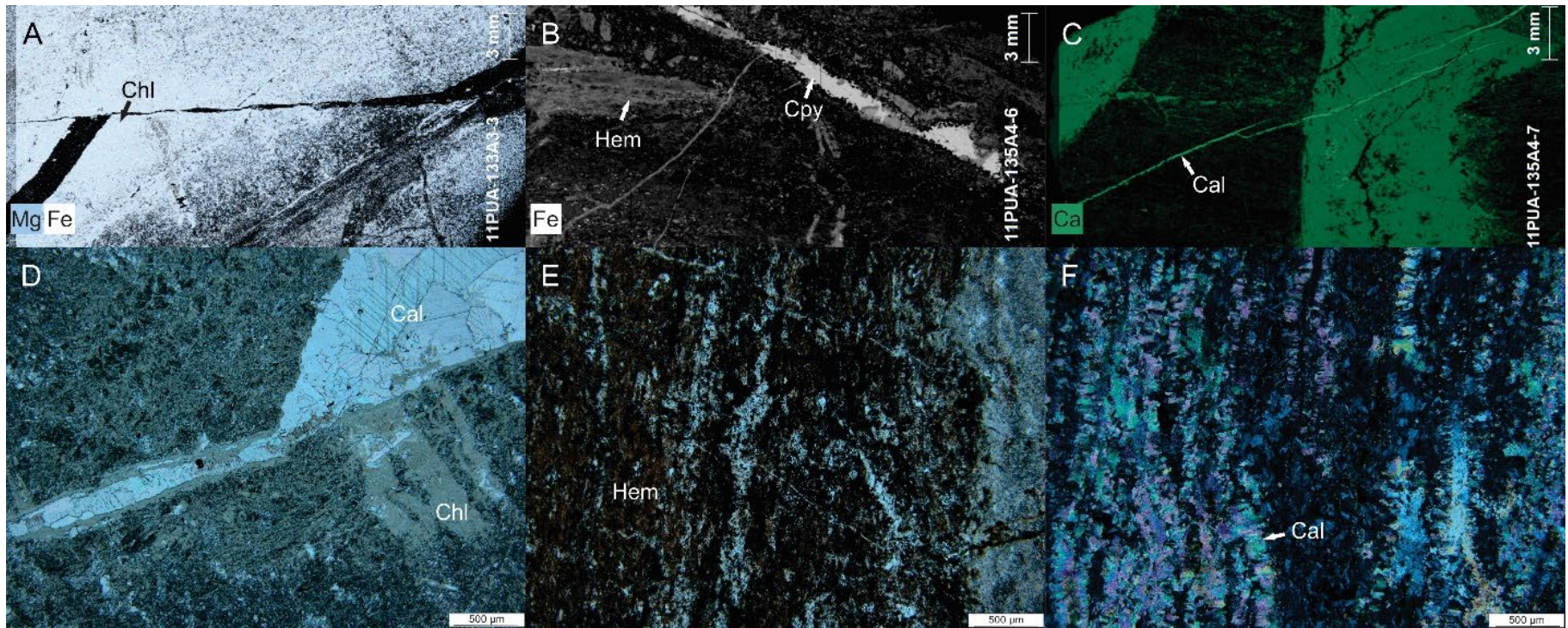


Figure 14: False colour micro-XRF elemental distribution maps and photomicrographs of LC alteration for samples 11PUA-133A3-3, 11PUA-135A4-6, and 11PUA-135A4-7. A&D) Sample 133A3-3, host tuff. High Mg & Fe content indicate chlorite alteration. This is shown in the PPL photomicrograph in D. B&E) Sample 11PUA-135A4-6 of a tuff, with high Fe content indicating areas of hematite replacement. An image of a thin section in PPL demonstrates the hematite alteration in E. C&F) Sample 135A4-7 of a tuff, showing high Ca content due to calcite replacement of host rock. Calcite replacement is shown in the XPL photomicrograph F). Mineral abbreviations are as follows: Cal = calcite, Chl = chlorite, Cpy = chalcopyrite, Hem = hematite. Other abbreviations: PPL = plane polarized light, XPL = cross polarized light, RL = reflected light.

In addition to the uranium mineralization occurring in the volcanic tuffs, uranium also infiltrates the matrix of some conglomerates of the overlying Baker Lake Group (Figure 15). These conglomerates are polymictic and consist of predominantly stubby laths of albite with minor grains of anhedral quartz, anhedral potassium feldspar, detrital zircon, and barite (Figure 15B, D). The uraninite in these samples is fine-grained, anhedral and commonly occurs with hematite, ilmenite, chalcopyrite, pyrite, and barite infilling the matrix (Figure 15C, D). Hematite infills as a cement or as anhedral grains throughout the matrix. Ilmenite and chalcopyrite occur as anhedral grains disseminated throughout the sample. Pyrite, if present, is forming subhedral to euhedral prismatic grains throughout the conglomerate. Barite is occurring in some conglomerates as veinlets and in others as radial intergrowths with hematite.

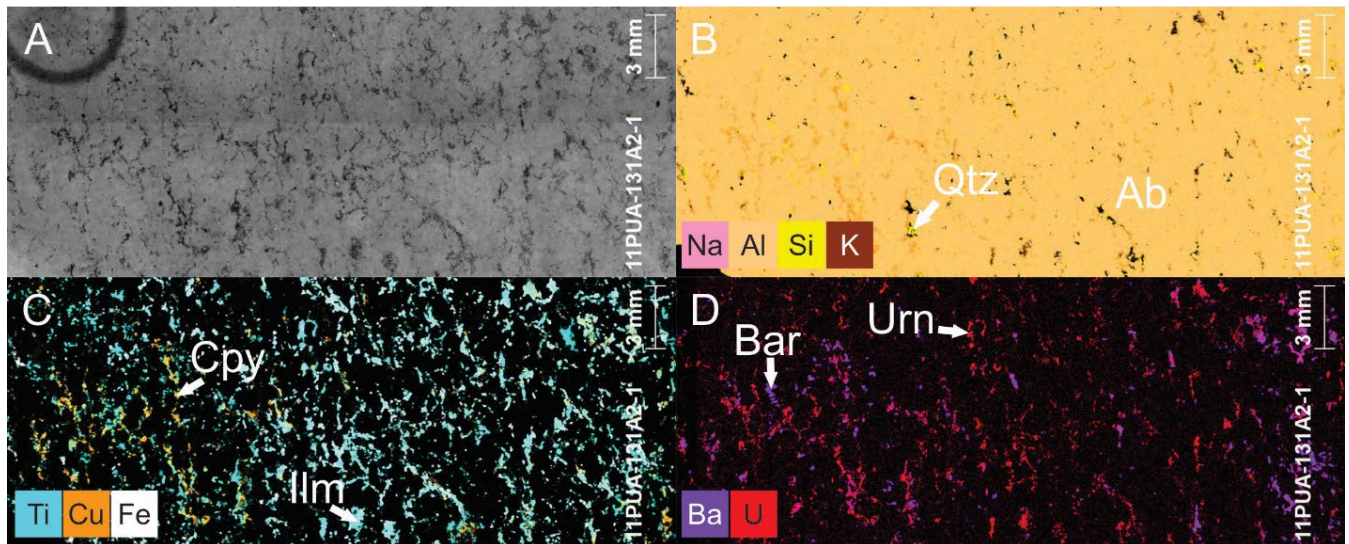


Figure 15: False colour micro-XRF elemental distribution maps of a conglomerate with minor uranium mineralization for sample 11PUA-131A2-1. A) Image of sample, a polymictic conglomerate. B) Matrix of albite, microcline, and quartz. Albite is shown by the high Na content, microcline by the areas with high K, and the grains of quartz are indicated by the high Si content. C) Chalcopyrite (high Cu), ilmenite (high Ti & Fe), and hematite (high Fe) throughout matrix of conglomerate. D) Disseminated uraninite, indicated by the high U, and barite, shown by the concentrations of high Ba. Mineral abbreviations are as follows: Ab = albite, Bar = barite, Cpy = chalcopyrite, Ilm = ilmenite, Urn = uraninite.

5.2. Uranium Mineral Chemistry

Analysis of uranium minerals using EDS was completed to identify the uranium mineral phases for the Lac Cinquante deposit. Following EDS, the corresponding data (Appendix E) was recalculated to atomic % and plotted on a series of ternary diagrams (U-Si-Ti, U-Si-Ca, U-Ca-Fe, U-Ca-Ti) to classify the uranium phases. The four following uranium phases were identified: uraninite, brannerite, uranophane, and coffinite (Figure 16A&B). Uraninite and brannerite are recognized as being vein-hosted and are described in detail in section 5.1. In addition to the vein-hosted uranium phases, coffinite and uranophane are also occurring at the LC deposit as alteration products of uraninite (Figure 16C). Since Ca and Si cations can substitute in for the U^{4+} site in the uraninite structure, this can lead to the eventual formation of alteration minerals, such as coffinite and uranophane (Kyser et al., 2005).

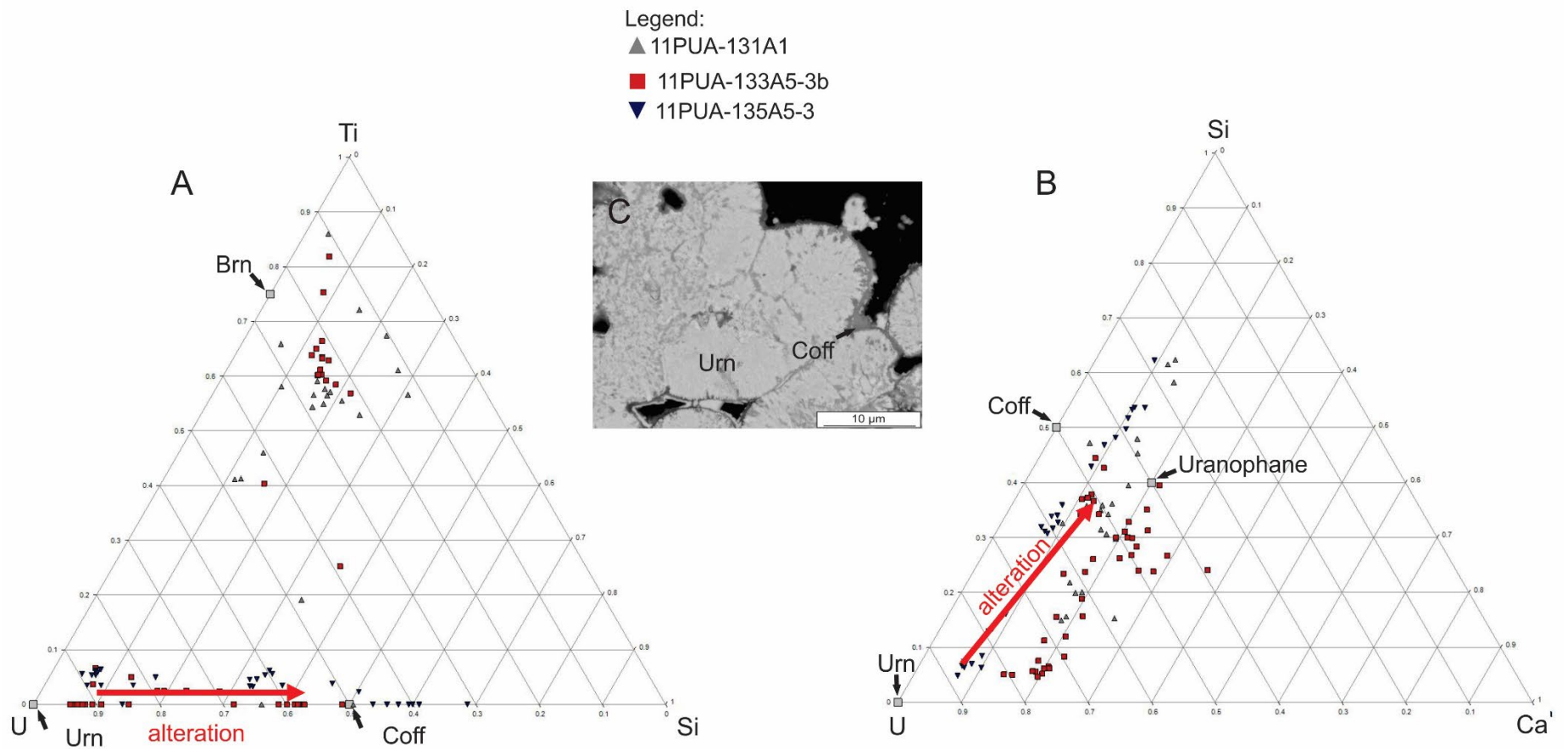


Figure 16: U-Ti-Si & U-Si-Ca ternary plots of uranium phases and BSE image of uranium phases for samples 11PUA-131A1 (conglomerate), 11PUA133A5-3b (tuff), and 11PUA-135A5-3 (tuff). A) U-Ti-Si ternary plot showing mineralization with ideal location of Urn, Brn, and Coff plotted. Samples plot near ideal location of Urn and Brn. Alteration of Urn to Coff is shown. B) U-Si-Ca ternary plot showing ideal locations of Urn, Coff, and uranophane plotted. Samples plot near ideal locations of Urn. Alteration of Urn towards Coff and uranophane is also demonstrated in this plot. C) BSE image shows Urn alteration to Coff along edges of grain boundary.

5.3. Laser Ablation Inductively Coupled Plasma Mass Spectrometry

Trace element compositions of 151 points of uraninite are listed in Appendix F. Rare earth element concentrations were normalized to chondrite (McDonough & Sun, 1995) and reveal four distinct profiles for the uraninite at the Lac Cinquante deposit. The mineralogically simple vein-hosted uraninite (vein-hosted uranium \pm pyrite, chalcopyrite, molybdenite, sphalerite, and galena) shows two distinct patterns (Figure 17 A, B). Thirty-two point-analyses over four samples comprise the first pattern (Figure 17A). The texture of uraninite of pattern 1 differs slightly from the uraninite of pattern 2, in that it consists of larger and thicker veins ($\sim 750 \mu\text{m}$) (Figure 10D). The pattern is steeply left leaning considering there is an enrichment in LREE/HREE ($C_{\text{eN}}/Y_{\text{bN}} = 27$). The Eu anomaly for this pattern is negligible ($\text{Eu}_{\text{N}}/\text{Eu}^* = 0.97$) and the $\Sigma\text{REE} = 660 \pm 31$ ppm.

The second pattern for the mineralogically simple vein-hosted uraninite is shown in Figure 17B. The uraninite from these samples forms thin ($\sim 50 \mu\text{m}$) veinlets (Figure 9F). The abundances of REEs in uraninite normalized to chondrite exhibit a rather flat lying without the enrichment in LREE/HREE seen in the above plot. This pattern is composed of 16 point-analyses between two samples and yields average $C_{\text{eN}}/Y_{\text{bN}} = 0.78$, indicating a slight enrichment in HREE with respect to LREE and no significant Eu anomaly with a value of $\text{Eu}_{\text{N}}/\text{Eu}^* = 1.0$ and $\Sigma\text{REE} = 240 \pm 11$ ppm.

The mineralogically complex vein-hosted uraninites, where vein-hosted uranium occurs with zircon, brannerite, barite, chalcopyrite, pyrite, molybdenite, sphalerite, and galena, have a very distinct pattern that is fairly flat-lying with a prominent positive Eu anomaly when normalized to chondrite (McDonough & Sun, 1995) (Figure 17C). A total of 100 point-analyses over four samples yield average $C_{\text{eN}}/Y_{\text{bN}} = 2.5$, demonstrating a slight enrichment in

LREE/HREE. The prominent positive Eu anomaly is calculated to a ratio of $\text{Eu}_N/\text{Eu}^* = 3.2$ and total REEs are $\Sigma 99 \pm 4.7$ ppm.

A single sample with disseminated uraninite and associations of hematite, chalcopyrite, pyrite, and galena was analysed at three different uraninite grains and resulted in a very distinct REE profile (Figure 17D) than the other three patterns discussed above. There is a lower abundance of total REEs compared to all other uraninite analysed ($\Sigma \text{REE} = 14 \pm 0.069$ ppm), but there is also a significant depletion of MREEs with respect to LREEs and HREEs. Additionally, there is a slight negative Eu anomaly: $\text{Eu}_N/\text{Eu}^* = 0.76$. The uraninite in this sample has a slight enrichment in LREE/HREE with a $\text{Ce}_N/\text{Yb}_N = 2.4$.

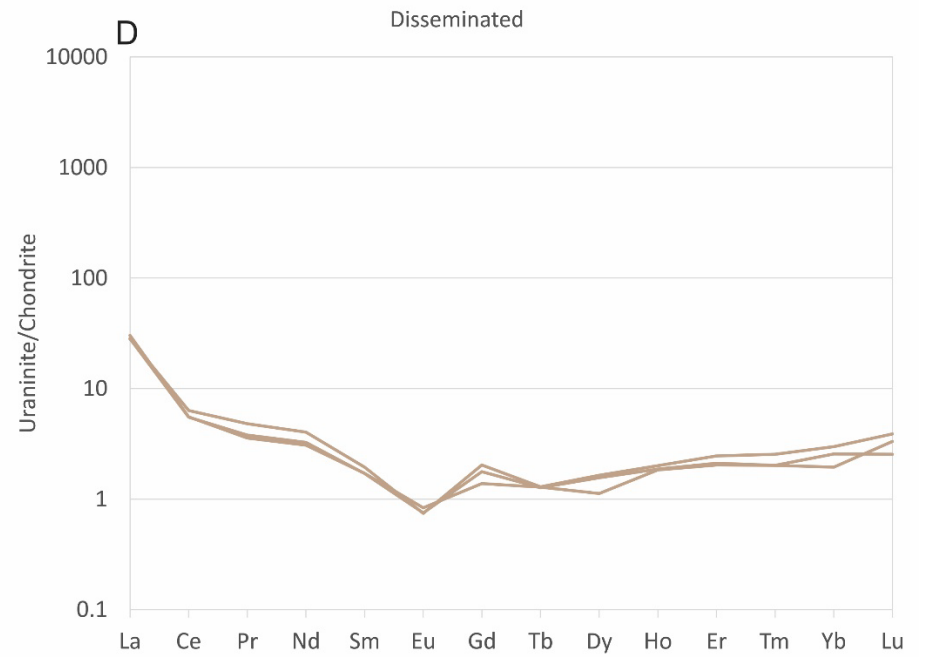
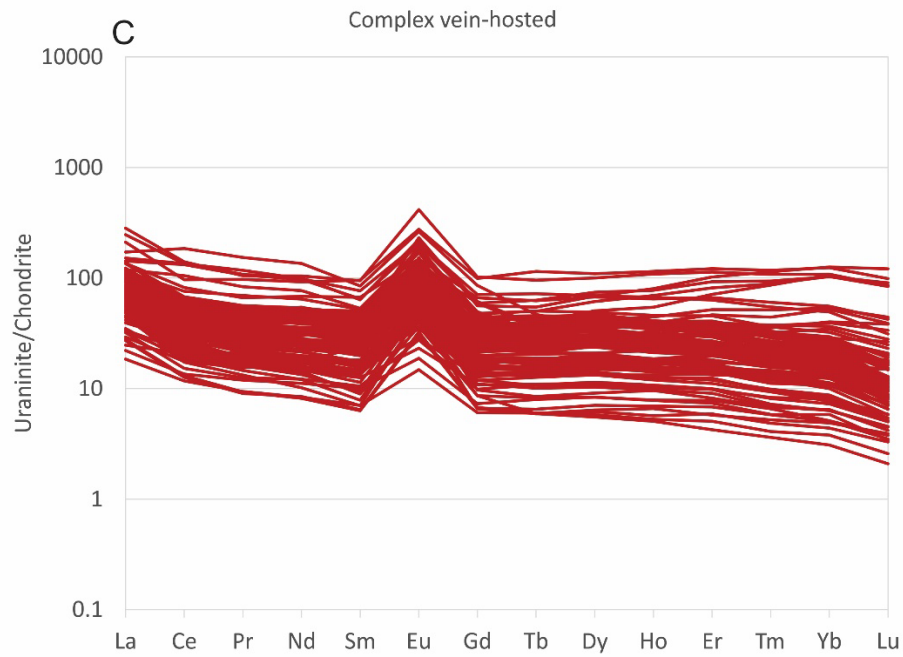
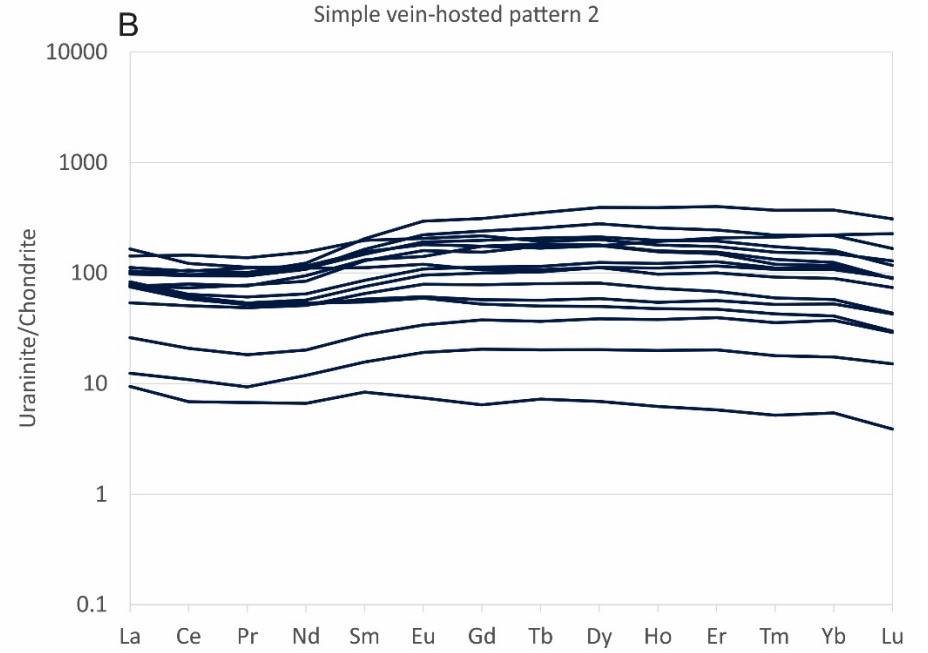
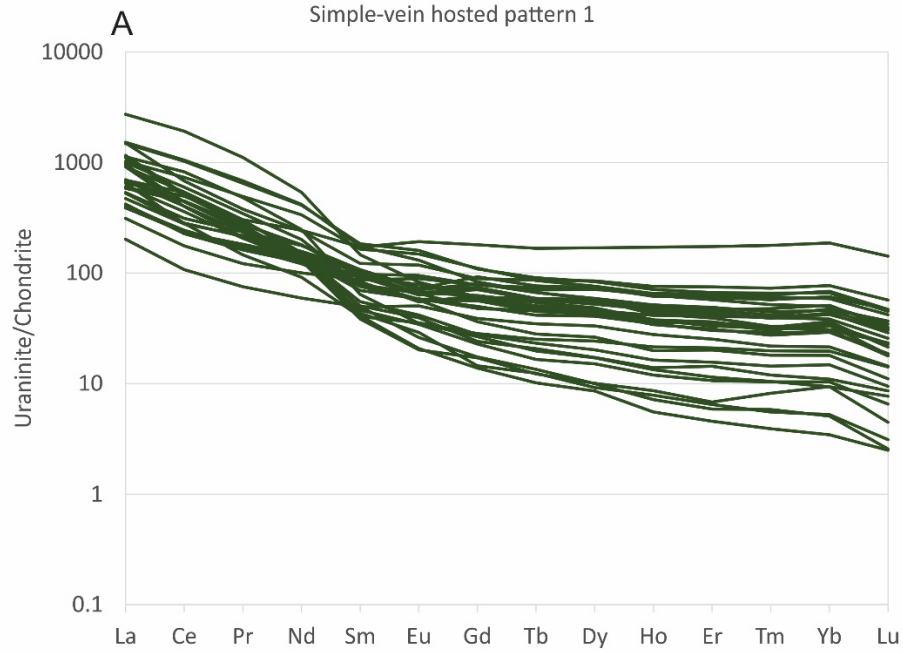


Figure 17: REE abundances in uraninite, normalized to chondrite (McDonough & Sun, 1995). A) Simple vein-hosted Urn pattern 1 of samples 11PUA-135A4-6, 11PUA-135A5-2, 11PUA-135A5-3, 11PUA-135A5-6. B) Simple vein-hosted uraninite pattern 2 of samples of samples 11PUA-134A2-1, 11PUA-134A2-3. C) Complex vein-hosted uraninite of samples 11PUA-133A5-3a, 11PUA-133A5-3a_1, 11PUA-133A5-3b, 11PUA-133A5-1, 11PUA-133A5-2. D) Disseminated uraninite of sample 11PUA-136A5-1.

In addition to LA-ICP-MS analysis of uraninite, brannerite was also analysed with two different samples corresponding to a total of sixteen point-analyses. There are two slightly different patterns that emerge when the REE abundances in brannerite are plotted after being normalized to chondrite (McDonough & Sun, 1995). The first pattern exhibits a slight, positive Eu anomaly (Figure 18A); notably, this anomaly is not as significant as the Eu anomaly in the uraninite, with a value of $Eu_N/Eu^* = 1.3$. This REE profile also has a slight enrichment of LREE/HREE as evidenced by $Ce_N/Yb_N = 5.6$, which is more of an enrichment than the uraninite hosted within the complex veins. The total enrichment in REEs is $\sum REE = 130 \pm 3.1$ ppm. The second pattern (Figure 18B) differs from the aforementioned REE profile because it has a slight negative Eu anomaly, where $Eu_N/Eu^* = 0.90$. This pattern has a similar enrichment in LREE with respect to HREE compared to pattern 1 in the brannerite profiles, because $Ce_N/Yb_N = 7.0$. The total enrichment in REEs for this pattern is $\sum REE = 150 \pm 3.3$ ppm.

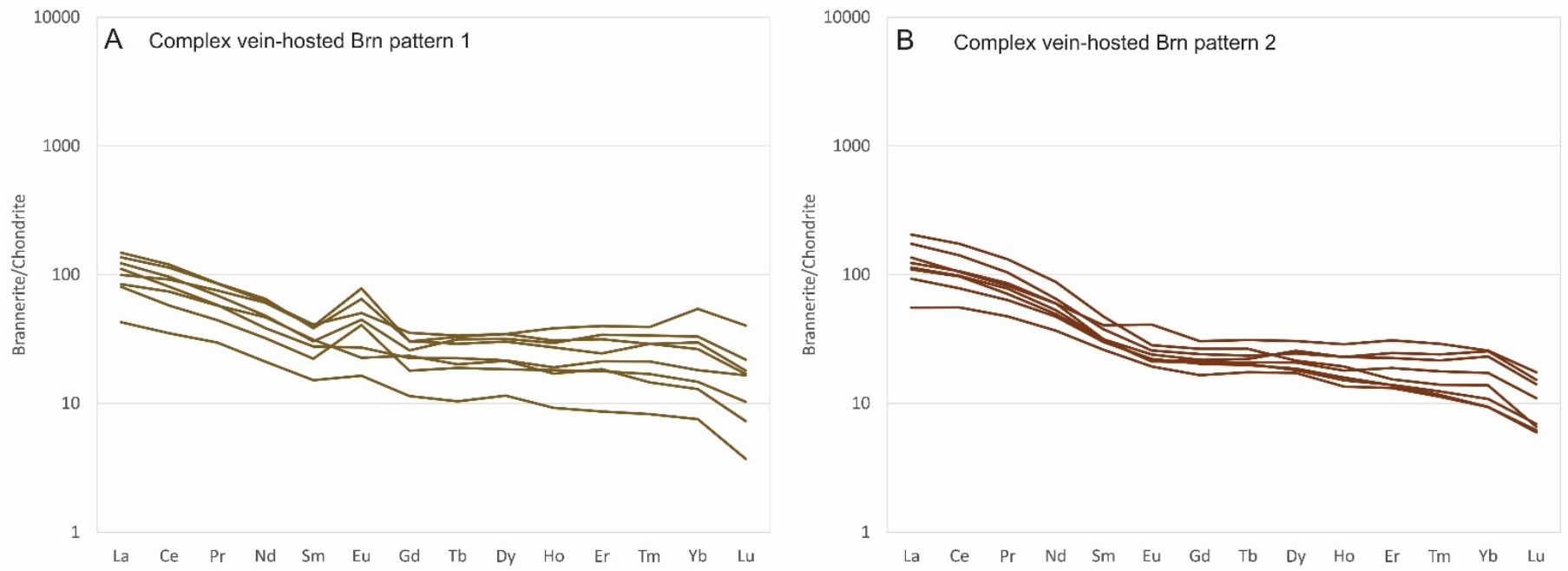


Figure 18: REE abundances in brannerite, normalized to chondrite (McDonough & Sun, 1995) for samples 11PUA-133A5-3a (tuff) and 11PUA-133A5-3b (tuff). A) Complex vein-hosted brannerite pattern 1. B) Complex vein-hosted brannerite pattern 2.

Trace element abundances (ppm) in uraninite and brannerite were plotted using box and whisker diagrams by type based on REE patterns (Figure 19, Figure 20). The uraninite shows high concentrations of HFSEs, such as Zr (8700 ± 8700 ppm) and Ti (5600 ± 14000 ppm) and LILEs, such as Ba (84 ± 180 ppm) and Sr (240 ± 210 ppm) (Figure 19). High Y (57 ± 78 ppm) is found in the uraninite at the LC as well. The uraninite also shows very low Th, with mean value $Th = 2.4 \pm 5.8$ ppm, however the abundance of this element is variable between the four styles of mineralization, and ranges from 0.017 ppm in the disseminated uraninite to 9.4 ppm in the simple vein-hosted pattern 1 uraninite (Figure 19). The disseminated uraninite is chemically distinct from the other two types of uranium mineralization. It has a higher overall content of Ba (410 ± 63 ppm) than the other styles of uranium mineralization (78 ± 180 ppm) but has lower concentrations of every other element.

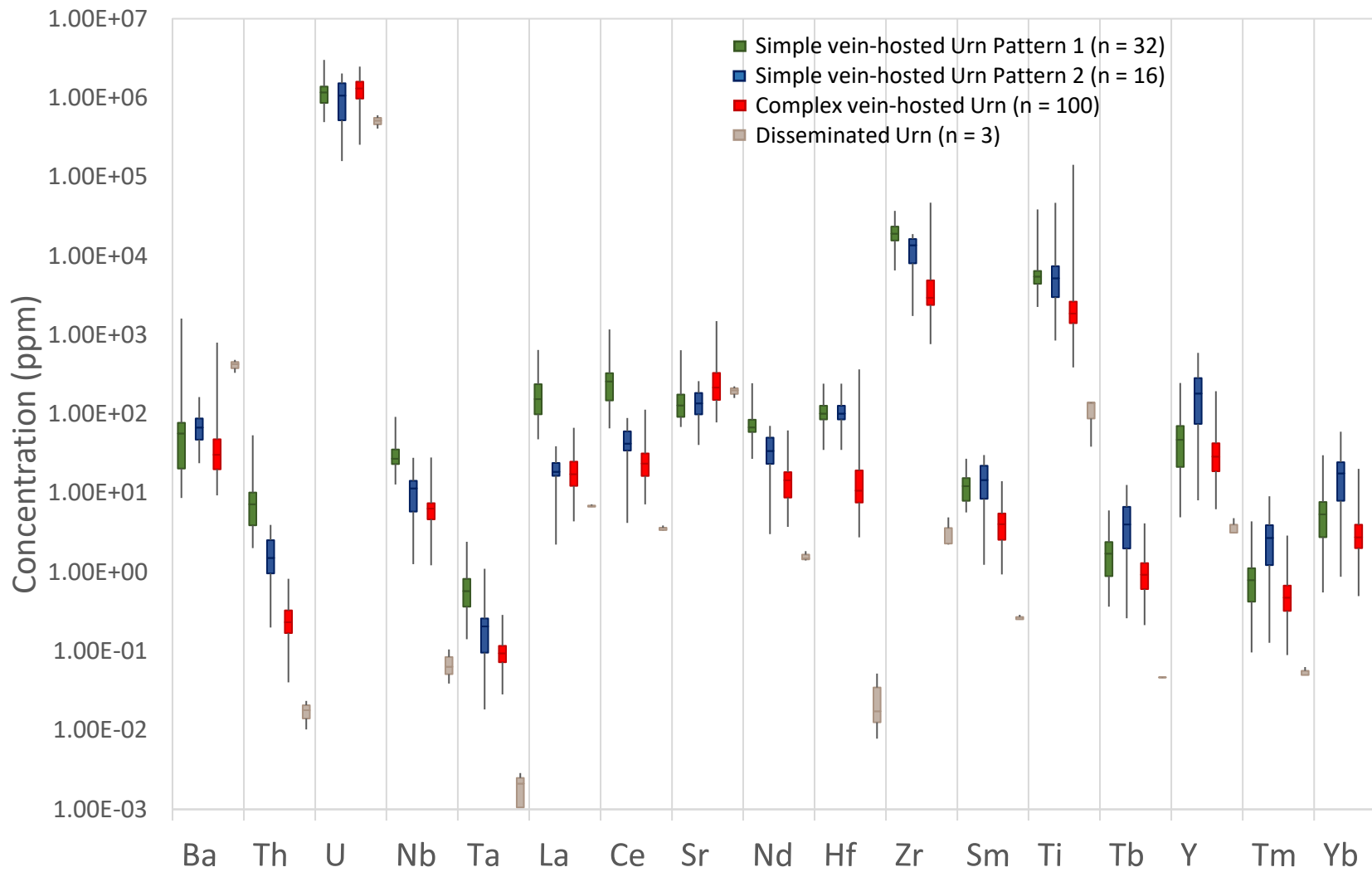


Figure 19: Trace element abundances (ppm) in uraninite.

Plotting the trace element abundances for brannerite (Figure 20) reveals an enrichment in Ba in the brannerite for both samples with the mean Ba = 930 ± 190 ppm. There is also a high concentration of Zr (8400 ± 3500 ppm). Similar to the uraninite, there is an enrichment in Sr (1600 ± 320 ppm). Thorium and Ta tend to be low in the brannerites Th = 0.060 ± 0.028 ppm and Ta = 0.53 ± 0.19 ppm.

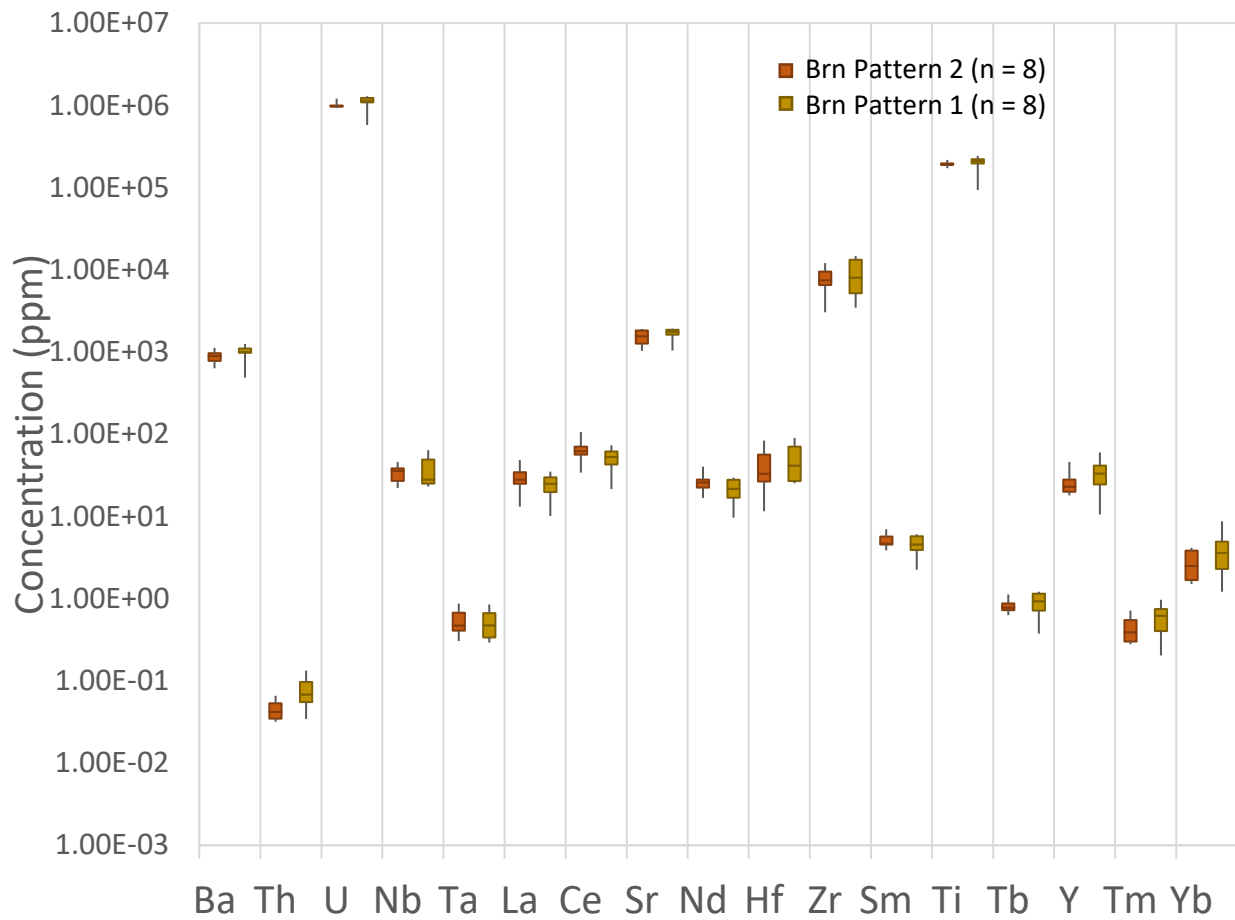


Figure 20: Trace element abundances (ppm) in brannerite.

Chapter 6 – Discussion

6.1. Paragenesis

This research indicates the first stage in the paragenetic sequence is the host rock formation with relict microcline, muscovite, plagioclase, quartz, apatite, and Ti-oxides (Figure 6). Bridge et al. (2013) reported a very different mineralogical assemblage for the host rocks that consists of plagioclase, diopside, hornblende, and chlorite with sulfides, minor graphite \pm biotite, \pm carbonate, \pm hematite, and classified the units as mafic tuff. The samples studied during this research appeared to be more felsic in composition and did not include the Ca-rich plagioclase (An₅₀₋₇₀) and hornblende described by Bridge et al. (2013). Bridge et al. (2013) did note interlayered felsic rocks with the mafic volcanics that have a mineral assemblage consisting of plagioclase, microcline, and quartz, and this unit seems to better match the observed host rocks of this study. The paper by Miller et al. (1986) reported the mineralized tuff zone as dominated by fine-grained quartz, chlorite, graphite, sericite-muscovite, sulfides (pyrite, chalcopyrite, and sphalerite) and minor carbonate. Findings from Miller et al. (1986) differ from Bridge et al. (2013) and are more similar to what this research has reported (quartz, muscovite).

This study indicates that pervasive albitization followed the formation of the host rock, replacing the majority of the initial mineral assemblage by fine-grained albite. Past research by Bridge et al. (2013) has simply reported the albitization of plagioclase as a result of minor alteration of hanging wall basalts amongst the more pervasive carbonate alteration (see section 2.4). On the other hand, the presence of albite has been explained by Miller et al. (1986), as part of the greenschist facies metamorphic mineral assemblage because of its occurrence with other index minerals such as chlorite and epidote. However, the rocks of this study do not contain metabasite index minerals such as actinolite, and epidote, apart from chlorite and albite. This

may indicate the host rocks are not mafic tuffs but are more felsic in composition (indicated by the microcline and quartz), and the greenschist metamorphic assemblage would therefore include albite and chlorite. A second possibility is the complete overprinting and replacement of the greenschist assemblage by albite from pervasive Na-metasomatism. Regardless of host rock composition and metamorphism, this study has shown by micro-XRF false colour elemental distribution maps coupled with petrography that pervasive albitization pre-dates the ore-phase based on cross cutting relationships (Figure 8, Figure 9).

The ore forming phase is subdivided into three styles of uranium mineralization: i) mineralogically simple vein-hosted uraninite + Cu-Fe-Mo-Pb sulfides in calcite and/or albite veins, ii) complex vein-hosted uraninite + brannerite + hydrothermal zircon \pm Cu-Fe-Mo-Pb sulfides, barite, fluorapatite in calcite and/or albite veins, and iii) disseminated uraninite \pm Cu-Fe sulfides, hematite in albitized host rock. The simple veins of uraninite are mineralogically distinct from the complex veins, lacking the brannerite, hydrothermal zircon, barite, and apatite. However, the LA-ICP-MS data shows similar enrichment in Zr, Ti, and Ba abundances within both uraninites (Figure 14). This is indicative of HFSE (Zr, Ti) mobility in the mineralizing fluids, suggesting the fluids that transported these usually immobile elements were likely high in F required for their mobility. Published research has shown that fluorine complexes increase the mobility of zirconium and consequently the formation of hydrothermal zircon (Taylor et al., 1989, Rubin et al., 1989, Rubin et al., 1993, Salvi et al., 2000). Finally, the disseminated uraninite is interpreted to have infiltrated the host rock due to the increase in porosity and permeability associated with albitization of the host rock. The occurrence of disseminated uraninite was also reported by Miller et al. (1986), who associated the mineralization with pervasively hematized and chloritized wall rocks. Comparing to past work done on this deposit,

the discovery of the high Ti, Zr, Ba, and P within the mineralizing fluids to the extent of saturating hydrothermal zircon, brannerite, barite, and fluorapatite within the complex ore veins has not been previously documented. Therefore, this merits a new interpretation of the LC deposit as more than a “mineralogically simple-vein hosted uranium deposit” (Bridge et al., 2013).

Finally, the samples have an extensive history of post ore alteration facing pervasive carbonatization, chloritization, and hematization. The age relationships of the chloritization and hematization at this deposit are unclear, however the pervasive carbonatization clearly post-dates the albitization. Past authors have also noted heavy alteration to carbonate, chlorite, and hematite (Miller et al., 1986, Bridge et al., 2013).

6.2. Classification of deposit type

This study has demonstrated that there are three styles of uranium mineralization occurring in mineralogically simple veins, complex veins, and disseminated in albitized host rock. Past research by Miller et al. (1983) considered the LC deposit a vein-type hydrothermal U + Pb + Mo + Ag + Cu ± Zn deposit with a complex elemental signature. Bridge et al. (2013) characterized this deposit as a mineralogically simple-vein hosted uranium deposit with an assemblage of uraninite + quartz, carbonates, chlorite, hematite ± molybdenite, pyrite chalcopyrite, Cu, Ag.

This study aims to reassess the classification of this deposit as vein-hosted by previous authors. The definition of a vein-hosted deposit (described in detail in section 2.1) is very broad, and the genetic model is poorly constrained and simply refers to the geometry of the mineral occurrence with a spatial association to a granitic body (IAEA, 2009). Considering the occurrence of the uranium mineralization at this deposit, the simple-vein hosted uraninite at the

LC exhibits a REE profile similar to that of a granite-sourced hydrothermal vein-type deposit with the characteristically highly fractionated pattern ($LREE/HREE > 1.0$), but is lacking a negative Eu anomaly (Figure 21) (Mercadier et al., 2011, Frimmel et al., 2013). Additionally, the LC uraninite is hosted within veins and is formed at relatively low temperature (230 – 350°C) (Bridge et al., 2013), which is consistent with the low temperatures typical of vein-hosted deposits (Cuney, 2009). However, the temperatures determined by Bridge et al. (2013), are related to retrograde chlorite formation, and therefore may be lower than the temperature of the mineralizing fluids. Despite the few similarities with LC and a vein-type deposit, there remain some inconsistencies with this classification. First, the mineralogy of this deposit is more complex with minerals such as brannerite, hydrothermal zircon, barite, and apatite that are atypical of a vein-hosted deposit. Furthermore, the geochemistry of this deposit includes high Zr, Ti, Ba, and Sr within ore minerals, suggesting high abundances of those elements within mineralizing fluids. When comparing to the vein-type systems of the Jachymov, Příbram, and Horní Slavkiv uranium districts these components are usually found in low abundance in uraninite, especially Zr that is mostly below detection limit (René et al., 2017, René et al., 2019).

Another possibility to consider is the classification of the LC deposit as a Na-metasomatic deposit, owing to the high abundance of albite both replacing the host rock and occurring within the mineralized veins (Figure 8, Figure 9). A comparison to various deposits and occurrences can be found in Table 1. According to the IAEA (2009), a metasomatic-type uranium deposit is defined as a uranium deposit that is related to alkaline Na- or K-metasomatites. “The metasomatites are developed in ancient shields with median masses, where they form stockworks controlled by long-lived ancient faults. Na-metasomatites are

predominantly albite in composition usually with minor carbonate and alkaline amphiboles and pyroxenes” (IAEA, 2009).

Na-metasomatic uranium deposits (also referred to as albitite-hosted uranium deposits) are poorly understood and poorly defined uranium deposits. Seemingly, the defining characteristic of Na-metasomatic related uranium is the association of uranium ores with albitites (Wilde, 2013). Micro-XRF elemental maps with various petrographic methods throughout this study have shown that the host rock has been significantly replaced by fine-grained albite. Past research has attributed the presence of albite and chlorite to greenschist facies metamorphism (Miller et al., 1986). Regardless, greenschist facies metamorphism and Na-metasomatism can occur in combination, as is the case at several uranium deposits worldwide, such as at the Valhalla deposit in Queensland, Australia (Polito et al., 2009) and the Gunnar deposit of the Beaverlodge uranium district in Saskatchewan, Canada (Dieng et al., 2015).

Structural controls are an important component to these systems with deposits typically occurring in brecciated, mylonitic zones of rock where fluid concentration can occur (Cuney et al., 2012, Wilde, 2013), such as the Gunnar deposit in Saskatchewan, Canada (Dieng et al., 2015), and the Aricheng South uranium occurrence in Guyana (Alexandre, 2010). Miller et al. (1986) reported that the uranium mineralization at the LC deposit has extensive fracturing and brecciation associated with a NW trending shear zone. Additionally, two major shear zones stretch across the Angikuni subbasin (Tulemalu shear zone and the eastern shear zone) (Aspler et al., 2000). These observations are consistent with the structural controls needed to concentrate fluids to form the albitites associated with these deposits.

A second observation that is consistent across many deposits is uranium mineralization that post-dates the albitization. As evidenced by the micro-XRF false colour elemental

distribution maps and petrographic observations (Figure 8, Figure 9), the albitization at LC predates the ore forming phase, which remains consistent with the paragenetic relationships recorded from many Na-metasomatic uranium deposits such as at the Aricheng South occurrence (Alexandre, 2010) and the Central Ukraine Uranium Province (Cuney et al., 2012). Furthermore, these deposits tend to have increased permeabilities and porosities from the early albitization that seem to be enhanced by dissolution of quartz and K-feldspar. The host rocks of these deposits typically reveal a major loss in SiO₂ and near complete removal of K₂O (Wilde, 2013). Although the samples at LC have seen an increase in permeability and porosity that is interpreted to have led to the formation of disseminations of uraninite, chalcopyrite, pyrite, and hematite and infilling of calcite and chlorite within the host rock, there is still a high abundance of quartz remaining with minor potassic phases, as shown in XRF false-colour elemental distribution maps (Figure 7, Figure 10, Figure 13).

Sodium-metasomatic deposits commonly host fluorapatite and hydrothermal zircon as evidenced by the Valhalla deposit (Polito et al., 2009) and Central Ukraine Province (Cuney et al., 2012), and large abundances of carbonate minerals are typical with these deposits (Wilde, 2013). There is usually a high content of Ti, and brannerite occurs in many of the deposits. Additionally, uranium mineralization is commonly associated with titanite, rutile, and ilmenite (Wilde, 2013). These mineralogical characteristics are identical to the LC, that hosts hydrothermal zircon (Figure 12E, I & J), apatite (Figure 12C), brannerite (Figure 12F, I & J), and Ti-oxides (Figure 12F) in the mineralogically complex veins with uranium mineralization and in surrounding host rock.

There are a few characteristics of this deposit that differ from Na-metasomatic related uranium deposits. The chondrite normalized REE profile of the LC simple vein-hosted pattern 2

uraninite does exhibit a slight enrichment in HREE/LREE (Figure 21B) which is similar to the REE profile of the Michelin deposit in Newfoundland, Canada (Figure 21F). However, all other REE profiles of the LC ore minerals are more similar to a hydrothermal vein-hosted system (Figure 21E) than Na-metasomatic due to their fractionated patterns, specifically simple vein-hosted pattern 1 (Figure 21). Additionally, the temperatures constrained by Bridge et al. (2013) at 230°C to 350°C are lower than the typical temperature range for Na-metasomatic related deposits at ~ 330°C to 380°C (Polito et al., 2009, Dieng et al., 2015, Cuney et al., 2012) (Table 1).

To conclude, the LC deposit formed at relatively low temperatures and the majority of the uranium minerals have a REE profile more similar to a vein-hosted deposit. However, this system is more mineralogically and geochemically complex than a granite related vein-hosted deposit and there are many similarities between the complex veins at the LC and other examples of Na metasomatic deposits (Table 1). These findings suggest the need to reclassify this deposit as Na-metasomatic, instead of vein hosted.

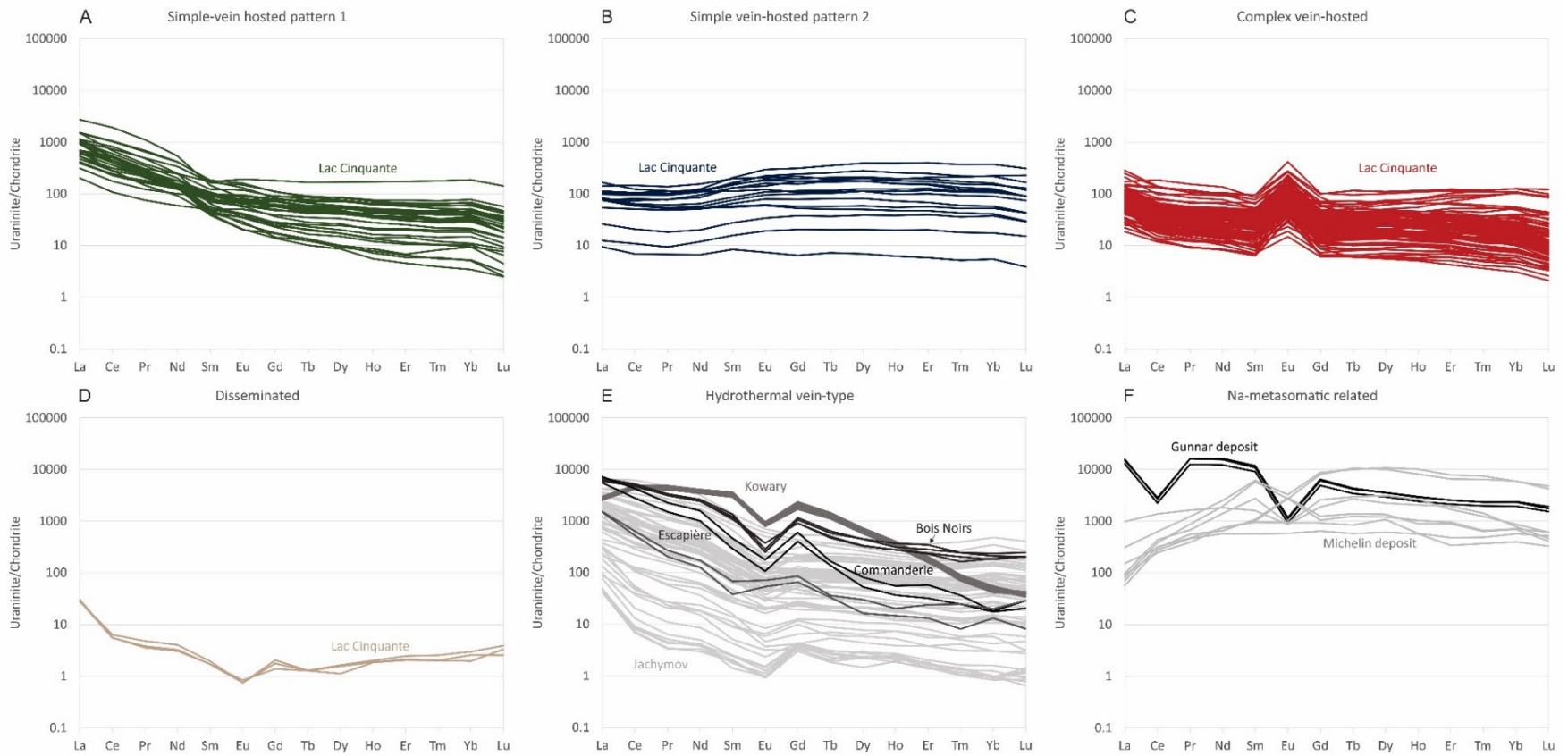


Figure 21: REE abundances of various uranium deposits, all normalized to chondrite (McDonough & Sun, 1995). A) to D) REE profiles of the uraninite at the LC deposit, data from this study. E) REE profiles of hydrothermal vein-type uraninite, modified from Mercadier et al. (2011) and Frimmel et al. (2013). F) REE profiles of Na-metasomatic related uraninite, modified from Dieng et al. (2015) and Duffet et al. (2020).

Table 1: Comparison of Lac Cinquante deposit to various uranium deposits.

Deposit	Lac Cinquante (Nunavut, Canada)	Aricheng South occurrence (northwestern Guyana)	Valhalla Deposit (Queensland, Australia)	Beaverlodge District: Gunnar Deposit (Northern Saskatchewan)	Central Ukraine Uranium Province	Beaverlodge District: Ace-Fay-Verna deposits (Northern Saskatchewan)
Classification of deposit	Na-metasomatic	Na-metasomatic	Na-metasomatic	Na-metasomatic	Na-metasomatic	Breccia type & vein-hosted
Basement rock (name, lithology, age)	No formal name. Archean metavolcanics with meta-tuff units	Not described	1900 Ma basement, name and lithology not described	Archean to late Paleoproterozoic basement granitoid and gneiss	Varies by deposit/occurrence	Donaldson Lake & Foot Bay gneisses
Metamorphism	Greenschist facies	None	Greenschist to amphibolite facies	Greenschist to amphibolite facies	Greenschist to amphibolite facies	Greenschist to amphibolite facies
Supracrustal rocks (name, lithology, age)	Dubawnt Supergroup that unconformably overly basement	Sedimentary units of the Paleoproterozoic Roraima Basin	1800 – 1668 Ma sedimentary and volcanic units of the Mount Isa Basin that unconformably overly basement	Unconformably overlain by Martin Lake basal conglomerates	Varies by deposit/occurrence	Unconformably overlain by Martin Lake basal conglomerates
Host rock (name, lithology, age)	No formal name. Archean meta-tuff units.	2.07 – 2.1 Ga Paleoproterozoic granodiorite of the Kurupung Batholith.	Strongly altered Paleoproterozoic metasediments and within the Leichhardt River Fault Trough.	Brecciated portions of albitized 2321 ± 3 Ma Gunnar granite	Paleoproterozoic gneisses, migmatites, and granites of the Ingul Megablock	Quartzite and conglomerates, phyllonite amphibolite, albite paragneiss, and granitic gneiss

Deposit	Lac Cinquante (Nunavut, Canada)	Aricheng South occurrence (northwestern Guyana)	Valhalla Deposit (Queensland, Australia)	Beaverlodge District: Gunnar Deposit (Northern Saskatchewan)	Central Ukraine Uranium Province	Beaverlodge District: Ace- Fay-Verna deposits (Northern Saskatchewan)
Structural controls	Extensive fracturing and brecciation associated with NW trending shear zone; mylonitic textures in metasediments	Uranium mineralization is occurring in two east/west trending fault breccia zones within the granodiorite and monzonite of the Kurupung Batholith.	Brecciated zones of host rock.	This deposit is sitting along the NW-SE trending St Mary's Channel fault, Fraser fault, and Zeemel fault merging with Fraser fault at ore body to form s broad zone of alteration and brecciation.	Most U deposits occur along N-S striking shear zones	These deposits are located along the Saint Louis Fault, striking NE. Ace & Fay orebodies are located in the footwall, the Verna orebody is hosted within the hanging wall in brecciated mylonites.

Deposit	Lac Cinquante (Nunavut, Canada)	Aricheng South occurrence (northwestern Guyana)	Valhalla Deposit (Queensland, Australia)	Beaverlodge District: Gunnar Deposit (Northern Saskatchewan)	Central Ukraine Uranium Province	Beaverlodge District: Ace- Fay-Verna deposits (Northern Saskatchewan)
Mineralogical assemblage	Two styles: i)uraninite with brannerite, hydrothermal zircon, pyrite, chalcopyrite, molybdenite, sphalerite, and galena within albite and calcite. ii) uraninite, pyrite, chalcopyrite, molybdenite, sphalerite, galena in calcite or albite.	Pre-ore alteration (chlorite): minor uraninite, magnetite, rutile, calcite, and chlorite. Early ore stage (calcite stage): Uraninite, and calcite within narrow fractures within albite or calcite. Trace rutile. Rare galena, monazite and small amounts of barite, thorite, and a Sr-Bar sulfate. Main ore stage: brannerite & hydrothermal zircon.	Early stage: Uncommon trace amounts of early disseminated uraninite and brannerite. Magnetite is disseminated as well. Main mineralization stage: Brecciated clasts cemented by brannerite, apatite, zircon, albite, reibeckite, calcite ± hematite. Late stage mineralization: Disseminated and vein- style uraninite in hematite, dolomite, calcite, chlorite, quartz, Pb-, Fe-, Cu- sulfide assemblage	Pitchblende occurring as small veinlets, breccia infillings, cavity infillings, fracture plane coatings, and disseminations throughout host albitized granite. Uraninite is occurring with chlorite, sericite, hematite, calcite, monazite, and titanite	U minerals (brannerite, uraninite, and U- ferropseudobrookite), apatite, andradite, carbonates, biotite, galena, native Pb, and hydrothermal zircon	Two styles: i) breccia-type ore with pitchblende, brannerite, coffinite, galena, quartz, calcite, chlorite, and pyrite, and ii) vein-type ore with pitchblende, brannerite quartz, calcite, chlorite, pyrite, chalcopyrite, galena, sphalerite, clausenthalite, and nolanite.

Deposit	Lac Cinquante (Nunavut, Canada)	Aricheng South occurrence (northwestern Guyana)	Valhalla Deposit (Queensland, Australia)	Beaverlodge District: Gunnar Deposit (Northern Saskatchewan)	Central Ukraine Uranium Province	Beaverlodge District: Ace- Fay-Verna deposits (Northern Saskatchewan)
Age of mineralization	Initial mineralization at 1828 ± 30 Ma. Remobilization dated to 1437 ± 5 Ma. Tectonic events caused resetting at 1260-1321 Ma, 895 Ma, 741-813 Ma, and 660-706 Ma	1995 ± 15 Ma	1551 ± 7 Ma to 1510 ± 15 Ma	2300 - 1850 Ma	1812 ± 42 Ma to 1753 ± 42 Ma	1850 - 1820 Ma
Formation temperatures	230 – 350°C	Pre-ore chlorite: 210 – 280° C, pre-ore carbonates: 250 – 350° C	340 – 380° C	315° C	340 – 370° C	330 - 315° C
Alteration	Pervasive albitization, hematization, chloritization, and carbonatization.	Chlorite and calcite with alteration of uraninite to coffinite, alteration of zircon, and minor alteration of magnetite to hematite and limonite.	Pre-ore alteration: albite, riebeckite, calcite, brannerite. Syn-ore alteration: brannerite, zircon, albite, riebeckite, calcite. Post-ore alteration: uraninite to coffinite, quartz, galena, pyrite, Cu-sulfides.	Chlorite, carbonate, specular hematite, and ilmenite.	Albitization, carbonatization, K-metasomatism, chloritization-epidotization	Albite, calcite, chlorite, hematite, and epidote with variable silicification.

Deposit	Lac Cinquante (Nunavut, Canada)	Aricheng South occurrence (northwestern Guyana)	Valhalla Deposit (Queensland, Australia)	Beaverlodge District: Gunnar Deposit (Northern Saskatchewan)	Central Ukraine Uranium Province	Beaverlodge District: Ace- Fay-Verna deposits (Northern Saskatchewan)
Deposit geochemistry (if reported)	Enrichment in Zr, Ti, Nb, Y, Ba, Sr of ores (uraninite and brannerite). Depletion of Th of ores (uraninite and brannerite). Enrichment in Rb, K, Ti of host rocks. Depletion in Th of host rocks.	Enrichment in Na, Ca, U, Hf. Depletion in K, Rb of host rocks.	Enrichment in Na, Ca, U, Zr, P, V, Y and Sr. Depletion in Si, K, Ba, Rb of host rocks.	High P ₂ O ₅ , Y ₂ O in ores (uraninite).	High Si, Ca in ores (brannerite). Low Th, REEs in ores (brannerite). Enrichment in Na, Ca, U, K, Sr, Zr, Hf, Ni, Co, Zn, Pb of host rocks. Depletion in Si, K, Rb of host rocks.	High MnO, Y ₂ O ₃ , SO ₃ , ThO, CaO, SiO ₂ , FeO, and TiO ₂ in ores (uraninite).
REE characteristics	Enrichment in LREE/HREE, negligible to positive Eu anomalies	Not analysed	Not analysed	Enrichment in LREE/HREE, negative Eu and Ce anomalies	Not analysed	Slight enrichment in LREE/HREE, slight negative Eu anomaly
References	This study, Miller et al. (1986), Bridge et al. (2013)	Alexandre, 2010	Polito et al., 2009	Dieng et al., 2015	Cuney et al., 2012	Dieng et al., 2015

6.3. Uranium source

The main objective of this study is to determine the origin of uranium for the LC deposit. Considering the REE pattern in uranium oxides is source controlled (Mercadier et al., 2011), the REE profiles of the LC will be compared to the two potential sources. The two suspected sources of uranium for the LC deposit are monazite, zircon, apatite, or exsolved fluids of the 1.85 – 1.79 Ga Hudson granites or the volcanic glass of, or fluids related to, the ultrapotassic volcanic rocks of the 1.83-1.81 Ga Christopher Island Formation. Ideally, a comparison would be made between the ore minerals and the trace elements of the minerals (apatite, zircon, monazite) that may be sourcing the uranium, however this data is unavailable in published literature and whole rock trace element data of the Hudson granites and CIF ultrapotassic minettes has been used to discriminate the source instead.

The mean REE profiles of the LC uraninite show four distinct patterns when normalized to chondrite (McDonough & Sun, 1995) (Figure 22A). Simple vein-hosted pattern 1 uraninite has a mean $\text{Eu}_N/\text{Eu}^* = 0.97$, simple-vein hosted pattern 2 uraninite has a $\text{Eu}_N/\text{Eu}^* = 1.01$, complex vein-hosted uraninite with $\text{Eu}_N/\text{Eu}^* = 3.2$ and disseminated $\text{Eu}_N/\text{Eu}^* = 0.76$ (Figure 22A). Both the simple vein-hosted patterns have nearly identical Eu anomalies to the CIF ($\text{Eu}_N/\text{Eu}^* = 0.97$) but are distinct from the Hudson granites with its more pronounced negative Eu anomaly ($\text{Eu}_N/\text{Eu}^* = 0.49$). The Eu anomaly of the complex vein-hosted is anomalously positive and much higher than both the CIF and the Hudson granites, suggesting high $\text{Eu}^{2+}/\text{Eu}^{3+}$ ratios (Figure 22C). The pronounced enrichment of Eu^{2+} in the complex vein-hosted uraninite is interpreted to be in part due to the albitization of the local mafic host rock in addition to the formation of apatite within veins. During crystallization of the local mafic host rocks, Eu^{2+} would have been preferentially fractionated into the Ca-rich plagioclase. Subsequent albitization

then released Eu^{2+} into the system. Furthermore, apatite coeval with uraninite formation is not geochemically compatible with Eu^{2+} and therefore will tend not to pull any Eu^{2+} out of the system, leaving the excess Eu^{2+} to fractionate into the uraninite, contributing to the positive Eu anomaly. The disseminated uraninite has a slight negative Eu anomaly and sits partway between the Hudson granite Eu anomaly and the CIF Eu anomaly. Overall, the REE profiles of the uraninite and brannerite at LC have negligible to positive Eu anomalies, which is most similar to the CIF. Additionally, the lack of a negative Eu anomaly, which is characteristic of uranium oxides from a granitic source i.e. the Hudson granites (Mercadier et al., 2011), further suggests the uranium is originating from the CIF.

In terms of LREE/HREE enrichments, the simple vein-hosted pattern 1 uraninite has a higher enrichment in LREE/HREE compared to all other patterns at LC but is lower than both the Hudson granites and CIF minettes (both $\text{Ce}_N/\text{Yb}_N \approx 55$). Despite the identical style of mineralization of the pattern 2 and pattern 1 uraninite (simple vein-hosted), pattern 2 exhibits a flat-lying profile and a slight depletion in LREE/HREE, typical of a mafic signature. Pattern 2 uraninite forms thin veinlets likely under lower fluid/rock ratios that are interpreted to have allowed for a higher contribution from the local mafic host rock, resulting in the flat-lying REE profile. In contrast, pattern 1 uraninite forms thick veins thus under high fluid/rock ratios and is thought to have had a high input of REEs from the mineralizing fluids and less input from the local mafic host rock, resulting in a pattern more similar to the source (Figure 22). The complex vein-hosted uraninite, brannerite, and disseminated uraninite have similar, and only slight enrichments in LREE/HREE and in comparison to the Hudson granites and CIF have much more flat-lying profiles. Another mineral forming coeval with uraninite within the complex veins is thought to have preferentially fractionated out the LREE-MREEs, such as apatite (Raimbault et

al., 1993), leaving that profile more depleted in these elements and correspondingly resulting in a less pronounced enrichment in LREE/HREE (Figure 22A, B) compared to the simple vein-hosted uraninites, Hudson granite, and CIF. The disseminated uraninite shows an interesting pattern, however this is thought to be a mixed analysis due to the fine-grained nature of this style of uraninite.

Analysis of trace elements within the LC uraninite and brannerite (Figure 22) show high abundances of Ba, Ti, Zr, and Sr. Although trace elements in the CIF and Hudson granites are similar (Figure 22D, E, F), the CIF is higher in Ba (5200 ± 2700 ppm), Ti (7100 ± 610 ppm), Zr (760 ± 48 ppm), and Sr (920 ± 350 ppm) compared to the Hudson granites Ba (1100 ± 520 ppm), Ti (1500 ± 610 ppm), Zr (250 ± 99 ppm), and Sr (290 ± 160 ppm). This makes the CIF a more likely source for the high Ba (84 ± 180 ppm), Ti (5600 ± 14000 ppm), Zr (8700 ± 8700 ppm), and Sr (240 ± 210 ppm) abundances found in the uraninite of the LC deposit. Although P was not included in the LA-ICP-MS analysis of the LC ore minerals, the system had to have been sufficiently saturated in P to mineralize apatite within the complex veins, suggesting high P in the fluids coming from the source. Spider diagrams show that the Hudson granites have a depletion in P when normalized to MORB, whereas the CIF is much higher in P (Figure 5), further suggesting the CIF was sourcing the uranium for the LC deposit.

Based on comparisons of the REE profiles and trace element abundances of the ore minerals at the Lac Cinquante deposit and the potential sources, the CIF is more consistent as the source for uranium and other components. The REE profile of the simple vein hosted pattern 1 uraninite at the LC deposit (Figure 22A, B, C) is more similar to the CIF, with nearly identical average Eu anomalies and fractionated patterns. Differences in REE patterns of complex veins can be explained by co-crystallizing phases. Additionally, most uranium oxides sourced from

granites exhibit a negative Eu anomaly (Mercadier et al., 2011), the lack of this anomaly in the LC ores further points to the CIF as a source as opposed to the Hudson granites. Furthermore, the CIF represents a better source for Ba, Ti, Zr, and P which could explain the enrichment of those elements in uraninite and brannerite as well as in the system as a whole to form brannerite, hydrothermal zircon and apatite. Considering uranium was sourced from the CIF, it is interpreted that CIF volcanism provided the heat necessary to drive hydrothermal circulation of mineralizing fluids that transported uranium from the CIF (or from exsolved fluids related to the CIF), where it was subsequently deposited in reducing conditions to form the uranium ore minerals of LC.

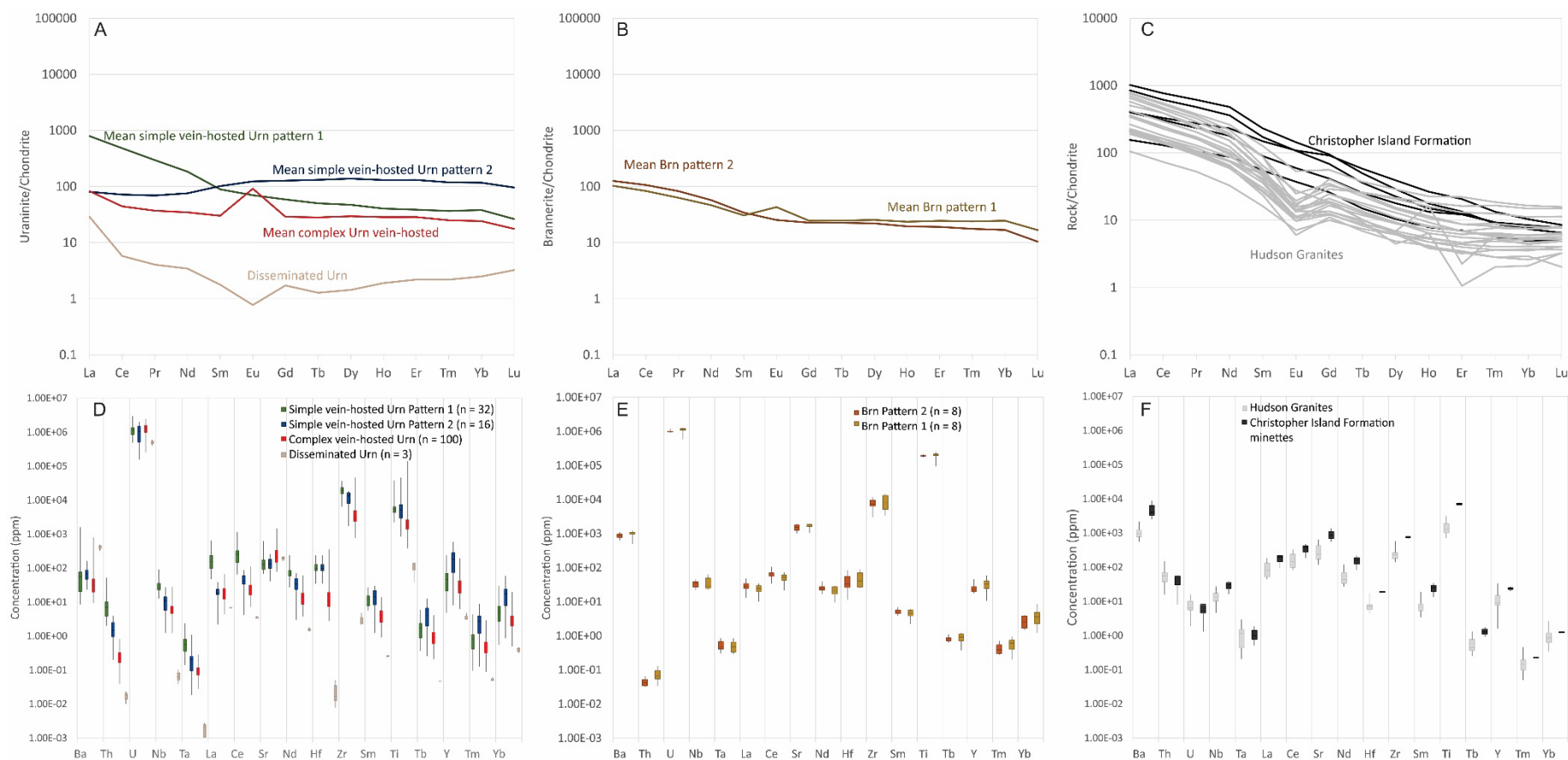


Figure 22: REE abundances and trace element abundances in uraninite, brannerite, Hudson granites, and Christopher Island Formation ultrapotassic minettes. The REE profiles are normalized to chondrite (McDonough & Sun, 1995). A) Mean REE profiles showing the abundances of REEs in the uraninite at LC. B) Mean REE profiles showing the abundances of REEs in the brannerite at LC. C) REE profiles showing the abundances of REEs in the Hudson granites and the Christopher Island Formation. D) Trace element abundances (ppm) of the uraninite at LC. E) Trace element abundances (ppm) of the brannerite at LC. F) Trace element abundances (ppm) of the Hudson granites and Christopher Island Formation ultrapotassic minettes.

6.4. Genetic model and implications for future exploration and research

Research by Aspler et al. (2000) suggested ~ 1.85 Ga Paleoproterozoic activity along the eastern shear zone and the Tulemalu shear zone in the Angikuni subbasin near the study area (Figure 2A). Additionally, Miller et al. (1986) described evidence of shearing in the deposit area, indicated by stretching of pillowed basalts and cataclastic textures. Active shearing in the deposit area at approximately 1.85 Ga would be consistent with the structural component needed to concentrate fluid flow for intense Na-metasomatism to occur. It has been shown throughout this study that Na-metasomatism pre-dates the ore forming phase at this deposit, therefore the 1.85 activity along the shear zones may have allowed fluids to circulate throughout the shear zone, leading to the albitization of the host rock, prior to the ore forming phase. However, this is merely speculation and further study to investigate the relationship between these structural components, metasomatism, and ore formation is highly recommended.

Geochronology (U-Pb) of the uranium mineralization at the LC has been dated by Bridge et al. (2013) and clusters around two ages: an initial mineralization event at 1.828 ± 29 Ga and 1.437 ± 31 Ga, interpreted to represent a resetting event. Considering the 1.833 – 1.811 Ga CIF (van Breeman et al., 2005) is the most likely source of uranium for this deposit, this implies the genetic model of the uranium deposit likely involved either the leaching of uranium from the volcanic glass of the ultrapotassic lavas, or uranium was sourced from fluids exsolved during the crystallization of the CIF. The emplacement of the CIF likely provided the heat to drive the hydrothermal circulation of the mineralizing fluids that transported uranium through fractures, faults, or shear zones until it precipitated as uraninite and brannerite in reducing conditions. Bridge et al. (2013) also reported draping of CIF flows across dipping strata as an indication of active faulting during the depositional period of the CIF. This is supported by Peterson et al.

(2002), who interpreted a series of normal faults forming a half graben system that was coeval with the deposition of the CIF. Additionally, petrogenetic studies indicate a genetic link between volcanism and faulting associated with basin initiation (Rainbird et al., 2003). As previously mentioned, activity along shear zones within the study area is also recorded near the time of deposition (Aspler & Chiarenzelli, 1996, Miller et al., 1986). Therefore, the interpretation is that minette magmas were derived from a reservoir of enriched upper mantle near the base of the crust (Cousens et al., 2001). Subsequently, the alkaline magmas were likely transported up through faults and shear zones that penetrated deep into the lithosphere (Rainbird et al., 2003). This may indicate the presence of pathways for concentrated fluid flow during the time of CIF intrusion and eruption and could imply uranium was easily transported through these faults and/or shear zones and was deposited. This finding has implications for uranium potential in other subbasins within the Baker Lake Basin that contain the CIF.

Due to the need for reclassification of this deposit, future exploration should focus on defining an alteration halo associated with the Na-metasomatism at this deposit to better constrain the distribution of uranium mineralization related to this alteration. Future research to better constrain the structural controls of the LC uranium could be helpful in understanding the movement of uranium and associated fluids during the Paleoproterozoic. Additional study on the fluid chemistry and more specifically the behaviour of HFSE (Zr, Ti) within the hydrothermal fluids in this system would be useful in deepening our understanding of this deposit. Further study could involve field examination of the CIF and the uranium distribution within the volcanic unit.

Chapter 7 – Conclusion

The Lac Cinquante uranium deposit has a complex mineralogical and geochemical signature. It is characterized by a high abundance in both HFSE (Zr, Ti) and LILE (Ba, Sr) in ore minerals (uraninite and brannerite) suggesting high mobility of rather immobile elements within mineralizing fluids. Mineralogically, this deposit consists of uraninite as the main ore-forming mineral associated with brannerite, hydrothermal zircon, apatite, barite, pyrite, chalcopyrite, molybdenite, and sphalerite. The abundance of HFSE and the presence of brannerite, hydrothermal zircon, and apatite within a pervasively albitized host rock is indicative of a Na-metasomatic related uranium deposit, therefore this study has indicated the need to reclassify this deposit as such. Furthermore, the concentrations of Zr, Ti, Sr, Ba in ores, as well as the abundance of P in the system to saturate apatite within the veins is indicative of the CIF as the source of the uranium since it is also high in these components. The chondrite normalized REE profiles of the ore minerals at LC have a negligible to positive Eu anomaly, is further supporting the CIF as the origin of uranium because uranium from a granitic source (Hudson granite) would have the characteristic negative Eu anomaly seen in the chondrite normalized REE profile of the Hudson granite. This discovery has implications for future uranium exploration in the Baker Lake Basin due to the widespread distribution of the CIF across many subbasins, and the potential for it to have sourced uranium deposits in other subbasins in the region.

Chapter 8 – References

- Alexandre, P. 2010. Mineralogy and geochemistry of the sodium metasomatism-related uranium occurrence of Aricheng South, Guyana. *Mineralium Deposita*, **45**: 351–367. doi:10.1007/s00126-010-0278-7.
- Alexandre, P., Kyser, K., Thomas, D., Polito, P., and Marlat, J. 2009. Geochronology of unconformity-related uranium deposits in the Athabasca Basin, Saskatchewan, Canada and their integration in the evolution of the basin. *Mineralium Deposita*, **44**: 41–59. doi:10.1007/s00126-007-0153-3.
- Alexandre, P., and Kyser, T.K. 2005. Effects of cationic substitutions and alteration in uraninite, and implications for the dating of uranium deposits. *The Canadian Mineralogist*, **43, Part 3**: 1005–1017. Mineralogical Association of Canada. doi:<https://doi.org/10.2113/gscanmin.43.3.1005>.
- Aspler, L.B., Chiarenzelli, J.R., Cousens, B.L., Davis, W.J., and MacLachlan, K. 2000. Archean rifted continental margin/back-arc basin and Archean to Paleoproterozoic transpression near the Snowbird tectonic zone at Angikuni Lake, western Churchill Province, Nunavut. *In GeoCanada 2000 Conference CD*, Calgary.
- Aspler, L.B., Chiarenzelli, J.R., Cousens, B.L., Rainbird, R.H., and Mustard, P.S. 2004. Fluvial, lacustrine and volcanic sedimentation in the Angikuni Sub-basin, and initiation of approximately 1.84-1.79 Ga Baker Lake Basin, western Churchill Province, Nunavut, Canada. *Precambrian Research*, **129**: 225–250. Elsevier. doi:<https://doi.org/10.1016/j.precamres.2003.10.004>.
- Aspler, L.B., Wisotzek, I.E., Chiarenzelli, J.R., Losonczy, M.F., Cousens, B.L., McNicoll, V.J., and Davis, W.J. 2001. Paleoproterozoic intracratonic basin processes, from breakup of Kenorland to assembly of Laurentia: Hurwitz Basin, Nunavut, Canada. *Sedimentary Geology*, **141–142**: 287–318. doi:[https://doi.org/10.1016/S0037-0738\(01\)00080-X](https://doi.org/10.1016/S0037-0738(01)00080-X).
- Berman, R.G., Davis, W.J., and Pehrsson, S. 2007. Collisional Snowbird tectonic zone resurrected; growth of Laurentia during the 1.9 Ga accretionary phase of the Hudsonian Orogeny. *Geology (Boulder)*, **35**: 911–914. Geological Society of America (GSA). doi:<https://doi.org/10.1130/G23771A.1>.
- Bons, P.D., Elburg, M.A., and Gomez-Rivas, E. 2012. A review of the formation of tectonic veins and their microstructures. *Journal of Structural Geology*, **43**: 33–62. doi:<https://doi.org/10.1016/j.jsg.2012.07.005>.
- Bostock, H.H., Van Breemen, O., and Loveridge, W.D. 1987. Proterozoic geochronology in the Taltson magmatic zone, NWT. *Radiogenic Age and Isotopic Studies: Geological Survey of Canada, Paper*,: 82–87.
- Bowring, S.A. 1985. U-Pb zircon geochronology of early Proterozoic Wopmay orogen, NWT Canada: an example of rapid crustal evolution. *Kansas Univ., Lawrence (USA)*.

- Bridge, N., Banerjee, N., Pehrsson, S., Fayek, M., Finnigan, C., Ward, J., and Berry, A. 2013. Lac Cinquante Uranium Deposit, Western Churchill Province, Nunavut, Canada. *Exploration and Mining Geology*, **21**: 27–50.
- Card, C.D., Bethune, K.M., Davis, W.J., Rayner, N., and Ashton, K.E. 2014. The case for a distinct Taltson orogeny: Evidence from northwest Saskatchewan, Canada. *Precambrian Research*, **255**: 245–265. doi:<https://doi.org/10.1016/j.precamres.2014.09.022>.
- Card, C.D., Bethune, K.M., Rayner, N., and Ashton, K.E. 2021. Tectonic significance of the Virgin River shear zone of the Canadian Shield and implications for the origin of the Snowbird tectonic zone of Laurentia. *Precambrian Research*, **361**: 106241. doi:<https://doi.org/10.1016/j.precamres.2021.106241>.
- Card, C.D., Pana, D., Portella, P., Thomas, D.J., Annesley, I.R., Jefferson, C.W., and Delaney, G. 2007. Basement rocks to the Athabasca basin, Saskatchewan and Alberta. *Bulletin-Geological Survey of Canada*, **588**: 69. MINISTER OF ENERGY, MINES AND RESOURCES CANADA.
- Chi, G., Ashton, K., Teng, D., Deru, X., Zenghua, L., Song, H., Liang, R., and Kennicott, J. 2020. Comparison of granite-related uranium deposits in the Beaverlodge District (Canada) and South China; a common control of mineralization by coupled shallow and deep-seated geologic processes in an extensional setting. *Ore Geology Reviews*, **117**: Article 103319. Elsevier. doi:<https://doi.org/10.1016/j.oregeorev.2020.103319>.
- Chi, G., Haid, T., Quirt, D., Fayek, M., Blamey, N., and Chu, H. 2017. Petrography, fluid inclusion analysis, and geochronology of the End uranium deposit, Kiggavik, Nunavut, Canada. *Mineralium Deposita*, **52**: 211–232. Springer.
- Cousens, B.L., Aspler, L.B., Chiarenzelli, J.R., Donaldson, J.A., Sandeman, H.A., Peterson, T.D., and LeCheminant, A.N. 2001. Enriched Archean lithospheric mantle beneath western Churchill Province tapped during Paleoproterozoic orogenesis. *Geology (Boulder)*, **29**: 827–830. Geological Society of America (GSA). doi:[https://doi.org/10.1130/0091-7613\(2001\)029<0827:EALMBW>2.0.CO;2](https://doi.org/10.1130/0091-7613(2001)029<0827:EALMBW>2.0.CO;2).
- Cuney, M. 2009. The extreme diversity of uranium deposits. *Mineralium Deposita*, **44**: 3–9. Springer-Verlag. doi:<https://doi.org/10.1007/s00126-008-0223-1>.
- Cuney, M. 2010. Evolution of uranium fractionation processes through time; driving the secular variation of uranium deposit types. *Economic Geology and the Bulletin of the Society of Economic Geologists*, **105**: 553–569. Economic Geology Publishing Company. doi:<https://doi.org/10.2113/gsecongeo.105.3.553>.
- Cuney, M. 2014. Felsic magmatism and uranium deposits. *Bulletin de la Societe Geologique de France*, **185**: 75–92. Societe Geologique de France. doi:<https://doi.org/10.2113/gssgfbull.185.2.75>.
- Cuney, M., Emetz, A., Mercadier, J., Mykchaylov, V., Shunko, V., and Yuslenko, A. 2012. Uranium deposits associated with Na-metasomatism from central Ukraine: A review of some of the major

- deposits and genetic constraints. *Ore Geology Reviews*, **44**: 82–106.
doi:<https://doi.org/10.1016/j.oregeorev.2011.09.007>.
- Cutts, J.A., Regis, D., Pehrsson, S.J., Graziani, R., Petts, D.C., Smit, M.A., and Knox, B. 2024. Circa 1.9 Ga Rae-Hearne collision from Lu–Hf garnet chronology in eclogites. *Terra Nova*, **n/a**. John Wiley & Sons, Ltd. doi:<https://doi.org/10.1111/ter.12709>.
- Dieng, S., Kyser, K., and Godin, L. 2013. Tectonic history of the North American shield recorded in uranium deposits in the Beaverlodge area, northern Saskatchewan, Canada. *Precambrian Research*, **224**: 316–340. doi:<https://doi.org/10.1016/j.precamres.2012.09.011>.
- Dieng, S., Kyser, K., and Godin, L. 2015. Genesis of multifarious uranium mineralization in the Beaverlodge area, northern Saskatchewan, Canada. *Economic Geology and the Bulletin of the Society of Economic Geologists*, **110**: 209–240. Economic Geology Publishing Company. doi:<https://doi.org/10.2113/econgeo.110.1.209>.
- Duffett, C.L., Potter, E.G., Petts, D.C., Acosta-Gongóra, P., Cousens, B.L., and Sparkes, G.W. 2020. The evolution of metasomatic uranium ore systems in the Kitts-Post Hill belt of the Central Mineral Belt, Labrador, Canada. *Ore Geology Reviews*, **126**: 103720. doi:<https://doi.org/10.1016/j.oregeorev.2020.103720>.
- Fayek, M., Harrison, T.M., Ewing, R.C., Grove, M., and Coath, C.D. 2002. O and Pb isotopic analyses of uranium minerals by ion microprobe and U–Pb ages from the Cigar Lake deposit. *Chemical Geology*, **185**: 205–225. doi:[https://doi.org/10.1016/S0009-2541\(01\)00401-6](https://doi.org/10.1016/S0009-2541(01)00401-6).
- Finch, R., Murakami, T., and Burns, P.C. 1999. Systematics and paragenesis of uranium minerals. *In* *Reviews in Mineralogy*. Mineralogical Society of America and Geochemical Society. Available from <https://login.library.smu.ca/login?url=https://www.proquest.com/scholarly-journals/systematics-paragenesis-uranium-minerals/docview/2361699529/se-2?accountid=13908>.
- Flowers, R.M., Bowring, S.A., and Williams, M.L. 2006. Timescales and significance of high-pressure, high-temperature metamorphism and mafic dike anatexis, Snowbird tectonic zone, Canada. *Contributions to Mineralogy and Petrology*, **151**: 558–581. doi:10.1007/s00410-006-0066-7.
- Frimmel, H.E., Schedel, S., and Brätz, H. 2014. Uraninite chemistry as forensic tool for provenance analysis. *Applied Geochemistry*, **48**: 104–121. doi:<https://doi.org/10.1016/j.apgeochem.2014.07.013>.
- Gibb, R.A., and Walcott, R.I. 1971. A precambrian suture in the Canadian shield. *Earth and Planetary Science Letters*, **10**: 417–422. doi:[https://doi.org/10.1016/0012-821X\(71\)90090-2](https://doi.org/10.1016/0012-821X(71)90090-2).
- Hanmer, S., Sandeman, H.A., Davis, W.J., Aspler, L.B., Rainbird, R.H., Ryan, J.J., Relf, C., and Peterson, T.D. 2004. Geology and Neoproterozoic tectonic setting of the central Hearne supracrustal belt, western Churchill Province, Nunavut, Canada. *Precambrian Research*, **134**: 63–83. Elsevier. doi:<https://doi.org/10.1016/j.precamres.2004.04.005>.

- Hanmer, S., Williams, M., and Kopf, C. 1995. Modest movements, spectacular fabrics in an intracontinental deep-crustal strike-slip fault: Striding-Athabasca mylonite zone, NW Canadian Shield. *Journal of Structural Geology*, **17**: 493–507. doi:[https://doi.org/10.1016/0191-8141\(94\)00070-G](https://doi.org/10.1016/0191-8141(94)00070-G).
- Hoffman, P.F. 1988. United plates of America, the birth of a craton; early Proterozoic assembly and growth of Laurentia. *Annual Review of Earth and Planetary Sciences*, **16**: 543–603. Annual Reviews. Available from <https://login.library.smu.ca/login?url=https://www.proquest.com/scholarly-journals/united-plates-america-birth-craton-early/docview/2359572850/se-2?accountid=13908>.
- Hoshino, M., Sanematsu, K., and Watanabe, Y. 2016. Chapter 279 - REE Mineralogy and Resources. *In Handbook on the Physics and Chemistry of Rare Earths*. Edited by B. Jean-Claude and P. Vitalij K. Elsevier. pp. 129–291. doi:<https://doi.org/10.1016/bs.hpcr.2016.03.006>.
- International Atomic Energy Agency. 2009. World Distribution of Uranium Deposits (UDEPO), with Uranium Deposit Classification, 2009 Edition. International Atomic Energy Agency.
- International Atomic Energy Agency. 2018. World Distribution of Uranium Deposits (UDEPO). IAEA-TECDOC-1843. International Atomic Energy Agency.
- Jefferson, C.W., Thomas, D.J., Gandhi, S.S., Ramaekers, P., Delaney, G., Brisbin, D., Cutts, C., Portella, P., and Olson, R.A. 2007. Unconformity-associated uranium deposits of the Athabasca Basin, Saskatchewan and Alberta. *Bulletin-geological survey of Canada*, **588**: 23. MINISTER OF ENERGY, MINES AND RESOURCES CANADA.
- Kopf, C.F. 2002. Archean and Early Proterozoic Events Along the Snowbird Tectonic Zone in Northern Saskatchewan, Canada. *Gondwana Research*, **5**: 79–83. doi:[https://doi.org/10.1016/S1342-937X\(05\)70891-1](https://doi.org/10.1016/S1342-937X(05)70891-1).
- Kouske, A.P., Suh, C.E., Ghogomu, R.T., and Ngako, V. 2012. Na-metasomatism and uranium mineralization during a two-stage albitization at Kitongo, northern Cameroon: structural and geochemical evidence. *International Journal of Geosciences*, **3**: 258. Scientific Research Publishing.
- Kraus, J., and Menard, T. 1997. A thermal gradient at constant pressure; implications for low-to medium-pressure metamorphism in a compressional tectonic setting, Flin Flon and Kiseeynew domains, Trans-Hudson Orogen, central Canada. *The Canadian Mineralogist*, **35**: 1117–1136. Mineralogical Association of Canada.
- Liang, R., Chi, G., Ashton, K., Blamey, N., and Fayek, M. 2017. Fluid compositions and P-T conditions of vein-type uranium mineralization in the Beaverlodge uranium district, northern Saskatchewan, Canada. *Ore Geology Reviews*, **80**: 460–483. doi:<https://doi.org/10.1016/j.oregeorev.2016.07.012>.
- MacLachlan, K., Davis, W.J., and Relf, C. 2005. U/Pb geochronological constraints on Neoproterozoic tectonism; multiple compressional events in the northwestern Hearne Domain, western Churchill

- Province, Canada. *Canadian Journal of Earth Sciences = Revue Canadienne des Sciences de la Terre*, **42**: 85–109. National Research Council of Canada. doi:<https://doi.org/10.1139/e04-104>.
- Martel, E., van Breemen, O., Berman, R.G., and Pehrsson, S. 2008. Geochronology and tectono-metamorphic history of the Snowbird Lake area, Northwest Territories, Canada; new insights into the architecture and significance of the Snowbird tectonic zone. *Precambrian Research*, **161**: 201–230. Elsevier. doi:<https://doi.org/10.1016/j.precamres.2007.07.007>.
- McDonough, W.F., and Sun, S. -s. 1995. The composition of the Earth. *Chemical Geology*, **120**: 223–253. doi:[https://doi.org/10.1016/0009-2541\(94\)00140-4](https://doi.org/10.1016/0009-2541(94)00140-4).
- Mercadier, J., Annesley, I.R., McKechnie, C.L., Bogdan, T.S., and Creighton, S. 2013. Magmatic and metamorphic uraninite mineralization in the western margin of the Trans-Hudson Orogen (Saskatchewan, Canada); a uranium source for unconformity-related uranium deposits? *Economic Geology and the Bulletin of the Society of Economic Geologists*, **108**: 1037–1065. Economic Geology Publishing Company. doi:<https://doi.org/10.2113/econgeo.108.5.1037>.
- Mercadier, J., Cuney, M., Lach, P., Boiron, M.-C., Bonhoure, J., Richard, A., and Anonymous. 2012. Origin of uranium deposits revealed by their rare earth element signature. *Mineralogical Magazine*, **76**: 2099. Mineralogical Society. Available from <https://login.library.smu.ca/login?url=https://www.proquest.com/scholarly-journals/origin-uranium-deposits-revealed-their-rare-earth/docview/2366483266/se-2?accountid=13908>.
- Miller, A.R. 1980. Uranium geology of the eastern Baker Lake basin, District of Keewatin, Northwest Territories, Canada. Available from http://inis.iaea.org/search/search.aspx?orig_q=RN:12632145.
- Miller, A.R., Stanton, R.A., Cluff, G.R., and Male, M.J. 1986. Uranium Deposits and Prospects of the Baker Lake Basin and Subbasins, Central District of Keewatin, Northwest Territories. *Uranium Deposits of Canada*, Evans, EL, Editor, Canadian Institute of Mining and Metallurgy, Special, **33**: 263–285.
- Padhi, A.K., Mukherjee, M.K., Tripathi, B.K., Pande, D., Bisht, B.S., and Sarkar, B.C. 2023. Polymetallic Uranium Mineralisation in Rohil, Rajasthan, Western India: Insights from Mode of Occurrences, Structural Controls, Alteration Geochemistry and Exploration. *Minerals*, **13**: 555. MDPI AG, Basel. doi:<https://doi.org/10.3390/min13040555>.
- Pehrsson, S.J., Berman, R.G., and Davis, W.J. 2013a. Paleoproterozoic orogenesis during Nuna aggregation: a case study of reworking of the Rae craton, Woodburn Lake, Nunavut. *Precambrian Research*, **232**: 167–188. Elsevier.
- Pehrsson, S.J., Berman, R.G., Eglington, B., and Rainbird, R. 2013b. Two Neoarchean supercontinents revisited: The case for a Rae family of cratons. *Precambrian Research*, **232**: 27–43. doi:<https://doi.org/10.1016/j.precamres.2013.02.005>.
- Peterson, T.D., van Breemen, O., Sandeman, H., Cousens, B., Ramo, O.T., Van Schmus, W.R., and Bettencourt, J.S. 2002. Proterozoic (1.85-1.75 Ga) igneous suites of the western Churchill Province; granitoid and ultrapotassic magmatism in a reworked Archean hinterland. *Precambrian Research*, **119**: 73–100. Elsevier. doi:[https://doi.org/10.1016/S0301-9268\(02\)00118-3](https://doi.org/10.1016/S0301-9268(02)00118-3).

- Qiu, L., Danping, Y., Ren, M., Cao, W., Shuangli, T., Qingyin, G., Liting, F., Junting, Q., Zhang, Y., and Yongwen, W. 2018. The source of uranium within hydrothermal uranium deposits of the Motianling mining district, Guangxi, south China. *Ore Geology Reviews*, **96**: 201–217. Elsevier. doi:<https://doi.org/10.1016/j.oregeorev.2018.04.001>.
- Raimbault, L., Baumer, A., Dubru, M., Benkerrou, C., Croze, V., and Zahm, A. 1993. REE fractionation between scheelite and apatite in hydrothermal conditions. *American Mineralogist*, **78**: 1275–1285.
- Rainbird, R.H., and Davis, W.J. 2007. U-Pb detrital zircon geochronology and provenance of the late Paleoproterozoic Dubawnt Supergroup; linking sedimentation with tectonic reworking of the western Churchill Province, Canada. *Geological Society of America Bulletin*, **119**: 314–328. Geological Society of America (GSA). doi:<https://doi.org/10.1130/B25989.1>.
- Rainbird, R.H., Hadlari, T., Aspler, L.B., Donaldson, J.A., LeCheminant, A.N., and Peterson, T.D. 2003. Sequence stratigraphy and evolution of the Paleoproterozoic intracontinental Baker Lake and Thelon basins, western Churchill Province, Nunavut, Canada. *Precambrian Research*, **125**: 21–53. Elsevier. doi:[https://doi.org/10.1016/S0301-9268\(03\)00076-7](https://doi.org/10.1016/S0301-9268(03)00076-7).
- Rainbird, R.H., Stern, R.A., Rayner, N., Jefferson, C.W., and Delaney, G. 2007. Age, provenance, and regional correlation of the Athabasca Group, Saskatchewan and Alberta, constrained by igneous and detrital zircon geochronology. *Bulletin-Geological Survey of Canada*, **588**: 193. MINISTER OF ENERGY, MINES AND RESOURCES CANADA.
- Ramaekers, P. 1990. Geology of the Athabasca Group (Helikian) in northern Saskatchewan. Saskatchewan Energy and Mines, Saskatchewan Geological Survey.
- Regan, S.P., Williams, M.L., Chiarenzelli, J.R., Grohn, L., Mahan, K.H., and Gallagher, M. 2017. Isotopic evidence for Neoproterozoic continuity across the Snowbird Tectonic Zone, western Churchill Province, Canada. *Precambrian Research*, **300**: 201–222. doi:<https://doi.org/10.1016/j.precamres.2017.07.022>.
- Rene, M., and Dolníček, Z. 2017. Uraninite, Coffinite and Brannerite from Shear-Zone Hosted Uranium Deposits of the Bohemian Massif (Central European Variscan Belt). *Minerals*, **7**: 50. MDPI AG, Basel. doi:<https://doi.org/10.3390/min7040050>.
- René, M., Dolníček, Z., Sejkora, J., Škácha, P., and Šrein, V. 2019. Uraninite, coffinite and ningyoite from vein-type uranium deposits of the Bohemian Massif (Central European Variscan Belt). *Minerals*, **9**: 123. MDPI.
- Riegler, T., Lescuyer, J.-L., Wollenberg, P., Quirt, D., and Beaufort, D. 2014. Alteration related to uranium deposits in the Kiggavik–Andrew Lake structural trend, Nunavut, Canada: New insights from petrography and clay mineralogy. *The Canadian Mineralogist*, **52**: 27–45. Mineralogical Association of Canada.
- Roddick, J.C., and Miller, A.R. 1994. An ^{40}Ar – ^{39}Ar age from the REE-enriched Enekatcha ultrapotassic intrusive suite and implications for timing of ultrapotassic magmatism in the central Churchill Province, Northwest Territories. *Geol. Surv. Can. Pap.*,: 69–74.

- Rout, D., Krishnamurthi, R., and Sinha, D.K. 2022. Mineralogy and paragenesis of the Meso-Proterozoic Rohil uranium deposit, North Delhi Fold Belt, Rajasthan, India. *Ore Geology Reviews*, **151**: 105204. doi:<https://doi.org/10.1016/j.oregeorev.2022.105204>.
- Rubin, J.N., Henry, C.D., and Price, J.G. 1989. Hydrothermal zircons and zircon overgrowths, Sierra Blanca Peaks, Texas. *American Mineralogist*, **74**: 865–869. Mineralogical Society of America.
- Rubin, J.N., Henry, C.D., and Price, J.G. 1993. The mobility of zirconium and other “immobile” elements during hydrothermal alteration. *Chemical Geology*, **110**: 29–47. doi:[https://doi.org/10.1016/0009-2541\(93\)90246-F](https://doi.org/10.1016/0009-2541(93)90246-F).
- Salvi, S., Fontan, F., Monchoux, P., Williams-Jones, A.E., and Moine, B. 2000. Hydrothermal mobilization of high field strength elements in alkaline igneous systems: evidence from the Tamazeght Complex (Morocco). *Economic Geology*, **95**: 559–576. Society of Economic Geologists.
- Sandeman, H.A., Hanmer, S., Davis, W.J., Ryan, J.J., and Peterson, T.D. 2004. Whole-rock and Nd isotopic geochemistry of Neoproterozoic granitoids and their bearing on the evolution of the central Hearne supracrustal belt, western Churchill Province, Canada. *Precambrian Research*, **134**: 143–167. Elsevier. doi:<https://doi.org/10.1016/j.precamres.2004.05.005>.
- Scott, J.M.J., Peterson, T.D., and McCurdy, M.W. 2012. U, Th, REE occurrences within Nueltin Granite at Nueltin Lake, Nunavut; recent observations. *Current Research - Geological Survey of Canada*,: 15. Geological Survey of Canada. doi:<https://doi.org/10.4095/289393>.
- Shabaga, B.M., Fayek, M., Quirt, D., Jefferson, C.W., and Camacho, A. 2017. Mineralogy, geochronology, and genesis of the Andrew Lake uranium deposit, Thelon Basin, Nunavut, Canada. *Canadian Journal of Earth Sciences*, **54**: 850–868. NRC Research Press.
- Shabaga, B.M., Fayek, M., Quirt, D., Jefferson, C.W., Ledru, P., Cuney, M., and Mercadier. 2021. Geochemistry and geochronology of the Kiggavik uranium deposit, Nunavut, Canada. *Mineralium Deposita*, **56**: 1245–1262. Springer-Verlag. doi:<https://doi.org/10.1007/s00126-020-01001-8>.
- Sharpe, R., and Fayek, M. 2011. The world’s oldest observed primary uraninite. *The Canadian Mineralogist*, **49**: 1199–1210. Mineralogical Association of Canada. doi:<https://doi.org/10.3749/canmin.49.5.1199>.
- Sharpe, R., Fayek, M., Quirt, D., and Jefferson, C.W. 2015. Geochronology and genesis of the Bong uranium deposit, Thelon Basin, Nunavut, Canada. *Economic Geology*, **110**: 1759–1777. Society of Economic Geologists.
- Taylor, R.P., Strong, D.F., and Kean, B.F. 1980. The Topsails igneous complex: Silurian–Devonian peralkaline magmatism in western Newfoundland. *Canadian Journal of Earth Sciences*, **17**: 425–439. NRC Research Press Ottawa, Canada.
- Tremblay, L.P. 1970. The significance of uranium in quartzite in the Beaverlodge area, Saskatchewan. *Canadian Journal of Earth Sciences = Revue Canadienne des Sciences de la Terre*, **7**: 280–305. National Research Council of Canada. doi:<https://doi.org/10.1139/e70-027>.

- van Breemen, O., Henderson, J.B., Loveridge, W.D., and Thompson, P.H. 1987. U–Pb zircon and monazite geochronology and zircon morphology of granulites and granite from the Thelon Tectonic Zone, Healey Lake and Artillery Lake map areas, NWT. *Radiogenic Age and Isotopic Studies, Report*, **1**: 82–87.
- van Breemen, O., Peterson, T.D., and Sandeman, H.A. 2005. U-Pb zircon geochronology and Nd isotope geochemistry of Proterozoic granitoids in the western Churchill Province: intrusive age pattern and Archean source domains. *Canadian Journal of Earth Sciences*, **42**: 339–377. Canadian Science Publishing NRC Research Press, Ottawa. Available from <https://login.library.smu.ca/login?url=https://www.proquest.com/scholarly-journals/u-pb-zircon-geochronology-nd-isotope-geochemistry/docview/218834970/se-2?accountid=13908>.
- van Breemen, O., Thompson, P.H., Hunt, P.A., and Culshaw, N. 1987. U–Pb zircon and monazite geochronology from the northern Thelon Tectonic Zone, District of Mackenzie. *Radiogenic age and isotopic studies, Report*, **1**: 82–87.
- White, D.J. 2005. High-temperature, low-pressure metamorphism in the Kiseynew domain, Trans-Hudson orogen: crustal anatexis due to tectonic thickening? *Canadian Journal of Earth Sciences*, **42**: 707–721. NRC Research Press Ottawa, Canada.
- Yu, C.-D., Wang, K.-X., Liu, X.-D., Cuney, M., Pan, J.-Y., Wang, G., Zhang, L., and Zhang, J. 2020. Uranium Mineralogical and Chemical Features of the Na-Metasomatic Type Uranium Deposit in the Longshoushan Metallogenic Belt, Northwestern China. *Minerals*, **10**: 335. Multidisciplinary Digital Publishing Institute. doi:10.3390/min10040335.
- Zhong, J., Wang, S.-Y., Gu, D.-Z., Cai, Y.-Q., Fan, H.-H., Shi, C.-H., and Hu, C.-N. 2020. Geology and fluid geochemistry of the Na-metasomatism U deposits in the Longshoushan uranium metallogenic belt, NW China: Constraints on the ore-forming process. *Ore Geology Reviews*, **116**: 103214. doi:<https://doi.org/10.1016/j.oregeorev.2019.103214>.

Appendix

Appendix A – List of samples and techniques

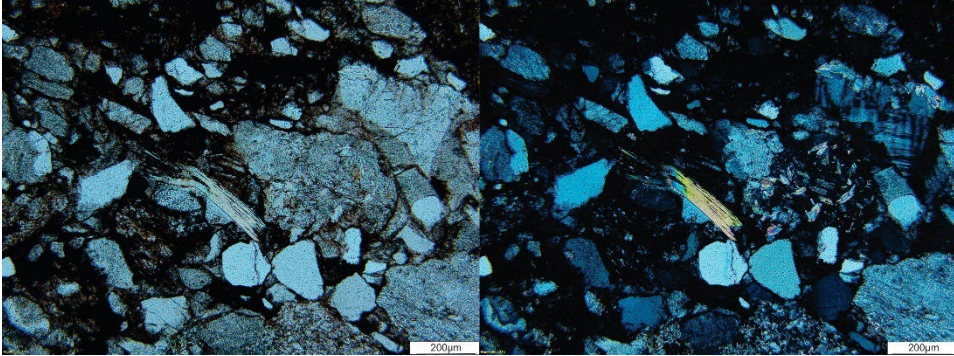
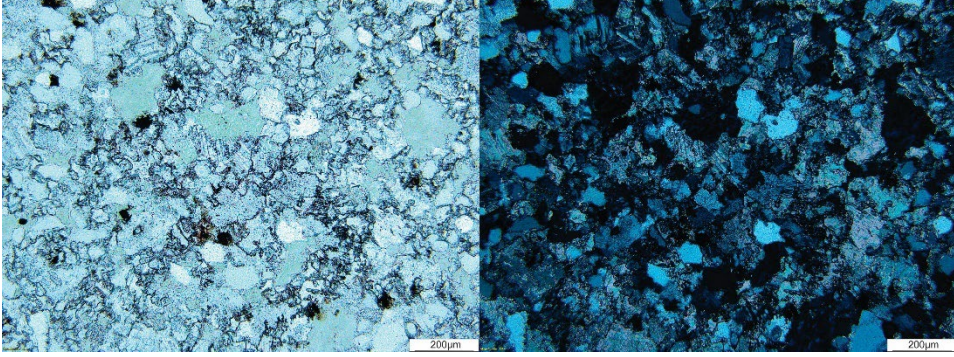
Sample Number	Rock Type	Location			Sample Type	Petrography	XRF	SEM	LA-ICP-MS
		UTM Zone	Easting	Northing					
11PUA-122A1-1	Conglomerate	14N	510070.92	6939340.8	Hand Sample		X		
11PUA-122A2-2a	Conglomerate	14N	510070.92	6939340.8	Hand Sample		X		
11PUA-122A2-2b	Conglomerate	14N	510070.92	6939340.8	Hand Sample	X	X		
11PUA-124A1-a	Polymictic conglomerate	14N	517072.84	6940803.1	Hand Sample		X		
11PUA-124A1-b	Polymictic conglomerate	14N	517072.84	6940803.1	Hand Sample	X	X		
11PUA-125B1	Carbonate, hematite vein	14N	515744.11	6940115.4	Hand Sample	X	X		
11PUA-128A2	Quartz-sulfides stockwerk	14N	501439.95	6941952.7	Hand Sample		X		

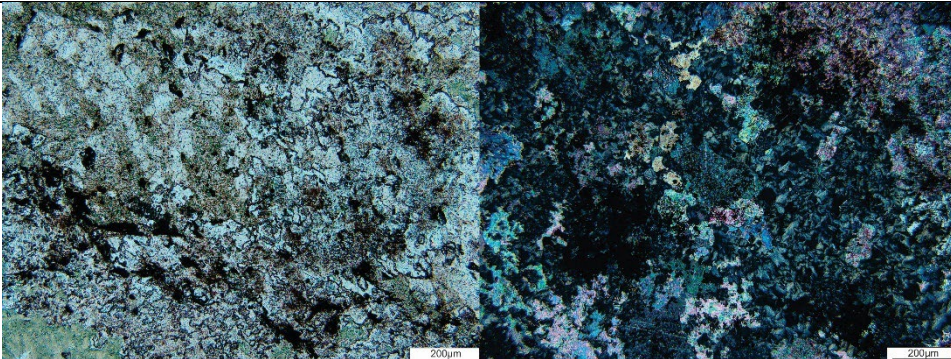
11PUA-128A4	Quartz-sulfides stockwerk	14N	501439.95	6941952.7	Hand Sample	X	X		
11PUA-131A1	Polymictic conglomerate	14N	503964.11	6935704.8	Hand Sample	X	X	X	
11PUA-131A2-1	Polymictic conglomerate	14N	503964.11	6935704.8	Hand Sample		X		
11PUA-133A3-2	Altered basalt	14N	519160	6940111	Drill Core 10-LC-35		X		
11PUA-133A3-3	Altered basalt	14N	519160	6940111	Drill Core 10-LC-35	X	X		
11PUA-133A5-1	Tuff	14N	519160	6940111	Drill Core 10-LC-35		X	X	X
11PUA-133A5-2	Tuff	14N	519160	6940111	Drill Core 10-LC-35		X	X	X
11PUA-133A5-2_1	Tuff	14N	519160	6940111	Drill Core 10-LC-35		X		
11PUA-133A5-3a	Tuff	14N	519160	6940111	Drill Core 10-LC-35	X	X	X	X
11PUA-133A5-3b	Tuff	14N	519160	6940111	Drill Core 10-LC-35		X	X	X
11PUA-133A5-3b_1	Tuff	14N	519160	6940111	Drill Core 10-LC-35	X	X		
11PUA-133A6-1	Tuff	14N	519160	6940111	Drill Core 10-LC-35	X	X		

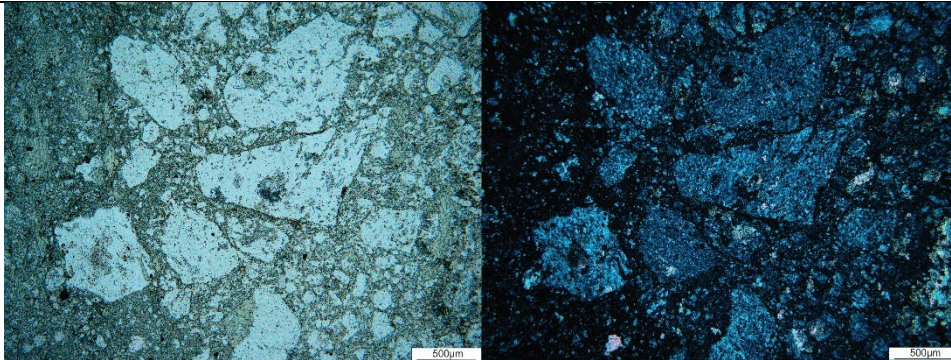
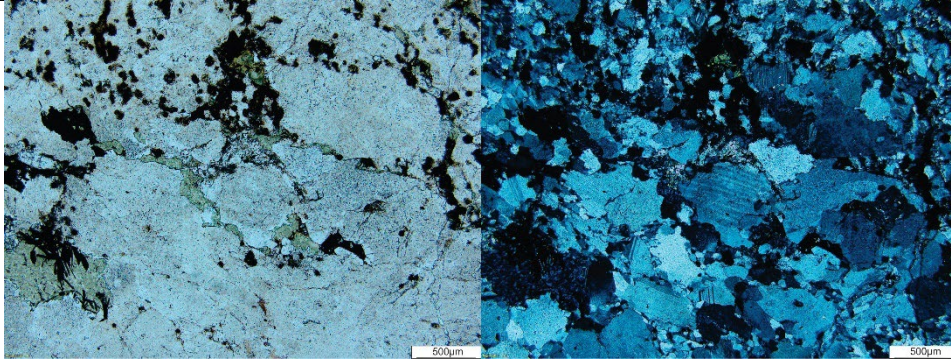
11PUA-134A2-1	Gash vein	14N	518676	6940370	Drill Core 10-LC-63		X	X	X
11PUA-134A2-3	Gash vein	14N	518676	6940370	Drill Core 10-LC-63	X	X	X	X
11PUA-134A2-4	Gash vein	14N	518676	6940370	Drill Core 10-LC-63		X		
11PUA-135A4-6	Tuff	14N	518626	6940383	Drill Core 10-LC-18	X	X	X	X
11PUA-135A4-7	Tuff	14N	518626	6940383	Drill Core 10-LC-18	X	X		
11PUA-135A5-2	Tuff	14N	518626	6940383	Drill Core 10-LC-18	X	X	X	X
11PUA-135A5-2_1	Tuff	14N	518626	6940383	Drill Core 10-LC-18		X		
11PUA-135A5-3	Tuff	14N	518626	6940383	Drill Core 10-LC-18	X	X	X	X
11PUA-135A5-4	Tuff	14N	518626	6940383	Drill Core 10-LC-18	X	X		
11PUA-135A5-5	Tuff	14N	518626	6940383	Drill Core 10-LC-18		X		
11PUA-135A5-6	Tuff	14N	518626	6940383	Drill Core 10-LC-18	X	X	X	X
11PUA-135A6-1	Tuff	14N	518626	6940383	Drill Core 10-LC-18	X	X		
11PUA-135A6-2	Tuff	14N	518626	6940383	Drill Core 10-LC-18		X		
11PUA-135A6-3	Tuff	14N	518626	6940383	Drill Core 10-LC-18		X		
11PUA-136A5-1	Tuff	14N	519108	6940123	Drill Core 10-LC-15	X	X	X	X

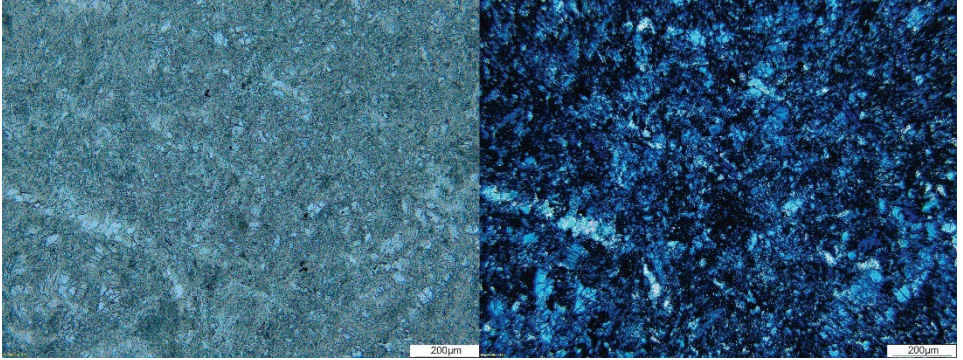
11PUA-136A5-2	Tuff	14N	519108	6940123	Drill Core 10-LC-15		X		
11PUA-136A5-3	Tuff	14N	519108	6940123	Drill Core 10-LC-15		X	X	X
11PUA-136A5-3_1	Tuff	14N	519108	6940123	Drill Core 10-LC-15		X		
11PUA-136A5-4	Tuff	14N	519108	6940123	Drill Core 10-LC-15		X		

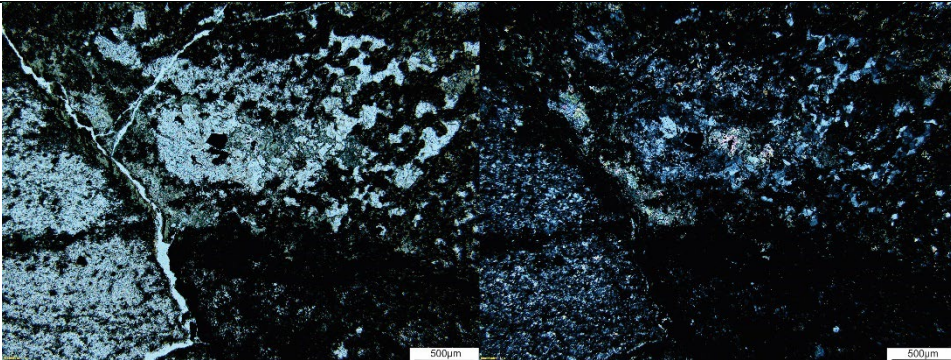
Appendix B – Petrographic Descriptions

Sample Number	Petrography (PPL, XPL, & RL)	Photomicrographs
<p>11PUA-122A1-2b (hand sample)</p> <p>Rock type: polymictic conglomerate</p>	<p><i>Clasts (50%):</i> Anhedral quartz grains (40%), subhedral laths of albite (25%), anhedral grains of k-feldspar (30%), and minor laths of muscovite (5%).</p> <p><i>Matrix (40%):</i> Fine-grained anhedral grains of quartz (65%), albite (10%), k-feldspar (20%), and rounded grains of hematite (2.5%) and ilmenite (2.5%).</p> <p><i>Cements (10%):</i> Infilling calcite (50%) and hematite cement (50%).</p> <p><i>Alteration:</i> Minor carbonate and hematite alteration.</p>	
<p>11PUA-124A1-b (hand sample)</p> <p>Rock type: polymictic conglomerate</p>	<p><i>Clasts (0%):</i> None.</p> <p><i>Matrix (50%):</i> Very fine-grained anhedral quartz grains (80%), anhedral grains of albite (15%), and minor laths of muscovite (5%).</p> <p><i>Cements (0%):</i> None. Grain-to-grain contact.</p> <p><i>Veinlets (50%):</i> Calcite vein crosscuts and get mineralization of acicular and radial hematite (20%) then calcite (80%).</p> <p><i>Alteration:</i> Pervasive alteration to hematite (30%), chlorite (30%), and carbonate (40%).</p>	

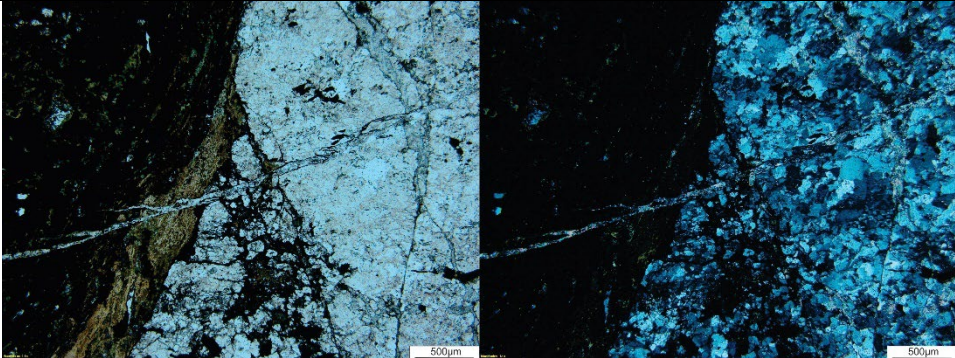
<p>11PUA-125B1 (hand sample)</p> <p>Rock type: carbonate, hematite vein</p>	<p><i>Matrix (20%)</i>: Anhedral quartz grains (5%), albite (10%), and k-feldspar grains (5%).</p> <p><i>Veinlets (15%)</i>: Albite (5%) vein and calcite (80%) veins crosscut sample. Pyrite (10%) and chalcopyrite (5%) crystallizes before calcite in calcite veins.</p> <p><i>Cements (5%)</i>: Minor calcite and hematite cements remaining cementing the grains of the host rock.</p> <p><i>Alteration (50%)</i>: Pervasive chlorite (50%), carbonate (40%), and hematite (10%) alteration replace the majority of the host rock, no initial textures are preserved. Carbonate alteration is invading the host rock as anhedral masses and predates the chlorite alteration. Hematite alteration is not as pervasive as carbonate and chlorite. Chlorite is exhibiting radial aggregates, replacing the minerals in the host rock and the veins.</p>	
---	--	--

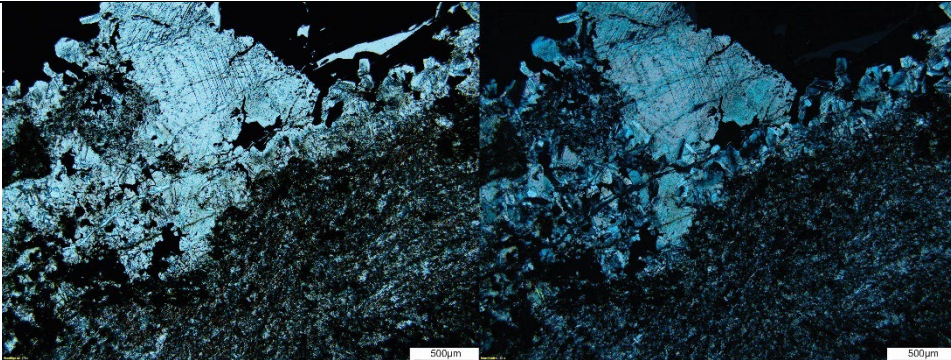
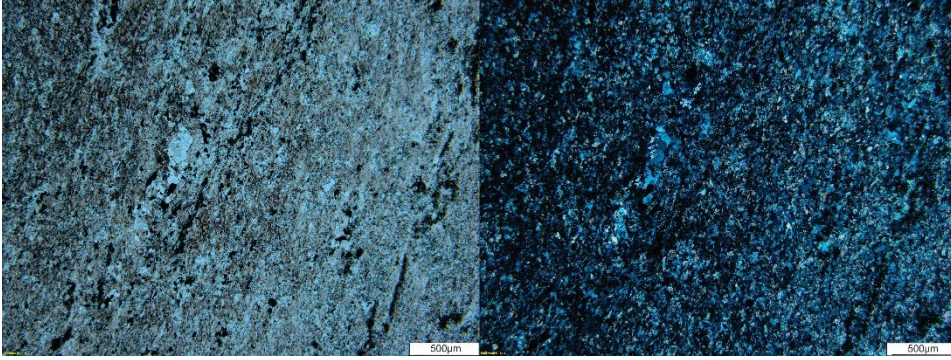
<p>11PUA-128A4 (hand sample)</p> <p>Rock type: quartz-sulfides stockwork (breccia??)</p>	<p><i>Clasts (40%):</i> Anhedral quartz (50%), anhedral albite (40%), and anhedral k-feldspar (10%).</p> <p><i>Matrix (20):</i> Anhedral quartz (60%), anhedral grains of albite (30%) and k-feldspar (10%).</p> <p><i>Cements (30%):</i> Calcite (5%), chlorite (70%), and hematite (20%) infilling between the quartz, albite, and k-feldspar. Uraninite (5%) concentrated within cements between grain boundaries.</p> <p><i>Alteration (10%):</i> Chlorite (70%) and hematite (20%) alteration concentrated along cements. Minor carbonate alteration to host rock (10%).</p>	
<p>11PUA-131A1 (hand sample)</p> <p>Rock type: polymictic conglomerate</p>	<p><i>Clasts (40%):</i> Anhedral quartz (30%), albite (50%), k-feldspar (10%) sandstone clasts (10%).</p> <p><i>Matrix (35%):</i> Fine-grained quartz (35%), euhedral hexagons of barite (5%), stubby subhedral grains of albite (45%), fine-grained disseminations of uraninite (5%), very fine-grained anhedral grains of disseminated chalcopryrite (5%), and acicular muscovite (5%)</p> <p><i>Cements (10%):</i> Calcite (50%), silica (10%), and hematite (40%) cements infilling matrix. Carbonate and silica</p>	

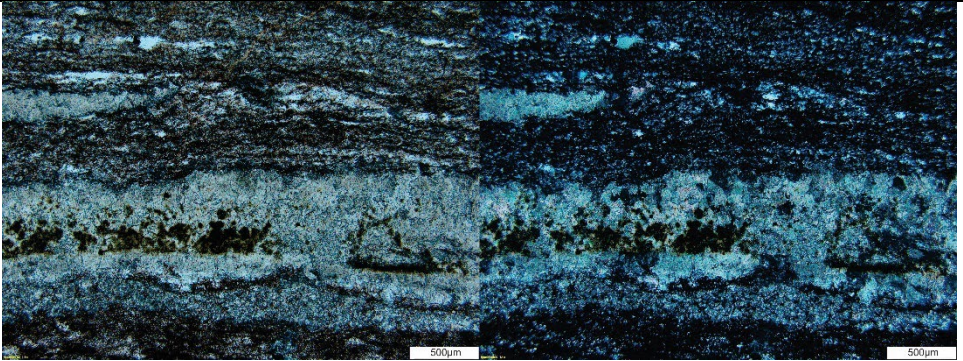
	<p>cements are infilling grain boundaries. Hematite cements are both infilling, but also mineralizing as acicular and radial growths in between the grains of the matrix.</p> <p><i>Alteration (5%):</i> Chlorite (100%) alteration is primarily replacing the minerals in the cements and is therefore concentrated as radial growths within the cement between the grains in the matrix.</p>	
<p>11PUA-133A3-3 (drill core 10LC-35 : 44.95 to 45.25m)</p> <p>Rock type: Altered basalt</p>	<p><i>Mineralogy (10%):</i> Subhedral, elongate grains of albite (90%) and minor euhedral K-feldspar (10%) remaining.</p> <p><i>Veinlets (15%):</i> Calcite (90%) and quartz (5%) veins crosscut sample. Chalcopyrite (5%) is occurring as anhedral grains within the veins.</p> <p><i>Alteration (75%):</i> Albitization of this sample, then pervasive carbonate (50%) alteration and chloritization (50%) occurred.</p>	

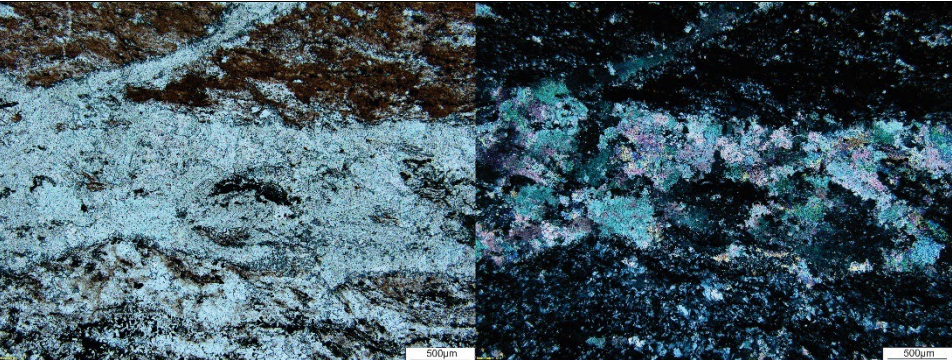
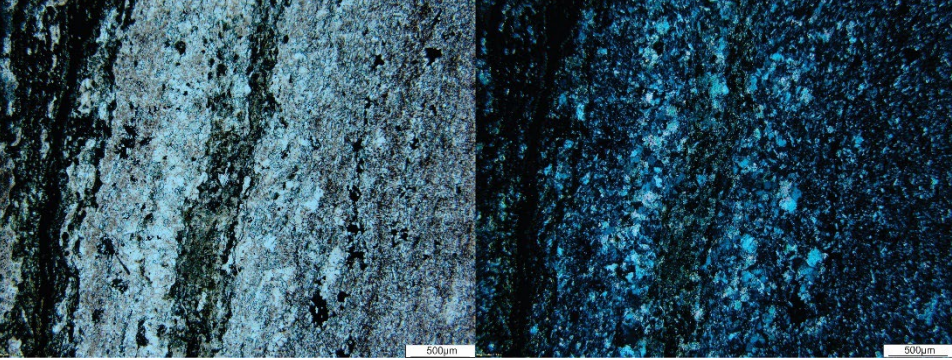
<p>11PUA-133A5-3a (drill core 10LC-35)</p> <p>Rock Type: Tuff</p>	<p><i>Mineralogy (20%)</i>: Anhedral albite (72.5%), anhedral quartz (25%), and anhedral grains of molybdenite (2.5%) are disseminated within the host rock.</p> <p><i>Veinlets (70%)</i>: Uraninite, pyrite, chalcopyrite, zircon, brannerite are hosted within calcite (50%) veins cross-cutting sample. Uraninite (20%) is botryoidal. Pyrite (10%) is euhedral and prismatic. Chalcopyrite (5%) is occurring as anhedral grains. Zircon (5%) cannot be distinguished using a polarizing microscope because it is metamict. Brannerite (5%) is large, blocky grains. Anhedral galena (2.5%) and sphalerite (2.5%) are also present in the calcite veins.</p> <p><i>Alteration (10%)</i>: Pervasive hematite (100%) replacement of host rock.</p>	
---	---	--

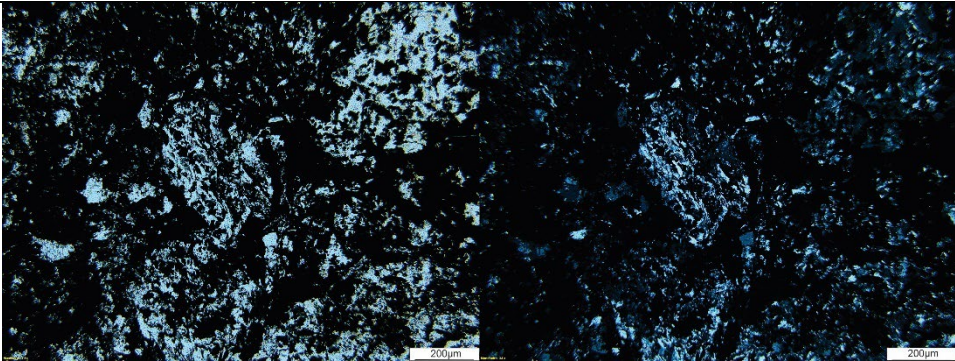
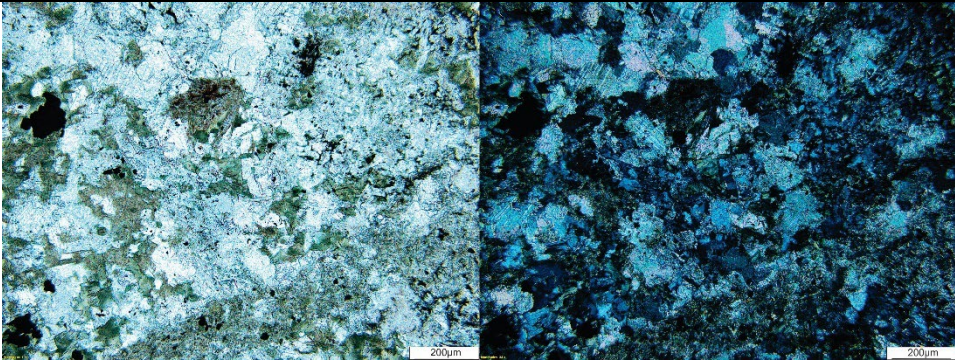
<p>11PUA-133A5-3b_1 (drill core 10LC-35 : 45.95 to 46.2m)</p> <p>Rock type: Tuff</p>	<p><i>Mineralogy (50%):</i> Anhedra very fine-grained albite (70%) and quartz (20%) with disseminated euhedral, prismatic pyrite (2.5%), disseminations of anhedra, elongate hematite (2.5%) grains, disseminated anhedra chalcocopyrite (2.5%), and anhedra molybdenite grains (2.5%).</p> <p><i>Veinlets (35%):</i> Calcite (30%) and albite (5%) veins cross-cut sample and concentrate botryoidal uraninite (20%), blocky brannerite (10%), botryoidal zircon (5%), euhedral, prismatic pyrite (2.5%), anhedra chalcocopyrite (10%), and anhedra sphalerite (2.5%) mineralization.</p> <p><i>Alteration (15%):</i> Carbonate (80%), chlorite (5%), and hematite (15%) alteration.</p>	
<p>11PUA-133A6-1 (drill core 10LC-35 : 46.65 to 47m)</p> <p>Rock type: Tuff</p>	<p><i>Mineralogy (80%):</i> Anhedra albite (55%), microcline (5%), anhedra quartz (30%), and acicular muscovite (5%) with muscovite defining a foliated fabric. Minor euhedral, prismatic pyrite (2.5%) and anhedra, chalcocopyrite (2.5%) grains are disseminated throughout host rock.</p> <p><i>Veinlets (10%):</i> Calcite veins crosscut sample. Prismatic pyrite (5%) and anhedra chalcocopyrite (10%) are</p>	

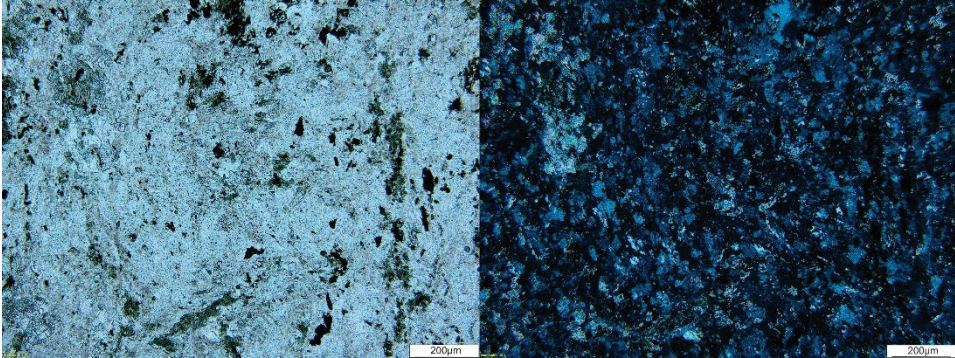
	<p>concentrated along the center of the veinlets.</p> <p><i>Alteration (10%):</i> Early albitization of the host rock. Minor chlorite alteration and carbonate alteration. Carbonate alteration is invading host rock, but chlorite alteration is mainly replacing the muscovite grains.</p>	
<p>11PUA-134A2-3 (drill core 10LC-63 : 62 to 62.4m)</p> <p>Rock type: Gash vein</p>	<p><i>Mineralogy (50%):</i> Host rock consists of quartz (40%), k-feldspar (10%), and albite (50%).</p> <p><i>Cements (5%):</i> Calcite (50%) and hematite (50%) cements fills the interstices between the grains of the host rock.</p> <p><i>Veinlets (40%):</i> A vein intrudes one half of this sample. Calcite (20%) veins crosscut sample and concentrate colloform uraninite (25%), anhedral disseminations of chalcopyrite throughout the vein (10%), anhedral grains of pyrite (2.5%), and grains of galena infilling around uraninite (2.5%).</p> <p><i>Alteration (5%):</i> Host rock is facing replacement by hematite.</p>	

<p>11PUA-135A4-6 (drill core 10LC-18 : 79.45 to 79.85m)</p> <p>Rock type: Tuff</p>	<p><i>Mineralogy (40%):</i> Albite host rock with disseminated anhedral hematite and chalcopryite.</p> <p><i>Veinlets (10%):</i> Calcite veins cross-cutting sample. The major vein has anhedral chalcopryite (30%) along the center of the vein, blocky grains of calcite (20%) within the vein, laths of albite (10%) rimming the edge of the vein. Uraninite (35%) mineralization is occurring surrounding the main vein It is mainly anhedral, but some grains are exhibiting a botryoidal texture. Fine-grained galena (5%) is occurring as anhedral grains.</p> <p><i>Alteration (50%):</i> Pervasive carbonate (60%), hematite (40%) alteration. Both are replacing albitized host rock.</p>	
<p>11PUA-135A4-7 (drill core 10LC-18 :)</p> <p>Rock type: Tuff</p>	<p><i>Mineralogy (55%):</i> Anhedral albite (75%) and anhedral quartz (12.5%). Disseminated anhedral grains of sphalerite (5%), pyrite (2.5%), chalcopryite (5%).</p> <p><i>Veinlets (10%):</i> Calcite (40%) veins cross-cutting albite host rock. One of these veins has uraninite (40%) concentrated along the vein exhibiting a botryoidal texture. Minor hematite (2.5%) has mineralized as acicular needles within a calcite vein. Anhedral grains of</p>	

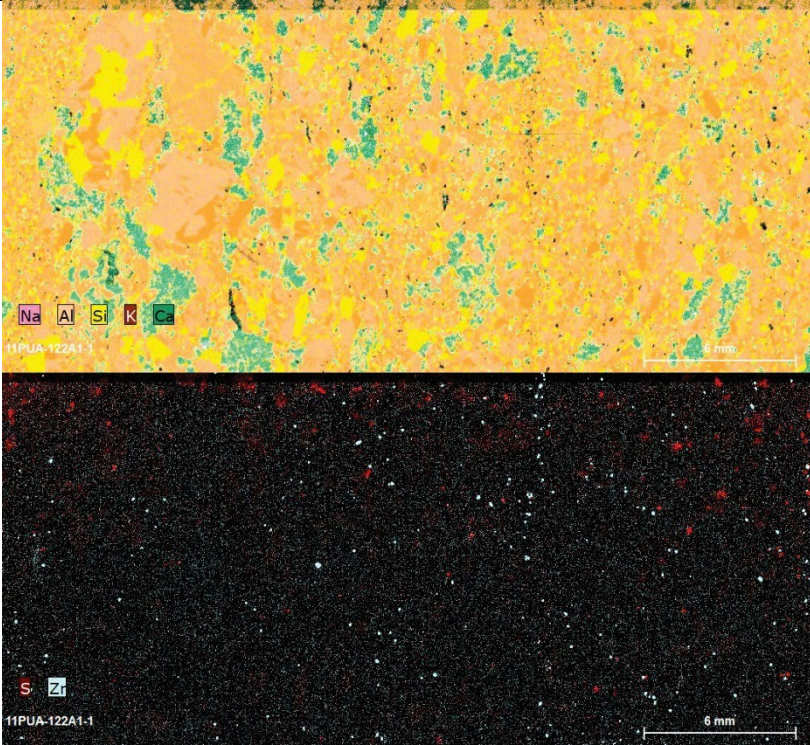
	<p>chalcopyrite (5%), pyrite (5%), sphalerite (5%), and minor galena (2.5%) are also occurring within these calcite veins.</p> <p><i>Alteration (35%):</i> Pervasive carbonate (70%) replacement. Hematite (20%) alteration and chlorite (10%) replacement.</p>	
<p>11PUA-135A5-2 (drill core 10LC-18: 80.1 to 80.6m)</p> <p>Rock type: Tuff</p>	<p><i>Mineralogy (60%):</i> Albite (100%).</p> <p><i>Veinlets (45%):</i> Calcite (65%) veins cutting across sample. Uraninite (15%) mineralization concentrated within calcite veins. Uraninite exhibits a botryoidal texture throughout the vein. Euhedral and prismatic pyrite (10%) veinlets crosscut sample. Anhedra chalcopyrite (5%) crystallizes in concentrations or dissemination throughout veinlets of calcite. Anhedra galena (2.5%) forms around uraninite grains. Anhedra sphalerite (2.5%) occurring throughout calcite veins.</p> <p><i>Alteration (5%):</i> Hematite replacement of host rock.</p>	

<p>11PUA-135A5-3 (drill core 10LC-18 : 80.1 to 80.6m)</p> <p>Rock type: Tuff</p>	<p><i>Mineralogy (20%):</i> Non-lineated, subhedral, elongate grains of albite (100%).</p> <p><i>Veinlets (30%):</i> Calcite (70%) veins cross-cutting sample. Anhedral uraninite (10%) mineralization within these calcite veins. Anhedral chalcopyrite (5%) mineralization within calcite veins. Anhedral chalcopyrite (10%) and bornite grains occurring along molybdenite (5%) occurring as veinlets.</p> <p><i>Alteration (50%):</i> Pervasive carbonate (45%), minor chlorite (5%), and pervasive hematite (50%) alteration.</p>	
<p>11PUA-135A5-4 (drill core 10LC-18 :)</p> <p>Rock type: Tuff</p>	<p><i>Mineralogy (30%):</i> Albite (72.5%) with minor quartz (2.5%). Disseminated grains of anhedral chalcopyrite (10%), anhedral to euhedral prismatic pyrite (5%), anhedral sphalerite (2.5%) and minor galena (2.5%) are also present.</p> <p><i>Veinlets (10%):</i> Calcite (60%) veins crosscut albitized host rock. Botryoidal vein-hosted uraninite (20%) is occurring in/along the calcite veins. Some uraninite is anhedral as well. Anhedral chalcopyrite (10%), pyrite (2.5%), sphalerite (2.5%), and galena (5%) are also concentrated within these veins.</p> <p><i>Alteration (60%):</i> Pervasive carbonate</p>	

	(70%) alteration of albite host rock. Hematite replacement (30%) of albite host rock.	
11PUA-135A5-6 (drill core 10LC-18 : 80.1 to 80.6m) Rock type: Tuff	<p><i>Mineralogy (10%):</i> Anhedral to subhedral grains of quartz (50%). Anhedral albite (10%). Laths of muscovite (40%), roughly defining a foliation.</p> <p><i>Veinlets (80%):</i> A uraninite (50%) vein and sulfide vein crosscut the majority of this sample. Uraninite is botryoidal to anhedral. Pyrite (30%) is subhedral to anhedral prismatic throughout the vein. Chalcopyrite (10%) is occurring as anhedral grains. Sphalerite (5%) and galena (5%) is anhedral as well.</p> <p><i>Alteration (10%):</i> Minor chlorite (100%) alteration.</p>	
11PUA-135A6-1 (drill core 10LC-18 : 81.6 to 81.9m) Rock type: Tuff	<p><i>Mineralogy (20%):</i> non-foliated elongate subhedral albite (80%) laths, anhedral quartz (10%) and predominantly randomly oriented acicular muscovite (10%).</p> <p><i>Veinlets (50%):</i> Calcite (10%) veins crosscut sample. Anhedral chalcopyrite (5%) is disseminated within calcite veins. Anhedral grains of uraninite (5%) are concentrated along calcite veinlets. Anhedral pyrite (80%) vein crosscuts</p>	

	<p>sample.</p> <p><i>Alteration (30%):</i> Carbonate (40%) and chlorite (70%) alteration. Carbonate replacement is invading the albite-host rock. Chlorite alteration is pervasive and is replacing the pre-existing minerals with radial masses.</p>	
<p>11PUA-136A5-1 (drill core 10LC-15 : 95.8 to 96.1m)</p> <p>Rock type: Tuff</p>	<p><i>Mineralogy (30%):</i> Euhedral to subhedral elongate grains of albite (57.5%). Minor acicular grains of muscovite (5%). Anhedral uraninite (35%) is disseminated throughout albitized host rock. Minor subhedral, prismatic pyrite (2.5%) disseminated throughout host rock.</p> <p><i>Veinlets (10%): Calcite (95%) and albite veins cross-cut sample. Minor anhedral chalcopyrite (2.5%) grains within calcite vein. Subhedral prismatic pyrite (2.5%) is also within the calcite vein.</i></p> <p><i>Alteration (60%):</i> Pervasive carbonate (70%) alteration. Hematite (20%) replacement is also occurring throughout host rock. Chlorite (10%) alteration is also occurring in the muscovite.</p>	

Appendix C – XRF Descriptions

Sample Number	XRF Descriptions	Type of U-mineralization	XRF Elemental Maps
<p>11PUA-122A1-1 (hand sample)</p> <p>Rock type: conglomerate</p>	<p><i>Clasts (20%):</i> Clasts of calcite (30%), K-feldspar (10%), quartz (20%), and albite (40%).</p> <p><i>Matrix (65%):</i> Calcite (15%), K-feldspar (15%), quartz (25%), and albite (35%) matrix. Disseminated hematite (5%), pyrite (2.5%). Minor disseminations of detrital zircon (2.5%).</p> <p><i>Cements (15%):</i> Calcite (50%), silica (20%) and hematite (20%) cements are infilling grains that make up the matrix.</p>	<p>None</p>	

<p>11PUA-122A-2a (hand sample)</p> <p>Rock type: conglomerate</p>	<p><i>Clasts (10%):</i> Albite (40%), quartz (40%), k-feldspar (15%), calcite (5%).</p> <p><i>Matrix (80%):</i> Albite (25%), quartz (25%), k-feldspar (25%), calcite (10%). Disseminated zircons (5%), ilmenite (5%), hematite (5%).</p> <p><i>Cements (10%):</i> Calcite (40%) and hematite (60%) cements.</p>	<p>None</p>	
---	--	-------------	--

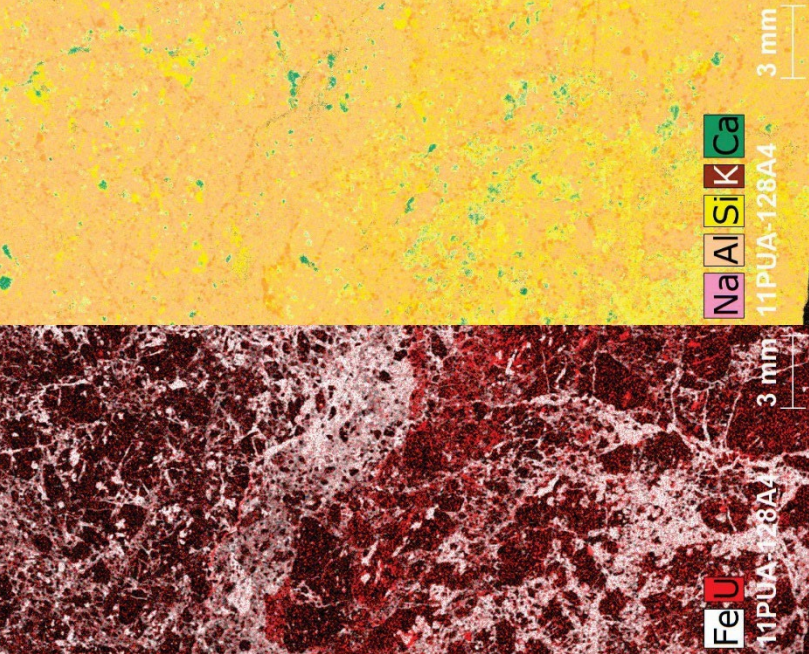
<p>11PUA-122A-2b (hand sample)</p> <p>Rock type: conglomerate</p>	<p><i>Clasts (25%):</i> Albite (35%), k-feldspar (15%), quartz (20%), calcite (30%).</p> <p><i>Matrix (65%):</i> Albite (25%), quartz (25%), k-feldspar (35%). Disseminated hematite (5%), detrital zircons (10%).</p> <p><i>Cements (10%):</i> Calcite (70%) and hematite (30%) cements.</p>	<p>None</p>	<p>The figure consists of two vertically stacked panels. The top panel is a colorized elemental map showing the distribution of Na, Al, Si, K, and Ca. The bottom panel is a grayscale map showing the distribution of Zr. Both panels include a 7 mm scale bar and the sample ID '11PUA-122A1-2b'.</p>
---	---	-------------	---

<p>11PUA-124A1-a (hand sample)</p> <p>Rock type: polymictic conglomerate</p>	<p><i>Clasts (0%): None.</i></p> <p><i>Matrix (85%):</i> Albite (80%), k-feldspar (5%), quartz (10%).</p> <p><i>Veins (15%):</i> Calcite (65%) veins cross-cutting sample. Hematite (20%), uraninite (5%), and chalcopyrite (10%) concentrated within calcite veins.</p> <p><i>Cements (0%):</i> None. Grain-to-grain contact.</p>	<p>Simple vein-hosted</p>	
--	--	---------------------------	--

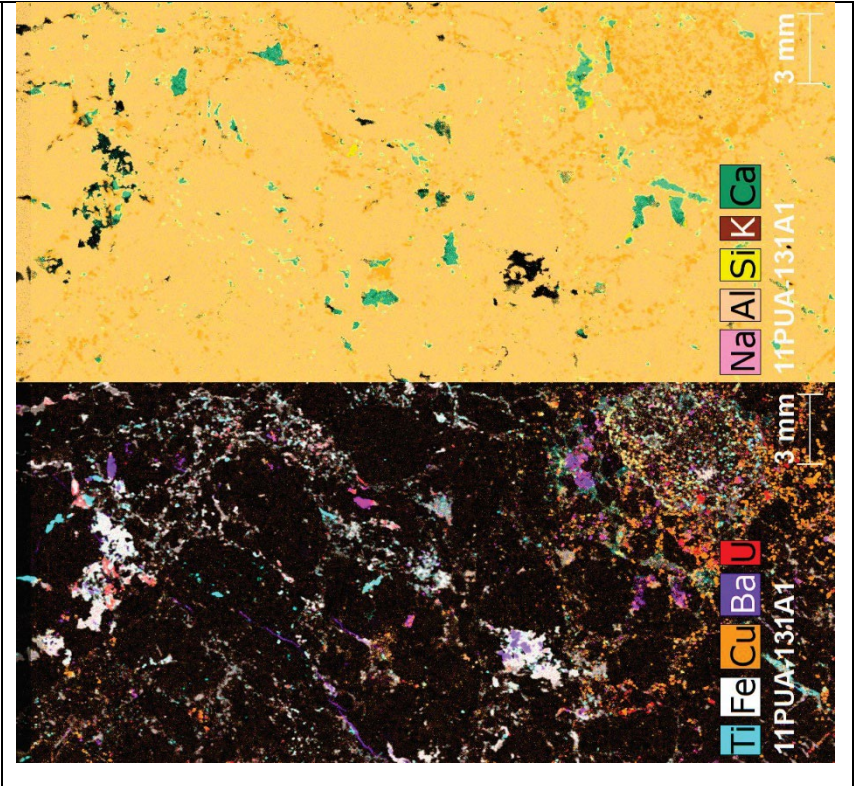
<p>11PUA-124A1-b (hand sample)</p> <p>Rock type: polymictic conglomerate</p>	<p><i>Clasts (0%):</i> None.</p> <p><i>Matrix (50%):</i> Quartz (80%), albite (15%), and minor muscovite (5%).</p> <p><i>Cements (0%):</i> None. Grain-to-grain contact.</p> <p><i>Veinlets (50%):</i> Calcite vein crosscuts sample. Hematite (20%) within calcite (80%).</p> <p><i>Alteration:</i> Pervasive alteration to hematite (30%), chlorite (30%), and carbonate (40%).</p>	<p>None</p>	<p>The figure consists of two vertically stacked panels showing mineralogical data for sample 11PUA-124A1-b. The top panel is a false-color map with a legend for Na, Al, Si, K, and Ca, and a 7 mm scale bar. The bottom panel is a false-color map with a legend for S, Ca, and Fe, and a 7 mm scale bar. Both panels show a complex, multi-colored pattern representing the distribution of these elements in the sample.</p>
--	---	-------------	--

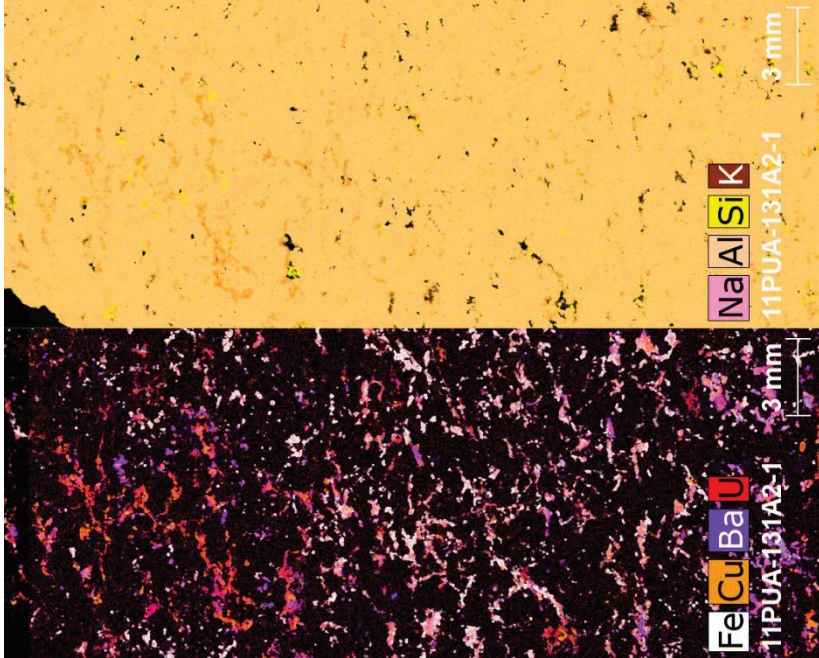
<p>11PUA-125B1 (hand sample)</p> <p>Rock type: carbonate, hematite vein</p>	<p><i>Mineralogy (20%)</i>: Quartz (5%), albite (10%), and k-feldspar (5%).</p> <p><i>Veins (15%)</i>: Albite (5%) vein and calcite (80%) veins crosscut sample. Uraninite in veinlets (5%). Pyrite (5%) and chalcopyrite (5%) in calcite veins.</p> <p><i>Cements (5%)</i>: Calcite and hematite cements.</p> <p><i>Alteration (50%)</i>: Pervasive chlorite (50%), carbonate (40%), and hematite (10%) replacement alteration. Chlorite alteration is most pervasive along uranium mineralization.</p>	<p>Simple vein-hosted</p>	<p>The image displays two stacked mineral maps for sample 11PUA-125B1. The top map is a color-coded mineral map with a legend on the right side listing elements: Na (purple), Al (green), Si (yellow), Ca (orange), U (red), and K (black). A 4 mm scale bar is visible in the bottom right corner. The bottom map is another color-coded mineral map with a legend on the right side listing elements: Mg (blue), Ca (green), Fe (red), Cu (orange), and U (black). A 4 mm scale bar is also visible in the bottom right corner. Both maps show a complex, irregular pattern of mineral distribution across the sample area.</p>
---	--	---------------------------	--

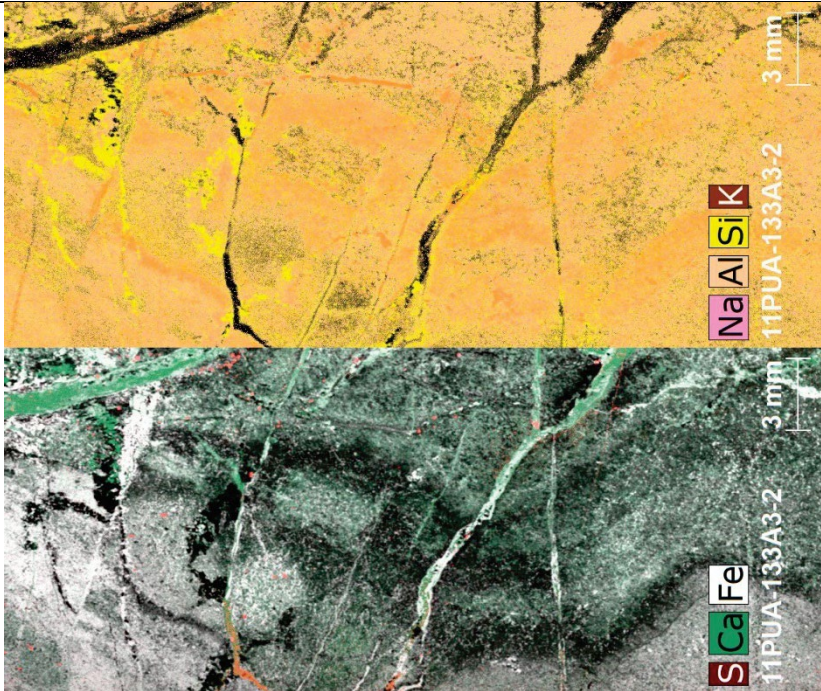
<p>11PUA-128A2 (hand sample)</p> <p>Rock type: quartz-sulfides stockwerk</p>	<p><i>Mineralogy (65%):</i> Albite (35%), k-feldspar (5%), quartz (30%), and calcite (10%). Chalcopyrite (10%), uraninite (5%), barite (5%), disseminated within albite host rock.</p> <p><i>Cements (35%):</i> Hematite (100%) cements.</p>	<p>Disseminated</p>	<p>The figure consists of two vertically stacked images of the same rock sample, 11PUA-128A2, each with a 3 mm scale bar. The top image is a color map showing the distribution of elements Na, Al, Si, K, and Ca. The bottom image is a grayscale map showing the distribution of elements Fe, Cu, and Ba.</p>
--	--	---------------------	---

<p>11PUA-128A4 (hand sample)</p> <p>Rock type: quartz-sulfides stockwerk</p>	<p><i>Clasts (40%):</i> Quartz (50%), albite (40%), and k-feldspar (10%).</p> <p><i>Matrix (20):</i> Quartz (60%), albite (30%) and k-feldspar (10%).</p> <p><i>Cements (30%):</i> Calcite (5%), chlorite (70%), and hematite (20%). Uraninite (5%) concentrated within cements between grain boundaries.</p> <p><i>Alteration (10%):</i> Chlorite (70%) and hematite (20%) alteration concentrated along cements. Minor carbonate alteration to host rock (10%).</p>	<p>Very minor (0.2 wt% U) disseminated</p>	
<p>11PUA-131A1 (hand sample)</p> <p>Rock type: polymictic conglomerate</p>	<p><i>Clasts (40%):</i> Quartz (40%), albite (50%), and k-feldspar (10%).</p> <p><i>Matrix (35%):</i> Quartz (35%), barite (5%), albite (45%), and muscovite (5%).</p> <p>Disseminations of uraninite (5%), chalcopyrite (5%).</p> <p><i>Cements (10%):</i> Calcite (50%), silica (10%), and hematite (40%) cements</p>	<p>Disseminated</p>	

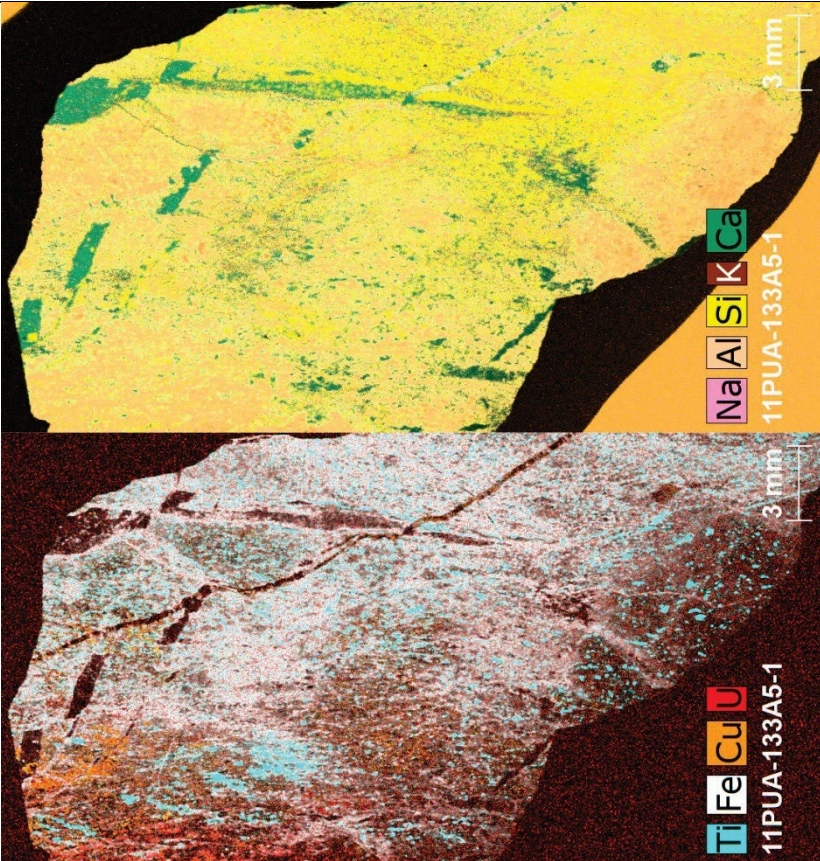
infilling matrix.
Alteration (5%): Chlorite (100%) alteration is primarily replacing the minerals in the cements.



<p>11PUA-131A2-1 (hand sample)</p> <p>Rock type: polymictic conglomerate</p>	<p><i>Mineralogy (80%):</i> Albite (70%), k-feldspar (5%), and quartz (2.5%). Hematite (7.5%), chalcopyrite (7.5%), uraninite (2.5%), and barite (5%) disseminated throughout sample.</p> <p><i>Cements (15%):</i> Infilling hematite (75%) and calcite (25%) cements.</p> <p><i>Alteration (5%):</i> Minor chlorite (100%) alteration.</p>	<p>Disseminated</p>	
--	---	---------------------	---

<p>11PUA-133A3-2 (drill core 10LC-35 : 44.95 to 45.25m)</p> <p>Rock type: Altered basalt</p>	<p><i>Mineralogy (5%):</i> Albite (95%), disseminated grains of hematite (5%).</p> <p><i>Veins (10%):</i> Calcite (60%) and quartz (20%) veins cross cutting sample. Hematite (15%) occurring within calcite veins. Chalcopyrite (2.5%), pyrite (2.5%) occurring along the calcite vein.</p> <p><i>Alteration (85%):</i> Pervasive carbonate (75%) alteration. Chlorite alteration (25%).</p>	<p>None</p>	
--	---	-------------	---

<p>11PUA-133A3-3 (drill core 10LC-35 : 44.95 to 45.25m)</p> <p>Rock type: Altered basalt</p>	<p><i>Mineralogy (10%):</i> Albite (90%), K-feldspar (10%).</p> <p><i>Veinlets (15%):</i> Calcite (90%) and quartz (5%) veins crosscut sample. Chalcopyrite (5%) within the veins.</p> <p><i>Alteration (75%):</i> Albitization of this sample, then pervasive carbonate (50%) alteration and chloritization (50%) occurred.</p>	<p>None</p>	<p>The figure consists of two vertically stacked images of the same sample area. The top image is a false-color map showing the distribution of various elements. A legend on the right side of the image lists Na (purple), Al (blue), Si (green), K (red), and Ca (yellow). A 3 mm scale bar is located in the top right corner. The bottom image is a grayscale map showing the distribution of Mg and Fe. A legend on the right side of the image lists Mg (light gray) and Fe (dark gray). A 3 mm scale bar is located in the top right corner. Both images show a prominent dark, diagonal feature, likely a veinlet, and a horizontal line across the middle.</p>
--	--	-------------	--

<p>11PUA-133A5-1 (drill core 10LC-35 : 45.65 to 45.85m)</p> <p>Rock type: Tuff</p>	<p><i>Mineralogy (5%):</i> Albite (100%).</p> <p><i>Veins (10%):</i> Calcite (72.5%) and quartz (10%) veins crosscut sample. Hematite (5%), rutile (5%) and chalcopyrite (5%) are occurring in disseminated concentrations throughout the sample. Uraninite (2.5%) veinlets also cut through sample.</p> <p><i>Alteration (85%):</i> Pervasive carbonate (60%) and hematite (40%) alteration.</p>	<p>Simple vein-hosted (very minor 0.1wt%)</p>	 <p>The figure consists of two mineral maps of the same rock sample, 11PUA-133A5-1, each with a 3 mm scale bar. The top map displays a yellow matrix with green veins, with a legend for Na, Al, Si, K, Ca. The bottom map displays a brown matrix with cyan veins, with a legend for Ti, Fe, Cu, U.</p>
--	---	---	--

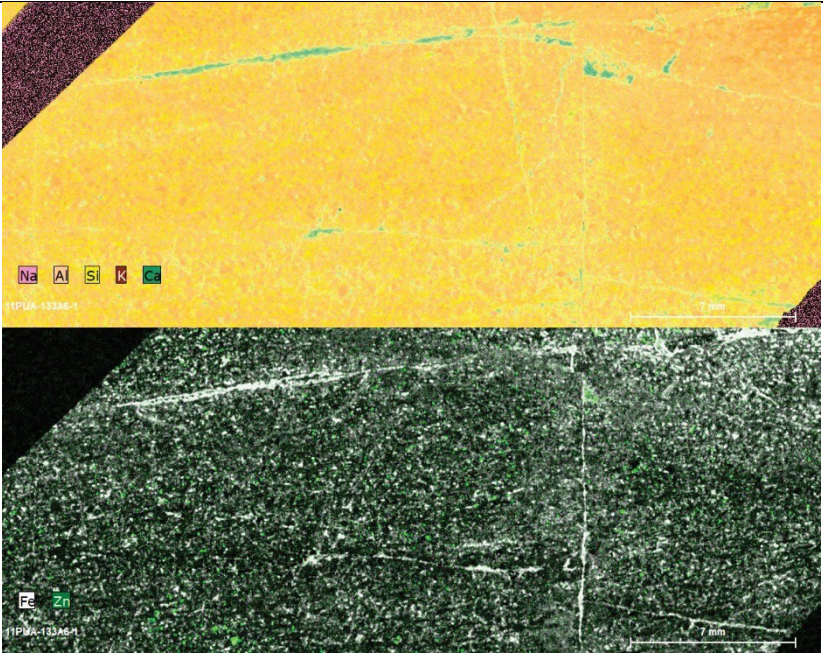
<p>11PUA-133A5-2 (drill core 10LC-35 : 45.65 to 45.85m)</p> <p>Rock type: Tuff</p>	<p><i>Mineralogy (60%):</i> Albite (5%) and quartz (5%) groundmass. Uraninite (85%) and molybdenite (5%) is invading the host rock surrounding the calcite vein.</p> <p><i>Veins (30%):</i> calcite (67.5%) and albite (10%) occurring as veins. Chalcopyrite (5%), pyrite (5%), rutile (2.5%), zircon (5%), sphalerite (2.5%), and galena (2.5%) disseminated throughout.</p> <p><i>Alteration (10%):</i> Carbonate alteration throughout this sample.</p>	<p>Complex vein-hosted</p>	
--	---	----------------------------	--

<p>11PUA-133A5-2_1 (drill core 10LC-35 : 45.65 to 45.85m)</p> <p>Rock type: Tuff</p>	<p><i>Mineralogy (60%):</i> Uraninite (90%) and molybdenite (10%) is invading the host rock surrounding the calcite vein.</p> <p><i>Veins (40%):</i> calcite (55%) occurring as veins. Chalcopyrite (5%), pyrite (10%), uraninite (15%), rutile (2.5%), zircon (5%), sphalerite (5%), and galena (2.5%) disseminated throughout.</p>	<p>Complex vein-hosted</p>	<p>The image displays three stacked elemental maps of a rock sample. The top map shows Ne, Al, Si, S, K, Ca. The middle map shows Ti, Cu, Zn, Zr, U. The bottom map shows Mo, U. Each map includes a 7 mm scale bar and the sample ID 11PUA-133A5-2.</p>
--	--	----------------------------	--

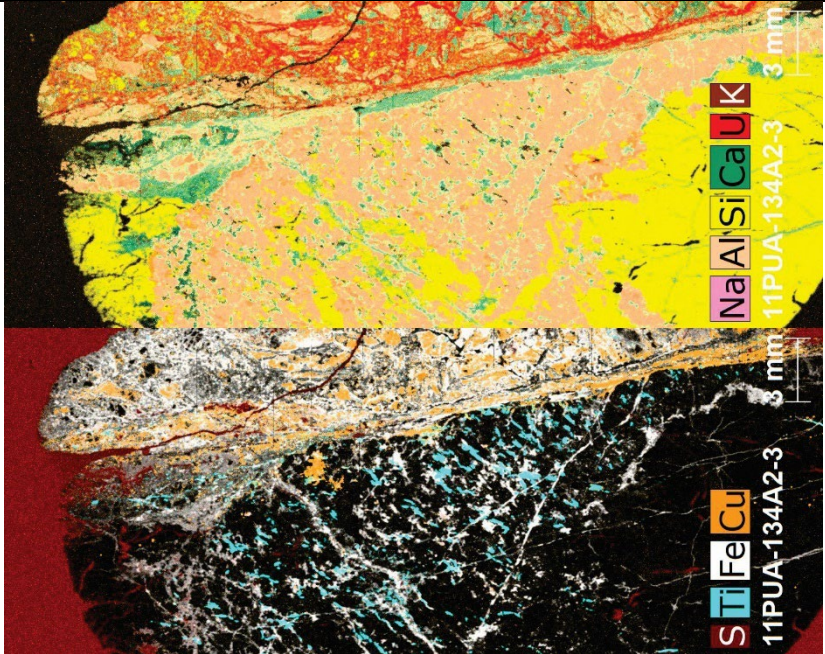
<p>11PUA-133A5-3a (drill core 10LC-35 : 45.95 to 46.2m)</p> <p>Rock type: Tuff</p>	<p><i>Mineralogy (20%):</i> Albite (72.5%), quartz (25%), and molybdenite (2.5%) are disseminated within the host rock.</p> <p><i>Veinlets (70%):</i> Uraninite (20%), pyrite (10%), chalcopyrite (5%), zircon (5%), brannerite (5%) are hosted within calcite (50%) veins cross-cutting sample. Galena (2.5%) and sphalerite (2.5%) are also present in the calcite veins.</p> <p><i>Alteration (10%):</i> Pervasive hematite (100%) replacement of host rock.</p>	<p>Complex vein-hosted</p>	
--	---	----------------------------	--

<p>11PUA-133A5-3b (drill core 10LC-35 : 45.95 to 46.2m)</p> <p>Rock type: Tuff</p>	<p><i>Mineralogy (40%):</i> Albitized (90%) host rock. Disseminated hematite (5%), molybdenite (10%).</p> <p><i>Veins (50%):</i> Calcite (45%) vein and albite (5%) vein crosscutting sample. Uraninite (20%), brannerite (5%), zircon (7.5%), chalcocopyrite (5%), pyrite (5%), and sphalerite (5%) within calcite vein. Minor molybdenite (2.5%) occurring within vein.</p> <p><i>Alteration (10%):</i> Host rock is facing carbonate (40%) and hematite (60%) alteration.</p>	<p>Complex vein-hosted</p>	<p>The figure consists of three vertically stacked elemental maps of a rock sample, labeled '11PUA-133A5-3b' in the bottom left of each map. Each map includes a 7 mm scale bar in the bottom right corner. The top map displays elements Na (purple), Al (green), Si (yellow), Ca (orange), and K (red). The middle map displays S (blue), Ca (orange), Ti (green), Cu (yellow), Zn (red), and U (purple). The bottom map displays Zr (green), Mo (yellow), U (purple), and Ba (red). The maps show a complex, irregular vein structure with varying mineral compositions across the sample.</p>
--	--	----------------------------	---

<p>11PUA-133A5-3b_1 (drill core 10LC-35 : 45.95 to 46.2m)</p> <p>Rock type: Tuff</p>	<p><i>Mineralogy (50%):</i> A (70%) and quartz (20%) with disseminated pyrite (2.5%), hematite (2.5%), chalcopryite (2.5%), molybdenite grains (2.5%).</p> <p><i>Veinlets (35%):</i> Calcite (30%) and albite (5%) veins cross-cut sample and concentrate uraninite (20%), brannerite (10%), zircon (5%), pyrite (2.5%), chalcopryite (10%), and sphalerite (2.5%) mineralization.</p> <p><i>Alteration (15%):</i> Carbonate (80%), chlorite (5%), and hematite (15%) alteration.</p>	<p>Complex vein-hosted</p>	
--	---	----------------------------	--

<p>11PUA-133A6-1 (drill core 10LC-35 : 46.65 to 47m)</p> <p>Rock type: Tuff</p>	<p><i>Mineralogy (80%):</i> Albite (55%), microcline (5%), quartz (27.5%), and muscovite (5%). Minor sphalerite (2.5%), pyrite (2.5%) and chalcopryrite (2.5%) are disseminated throughout host rock.</p> <p><i>Veins (10%):</i> Calcite veins crosscut sample. Pyrite (5%) and chalcopryrite (10%) are concentrated along the center of the veinlets.</p> <p><i>Alteration (10%):</i> Early albitization of the host rock. Minor chlorite alteration and carbonate alteration. Carbonate alteration is invading host rock.</p>	<p>None</p>	
---	---	-------------	---

<p>11PUA-134A2-1 (drill core 10LC-63 : 62 to 62.4m)</p> <p>Rock type: Gash vein</p>	<p><i>Mineralogy (40%):</i> Albite (87.5%). Disseminated rutile (5%), hematite (5%), molybdenite (2.5%).</p> <p><i>Veins (40%):</i> Calcite (70%) vein with vein-hosted uraninite (17.5%). Zirconium associated with uranium mineralization. Chalcopyrite (5%), pyrite (5%), and sphalerite (2.5%) within calcite vein.</p> <p><i>Alteration (20%):</i> Carbonate (70%) and hematite (30%) alteration of albitized host rock.</p>	<p>Simple vein-hosted</p>	
---	---	---------------------------	--

<p>11PUA-134A2-3 (drill core 10LC-63 : 62 to 62.4m)</p> <p>Rock type: Gash vein</p>	<p><i>Mineralogy (50%):</i> Host rock consists of quartz (40%), k-feldspar (10%), and albite (50%).</p> <p><i>Cements (5%):</i> Calcite (50%) and hematite (50%) cements fills the interstices between the grains of the host rock.</p> <p><i>Veinlets (40%):</i> A vein intrudes one half of this sample. Calcite (20%) veins crosscut sample and concentrate uraninite (25%), chalcopyrite (10%), of pyrite (2.5%), and galena (2.5%). Zirconium is associated with uranium-mineralization.</p> <p><i>Alteration (5%):</i> Host rock is facing replacement by hematite.</p>	<p>Simple vein-hosted</p>	
---	---	---------------------------	---

<p>11PUA-134A2-4 (drill core 10LC-63 : 62 to 62.4m)</p> <p>Rock type: Gash vein</p>	<p><i>Mineralogy (10%):</i> Albite (100%) groundmass.</p> <p><i>Veins (15%):</i> calcite and uraninite veinlets crosscut sample. Calcite (80%) vein concentrates pyrite (10%), hematite (5%), chalcocopyrite (5%).</p> <p>Molybdenum (60%) occurring along uraninite (40%) veinlet.</p> <p><i>Alteration (75%):</i> Pervasive carbonate (50%), hematite (30%), and chlorite (20%) alteration.</p>	<p>Simple vein-hosted</p>	
---	---	---------------------------	--

<p>11PUA-135A4-4 (drill core 10LC-18 : 79.45 to 79.85m)</p> <p>Rock type: Mz tuff</p>	<p><i>Mineralogy (50%):</i> Albite (90%) groundmass. Disseminated pyrite (5%), chalcopyrite (2.5%), sphalerite (2.5%).</p> <p><i>Veins (10%):</i> Calcite (90%) veins crosscut sample. Uraninite (2.5%), chalcopyrite (5%), sphalerite (2.5%) may be vein related.</p> <p><i>Alteration (40%):</i> Pervasive alteration to carbonate.</p>	<p>Unsure</p>	<p>The figure consists of two stacked elemental maps of a rock sample. The top map displays the distribution of Na, Al, Si, Ca, and K, with a 3 mm scale bar. The bottom map displays the distribution of Ca, Cu, Zn, and U, also with a 3 mm scale bar. Both maps show a network of veins and a groundmass.</p>
---	---	---------------	--

<p>11PUA-135A4-6 (drill core 10LC-18 : 79.45 to 79.85m)</p> <p>Rock type: Mz tuff</p>	<p><i>Mineralogy (40%)</i>: Albite host rock with disseminated hematite and chalcopyrite.</p> <p><i>Veinlets (10%)</i>: Calcite veins cross-cutting sample. The major vein has chalcopyrite (30%), calcite (20%), and albite (10%), and galena (5%). Uraninite (35%) mineralization is occurring surrounding the main vein.</p> <p><i>Alteration (50%)</i>: Pervasive carbonate (60%), hematite (40%) alteration. Both are replacing albitized host rock.</p>	<p>Simple vein-hosted</p>	
---	---	---------------------------	--

<p>11PUA-135A4-7 (drill core 10LC-18 : 79.45 to 79.85m)</p> <p>Rock type: Mz tuff</p>	<p><i>Mineralogy (55%):</i> Albite (75%) and quartz (12.5%). Disseminated sphalerite (5%), pyrite (2.5%), chalcocopyrite (5%).</p> <p><i>Veinlets (10%):</i> Calcite (40%) veins cross-cutting albite host rock. Uraninite (40%) is concentrated along the vein. Uranium mineralization is associated with zirconium. Hematite (2.5%), chalcocopyrite (5%), pyrite (5%), sphalerite (5%), and minor galena (2.5%) are also occurring within these calcite veins.</p> <p><i>Alteration (35%):</i> Pervasive carbonate (70%) replacement. Hematite (20%) alteration and chlorite (10%) replacement.</p>	<p>Simple vein-hosted</p>	<p>The figure consists of two vertically stacked panels. The top panel is a false-color map showing mineral distribution, with a legend on the right side listing Na (pink), Al (yellow), Si (green), K (dark green), and Ca (orange). A 3 mm scale bar is located in the top right corner. The bottom panel is another false-color map, with a legend on the right side listing Fe (red), Cu (orange), Zn (green), and U (dark green). A 3 mm scale bar is also present in the top right corner of this panel. Both panels show a complex pattern of mineral concentrations, with a prominent dark green vein-like feature running through the center.</p>
---	---	---------------------------	---

<p>11PUA-135A5-2 (drill core 10LC-18: 80.1 to 80.6m)</p> <p>Rock type: Mz tuff</p>	<p><i>Mineralogy (60%):</i> Albite (100%).</p> <p><i>Veinlets (45%):</i> Calcite (65%) veins cutting across sample. Uraninite (15%) mineralization concentrated within calcite veins. Zirconium associated with uranium mineralization. Pyrite (10%) veinlets crosscut sample. Chalcopyrite (5%) crystallizes in concentrations or dissemination throughout veinlets of calcite. Galena (2.5%) and sphalerite (2.5%) are occurring throughout calcite veins.</p> <p><i>Alteration (5%):</i> Hematite replacement of host rock.</p>	<p>Simple vein-hosted</p>	
--	--	---------------------------	--

<p>11PUA-135A5-2_1 (drill core 10LC-18 : 80.1 to 80.6m)</p> <p>Rock type: Mz tuff</p>	<p><i>Mineralogy (10%):</i> Groundmass is albite (100%).</p> <p><i>Veins (30%):</i> Calcite (55%) veins cross cutting sample. Pyrite (15%) vein cross cutting sample and pyrite (2.5%) is also disseminated within calcite veins. Chalcopyrite (7.5%) is disseminated within calcite veins.</p> <p>Uraninite (15%) occurring within calcite veins. Zirconium associated with uranium mineralization.</p> <p>Galena (2.5%) and minor (2.5%) sphalerite within sample.</p> <p><i>Alteration (60%):</i> Pervasive carbonate (55%) and hematite (45%) replacement.</p>	<p>Simple vein-hosted</p>	
---	--	---------------------------	--

<p>11PUA-135A5-3 (drill core 10LC-18 : 80.1 to 80.6m)</p> <p>Rock type: Mz tuff</p>	<p><i>Mineralogy (20%):</i> Albite (100%).</p> <p><i>Veinlets (30%):</i> Calcite (70%) veins cross-cutting sample. Uraninite (10%) mineralization within these calcite veins. Zirconium associated with uranium mineralization. Chalcopyrite (5%) mineralization is also occurring within calcite veins. Chalcopyrite (10%) and bornite grains occurring concentrated along molybdenite (5%) that is occurring as veinlets.</p> <p><i>Alteration (50%):</i> Pervasive carbonate (45%), minor chlorite (5%), and pervasive hematite (50%) alteration.</p>		<p>The image displays two stacked elemental maps of a rock sample. The top map shows the distribution of Na, Al, Si, K, Ca, and Fe. The bottom map shows the distribution of Fe, Cu, Mo, and U. Both maps include an 8 mm scale bar and the sample ID '11PUA-135A5-3'.</p>
---	--	--	--

<p>11PUA-135A5-4 (drill core 10LC-18 : 80.1 to 80.6m)</p> <p>Rock type: Mz tuff</p>	<p><i>Mineralogy (30%):</i> Albite (72.5%) with minor quartz (2.5%). Disseminated chalcopyrite (10%), pyrite (5%), sphalerite (2.5%) and minor galena (2.5%) are also present.</p> <p><i>Veinlets (10%):</i> Calcite (60%) veins crosscut albitized host rock. Vein-hosted uraninite (20%) is occurring in/along the calcite veins and is associated with high zirconium. Chalcopyrite (10%), pyrite (2.5%), sphalerite (2.5%), and galena (5%) are also concentrated within these veins.</p> <p><i>Alteration (60%):</i> Pervasive carbonate (70%) alteration of albite host rock. Hematite replacement (30%) of albite host rock.</p>		
---	---	--	--

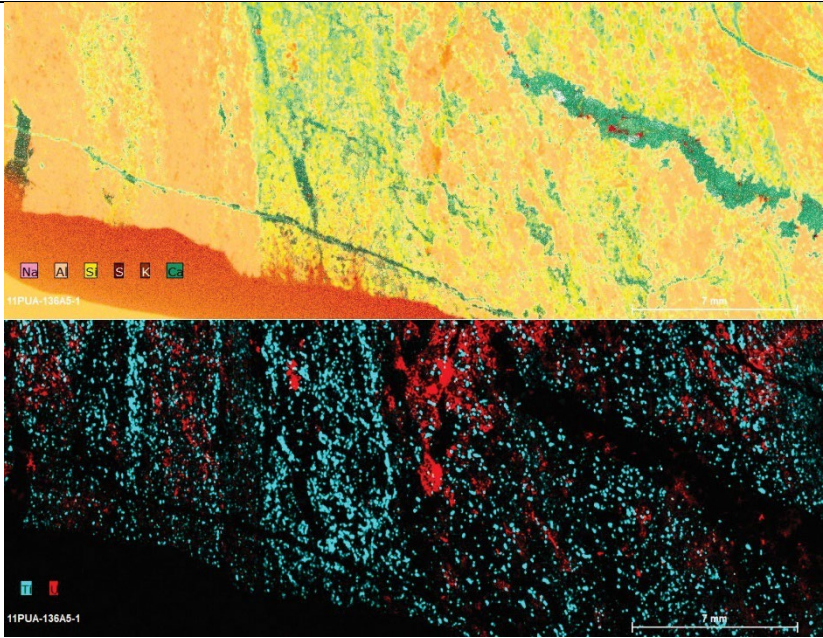
<p>11PUA-135A5-5 (drill core 10LC-18: 80.1 to 80.6m)</p> <p>Rock type: Mz tuff</p>	<p><i>Mineralogy (15%):</i> Albite (100%).</p> <p><i>Veins (65%):</i> Uraninite (20%) in this sample is concentrated along calcite (30%) veins. Uranium mineralization is associated with high zirconium. Chalcopyrite (25%) spatially associated with uranium mineralization. Pyrite veins crosscut sample (20%). Sphalerite (5%) is disseminated within calcite.</p> <p><i>Alteration (30%):</i> Pervasive carbonate (70%) and hematite (30%) alteration.</p>		
--	---	--	--

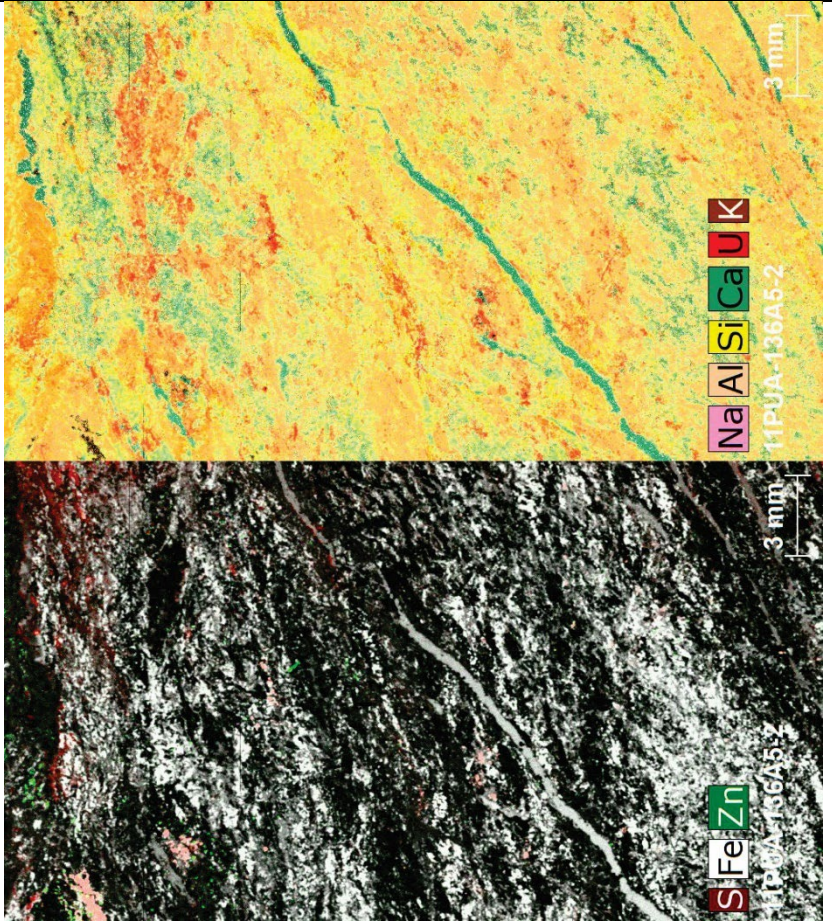
<p>11PUA-135A5-6 (drill core 10LC-18 : 80.1 to 80.6m)</p> <p>Rock type: Mz tuff</p>	<p><i>Mineralogy (10%):</i> Quartz (50%), albite (10%) and muscovite (40%).</p> <p><i>Veinlets (80%):</i> A uraninite (47.5%) vein and sulfide vein crosscut the majority of this sample. Uraninite is associated with high zirconium. Pyrite (30%), chalcopyrite (10%), sphalerite (5%), galena (5%), and barite (2.5%) are concentrated in/along the veins.</p> <p><i>Alteration (10%):</i> Minor chlorite (100%) alteration.</p>	<p>Simple vein-hosted</p>	<p>The image displays two stacked elemental maps of the sample. The top map shows the distribution of Ne, Al, Si, K, Ca, and U. The bottom map shows the distribution of S, Ti, Cu, Zn, and Ba. Both maps include a 7 mm scale bar.</p>
---	---	---------------------------	---

<p>11PUA-135A6-1 (drill core 10LC-18 : 81.6 to 81.9m)</p> <p>Rock type: Mz tuff</p>	<p><i>Mineralogy (20%)</i>: Albite (80%), quartz (10%), and muscovite (10%).</p> <p><i>Veinlets (50%)</i>: Calcite (10%) veins crosscut sample. Disseminated chalcopyrite (5%) within calcite veins. Uraninite (5%) is concentrated along calcite veinlets. Pyrite (80%) vein crosscuts sample.</p> <p><i>Alteration (30%)</i>: Carbonate (40%) and chlorite (70%) alteration.</p>	<p>Simple vein-hosted</p>	
---	--	---------------------------	--

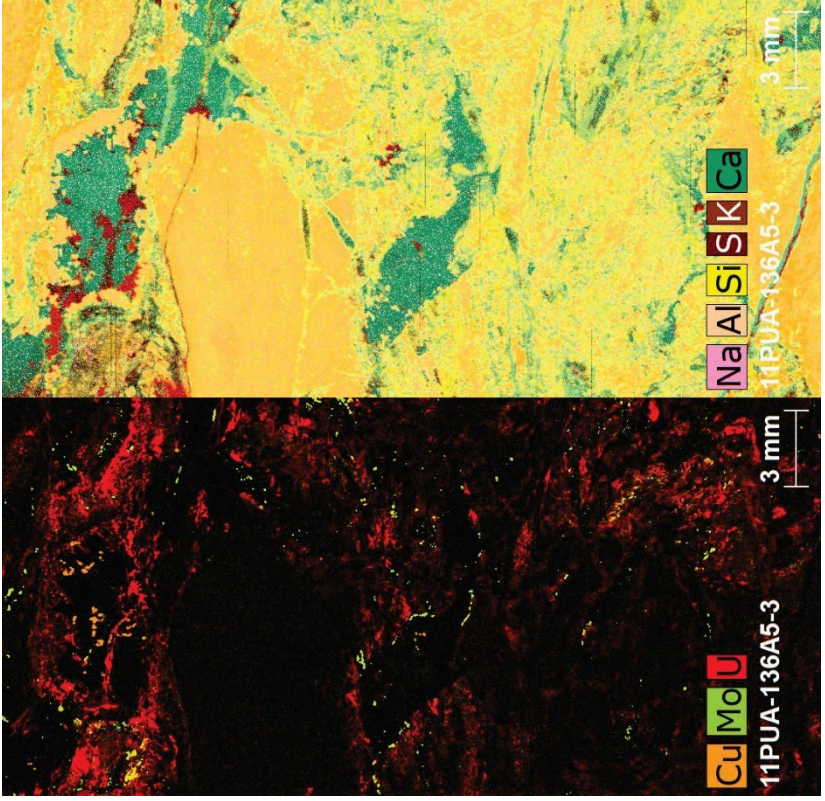
<p>11PUA-135A6-2 (drill core 10 LC-18 : 81.6 to 81.9m)</p> <p>Rock type: Mz tuff</p>	<p><i>Mineralogy (20%):</i> Albite (85%) and muscovite (10%). Disseminated hematite (5%), chalcopyrite (5%).</p> <p><i>Veins (60%):</i> Pyrite (90%) vein. Calcite (10%) veins crosscut sample.</p> <p><i>Alteration (20%):</i> Carbonate (55%) and hematite (45%) alteration.</p>		<p>The image displays two stacked elemental maps of a rock sample. The top map shows the distribution of Ne, Al, Si, S, K, and Ca. The bottom map shows the distribution of Ce, Cu, and U. Both maps include a 7 mm scale bar and the sample ID 11PUA-135A6-2.</p>
--	--	--	--

<p>11PUA-135A6-3 (drill core 10 LC-18 : 81.6 to 81.9m)</p> <p>Rock type: Mz tuff</p>	<p><i>Mineralogy (35%):</i> Albite () and muscovite ().</p> <p><i>Veins (45%):</i> Calcite (10%) veins cutting across the host rock plagioclase. Chalcopyrite (5%) disseminations concentrated along calcite veins. Uranium mineralization (5%) concentrated along calcite veins.</p> <p>Pyrite (80%) vein cutting across host rock.</p> <p><i>Alteration (20%):</i> Carbonate (60%) and hematite (40%) replacement.</p>		
--	--	--	--

<p>11PUA-136A5-1 (drill core 10LC-15 : 95.8 to 96.1m)</p> <p>Rock type: Mz tuff</p>	<p><i>Mineralogy (30%):</i> Albite (57.5%), muscovite (5%). Uraninite (35%) is disseminated throughout albitized host rock. Minor pyrite (2.5%) disseminated throughout host rock.</p> <p><i>Veins (10%):</i> Calcite (95%) and albite veins cross-cut sample. Minor chalcopyrite (2.5%) grains within calcite vein. Pyrite (2.5%) is also within the calcite vein.</p> <p><i>Alteration (60%):</i> Pervasive carbonate (70%) alteration. Hematite (20%) replacement is also occurring throughout host rock. Chlorite (10%) alteration.</p>		
---	---	--	---

<p>11PUA-136A5-2 (drill core 10LC-15 : 95.8 to 96.1m)</p> <p>Rock type: Mz tuff</p>	<p><i>Mineralogy (15%):</i> Albite (75%), disseminated hematite (12.5%), and minor pyrite (2.5%). Uraninite (10%) mineralization throughout pervasively carbonate-altered host rock.</p> <p><i>Veins (5%):</i> Calcite (100%) veins crosscut sample.</p> <p><i>Alteration (80%):</i> Pervasive carbonate (80%) and hematite (20%) alteration.</p>		 <p>The figure consists of two mineral maps of sample 11PUA-136A5-2, each with a 3 mm scale bar. The top map displays a color-coded distribution of elements: Na (pink), Al (yellow), Si (green), Ca (blue), U (red), and K (purple). The bottom map displays a color-coded distribution of elements: S (red), Fe (green), and Zn (blue). Both maps show a complex, heterogeneous mineral distribution with distinct veins and alteration zones.</p>
---	---	--	--

<p>11PUA-136A5-3 (drill core 10LC-15 : 95.8 to 96.1m)</p> <p>Rock type: Mz tuff</p>	<p><i>Mineralogy (55%):</i> Albite (65%). Uraninite (20%) throughout host rock. Zirconium associated with uranium mineralization. Molybdenite (5%) associated with uraninite. Sphalerite (5%), pyrite (5%) disseminated throughout sample.</p> <p><i>Veins (5%):</i> Calcite (95%) vein crosscutting sample with pyrite mineralization down the center (5%).</p> <p><i>Alteration (40%):</i> Hematite (60%) and carbonate (40%) alteration.</p>		<p>The figure consists of two vertically stacked elemental maps of the same sample, 11PUA-136A5-3. The top map displays the distribution of Na (purple), Al (yellow), Si (green), K (red), and Ca (blue). A scale bar in the top right corner indicates 3 mm. The bottom map displays the distribution of Fe (red), Mo (green), and U (blue). A scale bar in the top right corner indicates 1 mm. Both maps show a complex, heterogeneous distribution of these elements across the sample area.</p>
---	---	--	--

<p>11PUA-136A5-3_1 (drill core 10LC-15 : 95.8 to 96.1m)</p> <p>Rock type: Mz tuff</p>	<p><i>Mineralogy (40%):</i> Albite (100%).</p> <p><i>Veins (20%):</i> Uraninite (10%), molybdenite (5%), pyrite (5%), sphalerite (2.5%), galena (2.5%), and sphalerite (2.5%) mineralized within calcite (72.5%) veins.</p> <p><i>Alteration (40%):</i> Pervasive carbonate (70%) replacement. Hematite (30%) alteration.</p>	<p>Simple vein-hosted</p>	 <p>The figure consists of two stacked elemental maps of a drill core sample. The top map displays the distribution of Na, Al, Si, S, K, and Ca, with a 3 mm scale bar. The bottom map displays the distribution of Cu, Mo, and U, also with a 3 mm scale bar. Both maps are labeled '11PUA-136A5-3'.</p>
---	---	---------------------------	--

<p>11PUA-136A5-4 (drill core 10LC-15 : 95.8 to 96.1m)</p> <p>Rock type: Mz tuff</p>	<p><i>Mineralogy (55%):</i> Albite (100%).</p> <p><i>Veins (5%):</i> Calcite (100%) veins cross cutting sample.</p> <p><i>Alteration (40%):</i> Carbonate (75%) replacement and hematite (25%) alteration.</p>	<p>None</p>	<p>The figure consists of two vertically stacked elemental maps of a rock sample. The top map displays the distribution of Na, Al, Si, K, and Ca, with a 3 mm scale bar. The bottom map displays the distribution of S, Fe, and Zn, also with a 3 mm scale bar. Both maps show a central vertical vein structure.</p>
---	--	-------------	---

Appendix D – Sample List and Descriptions

Sample #	Sample Type	Rock Type	Sample Depth (m)		Location			Basic Sample Description
			Start	End	UTM Zone	Easting	Northing	
11PUA-122A1-1	Hand Sample	Conglomerate	N/A	N/A	14N	510070.9	6939341	Hematitic basal conglomerate with trace of U
11PUA-122A1-2a	Hand Sample	Conglomerate	N/A	N/A	14N	510070.9	6939341	Hematitic basal conglomerate with trace of U
11PUA-122A1-2b	Hand Sample	Conglomerate	N/A	N/A	14N	510070.9	6939341	Hematitic basal conglomerate with trace of U
11PUA-124A1-a	Hand Sample	Polymictic conglomerate	N/A	N/A	14N	517072.8	6940803	Polymictic conglomerate/basal breccia with quartz-carbonate-hematite-U cement
11PUA-124A1-b	Hand Sample	Polymictic conglomerate	N/A	N/A	14N	517072.8	6940803	Polymictic conglomerate/basal breccia with quartz-carbonate-hematite-U cement
11PUA-125B1	Hand Sample	Carbonate, hematite veins	N/A	N/A	14N	515744.1	6940115	Carbonate hematite veins with anomalous U
11PUA-128A1	Hand Sample	Quartz-sulfides stockwork	N/A	N/A	14N	501440	6941953	Quartz-sulfides stockwork
11PUA-128A2	Hand Sample	Quartz-sulfides stockwork	N/A	N/A	14N	501440	6941953	Quartz-sulfides stockwork
11PUA-128A3	Hand Sample	Quartz-sulfides stockwork	N/A	N/A	14N	501440	6941953	Quartz-sulfides stockwork

11PUA-128A4	Hand Sample	Quartz-sulfides stockwork	N/A	N/A	14N	501440	6941953	Quartz-sulfides stockwork
11PUA-131A1	Hand Sample	Polymictic conglomerate	N/A	N/A	14N	503964.1	6935705	Polymictic conglomerate with U
11PUA-131A2-1	Hand Sample	Polymictic conglomerate	N/A	N/A	14N	503964.1	6935705	Polymictic conglomerate with U
11PUA-131A2-2	Hand Sample	Polymictic conglomerate	N/A	N/A	14N	503964.1	6935705	Polymictic conglomerate with U
11PUA-133A3-1	Drill Core 10LC-35	Altered basalt	44.95	45.25	14N	519160	6940111	Moderate to strong hematite alteration. 5% quartz carbonate veinlets. Strong pervasive carbonate alteration. Trace pyrite and chalcopyrite dissemination
11PUA-133A3-2	Drill Core 10LC-35	Altered basalt	44.95	45.25	14N	519160	6940111	Moderate to strong hematite alteration. 5% quartz carbonate veinlets. Strong pervasive carbonate alteration. Trace pyrite and chalcopyrite dissemination
11PUA-133A3-3	Drill Core 10LC-35	Altered basalt	44.95	45.25	14N	519160	6940111	Moderate to strong hematite alteration. 5% quartz carbonate veinlets. Strong pervasive carbonate alteration. Trace pyrite and chalcopyrite dissemination

11PUA-133A5-1	Drill Core 10LC-35	Tuff	45.95	46.2	14N	519160	6940111	Laminated chlorite, graphite rich tuff. Moderate patchy hematite alteration. <1% disseminated chalcopyrite and pyrite. 5% quartz carbonate veins
11PUA-133A5-2a	Drill Core 10LC-35	Tuff	45.95	46.2	14N	519160	6940111	Laminated chlorite, graphite rich tuff. Moderate patchy hematite alteration. <1% disseminated chalcopyrite and pyrite. 5% quartz carbonate veins
11PUA-133A5-2b	Drill Core 10LC-35	Tuff	45.95	46.2	14N	519160	6940111	Laminated chlorite, graphite rich tuff. Moderate patchy hematite alteration. <1% disseminated chalcopyrite and pyrite. 5% quartz carbonate veins
11PUA-133A5-3a*	Drill Core 10LC-35	Tuff	45.95	46.2	14N	519160	6940111	Laminated chlorite, graphite rich tuff. Moderate patchy hematite alteration. <1% disseminated chalcopyrite and pyrite. 5% quartz carbonate veins
11PUA-133A5-3a*	Drill Core 10LC-35	Tuff	45.95	46.2	14N	519160	6940111	Laminated chlorite, graphite rich tuff. Moderate patchy hematite alteration. <1% disseminated chalcopyrite and pyrite. 5% quartz carbonate veins

11PUA-133A5-3b*	Drill Core 10LC-35	Tuff	45.95	46.2	14N	519160	6940111	Laminated chlorite, graphite rich tuff. Moderate patchy hematite alteration. <1% disseminated chalcopyrite and pyrite. 5% quartz carbonate veins
11PUA-133A5-3b*	Drill Core 10LC-35	Tuff	45.95	46.2	14N	519160	6940111	Laminated chlorite, graphite rich tuff. Moderate patchy hematite alteration. <1% disseminated chalcopyrite and pyrite. 5% quartz carbonate veins
11PUA-133A5-4	Drill Core 10LC-35	Tuff	45.95	46.2	14N	519160	6940111	Laminated chlorite, graphite rich tuff. Moderate patchy hematite alteration. <1% disseminated chalcopyrite and pyrite. 5% quartz carbonate veins
11PUA-133A6-1	Drill Core 10LC-35	Tuff	46.65	47	14N	519160	6940111	Laminated chlorite, graphite rich tuff. Moderate patchy hematite alteration. <1% disseminated chalcopyrite and pyrite. 5% quartz carbonate veins
11PUA-134A2-1	Drill Core 10-LC-63	Gash vein	62	62.4	14N	518676	6940370	Red pitchblende rich hematite altered locally weakly brecciated gash vein. Trace pyrite

11PUA-134A2-2a	Drill Core 10-LC-63	Gash vein	62	62.4	14N	518676	6940370	Red pitchblende rich hematite altered locally weakly brecciated gash vein. Trace pyrite
11PUA-134A2-2b	Drill Core 10-LC-63	Gash vein	62	62.4	14N	518676	6940370	Red pitchblende rich hematite altered locally weakly brecciated gash vein. Trace pyrite
11PUA-134A2-3a	Drill Core 10-LC-63	Gash vein	62	62.4	14N	518676	6940370	Red pitchblende rich hematite altered locally weakly brecciated gash vein. Trace pyrite
11PUA-134A2-3b	Drill Core 10-LC-63	Gash vein	62	62.4	14N	518676	6940370	Red pitchblende rich hematite altered locally weakly brecciated gash vein. Trace pyrite
11PUA-134A2-4	Drill Core 10-LC-63	Gash vein	62	62.4	14N	518676	6940370	Red pitchblende rich hematite altered locally weakly brecciated gash vein. Trace pyrite
11PUA-135A4-3	Drill Core 10LC-18	Tuff	79.45	79.85	14N	518626	6940383	Red , black tuff. Strongly foliated and cut by 3% qtz carbonate veins parallell to foliation. Scattered pitchblende and minor chalcopyrite, pyrrhotite in veinlets

11PUA-135A4-4	Drill Core 10LC-18	Tuff	79.45	79.85	14N	518626	6940383	Red , black tuff. Strongly foliated and cut by 3% qtz carbonate veins paralell to foliation. Scattered pitchblende and minor chalcopryrite, pyrrhotite in veinlets
11PUA-135A4-6a	Drill Core 10LC-18	Tuff	79.45	79.85	14N	518626	6940383	Red , black tuff. Strongly foliated and cut by 3% qtz carbonate veins paralell to foliation. Scattered pitchblende and minor chalcopryrite, pyrrhotite in veinlets
11PUA-135A4-6b	Drill Core 10LC-18	Tuff	79.45	79.85	14N	518626	6940383	Red , black tuff. Strongly foliated and cut by 3% qtz carbonate veins paralell to foliation. Scattered pitchblende and minor chalcopryrite, pyrrhotite in veinlets
11PUA-135A4-7	Drill Core 10LC-18	Tuff	79.45	79.85	14N	518626	6940383	Red , black tuff. Strongly foliated and cut by 3% qtz carbonate veins paralell to foliation. Scattered pitchblende and minor chalcopryrite, pyrrhotite in veinlets

11PUA-135A5-2a	Drill Core 10LC-18	Tuff	80.1	80.6	14N	518626	6940383	Red , black tuff. Strongly foliated and cut by 3% qtz carbonate veins paralell to foliation. Scattered pitchblende and minor chalcopyrite, pyrrhotite in veinlets
11PUA-135A5-2b	Drill Core 10LC-18	Tuff	80.1	80.6	14N	518626	6940383	Red , black tuff. Strongly foliated and cut by 3% qtz carbonate veins paralell to foliation. Scattered pitchblende and minor chalcopyrite, pyrrhotite in veinlets
11PUA-135A5-3	Drill Core 10LC-18	Tuff	80.1	80.6	14N	518626	6940383	Red , black tuff. Strongly foliated and cut by 3% qtz carbonate veins paralell to foliation. Scattered pitchblende and minor chalcopyrite, pyrrhotite in veinlets
11PUA-135A5-4	Drill Core 10LC-18	Tuff	80.1	80.6	14N	518626	6940383	Red , black tuff. Strongly foliated and cut by 3% qtz carbonate veins paralell to foliation. Scattered pitchblende and minor chalcopyrite, pyrrhotite in veinlets

11PUA-135A5-5a	Drill Core 10LC-18	Tuff	80.1	80.6	14N	518626	6940383	Red , black tuff. Strongly foliated and cut by 3% qtz carbonate veins paralell to foliation. Scattered pitchblende and minor chalcopyrite, pyrrhotite in veinlets
11PUA-135A5-5b	Drill Core 10LC-18	Tuff	80.1	80.6	14N	518626	6940383	Red , black tuff. Strongly foliated and cut by 3% qtz carbonate veins paralell to foliation. Scattered pitchblende and minor chalcopyrite, pyrrhotite in veinlets
11PUA-135A5-6	Drill Core 10LC-18	Tuff	80.1	80.6	14N	518626	6940383	Red , black tuff. Strongly foliated and cut by 3% qtz carbonate veins paralell to foliation. Scattered pitchblende and minor chalcopyrite, pyrrhotite in veinlets
11PUA-135A6-1	Drill Core 10LC-18	Tuff	80.1	80.6	14N	518626	6940383	Red , black tuff. Strongly foliated and cut by 3% qtz carbonate veins paralell to foliation. Scattered pitchblende and minor chalcopyrite, pyrrhotite in veinlets

11PUA-135A6-2	Drill Core 10LC-18	Tuff	80.1	80.6	14N	518626	6940383	Red , black tuff. Strongly foliated and cut by 3% qtz carbonate veins paralell to foliation. Scattered pitchblende and minor chalcopyrite, pyrrhotite in veinlets
11PUA-135A6-3	Drill Core 10LC-18	Tuff	80.1	80.6	14N	518626	6940383	Red , black tuff. Strongly foliated and cut by 3% qtz carbonate veins paralell to foliation. Scattered pitchblende and minor chalcopyrite, pyrrhotite in veinlets
11PUA-135A6-4	Drill Core 10LC-18	Tuff	80.1	80.6	14N	518626	6940383	Red , black tuff. Strongly foliated and cut by 3% qtz carbonate veins paralell to foliation. Scattered pitchblende and minor chalcopyrite, pyrrhotite in veinlets
11PUA-136A5-1	Drill Core 10LC-15	Tuff	95.8	96.1	14N	519108	6940123	Graphite, chlorite, sulfide tuff. 5% pyrite, 3% chalcopyrite. Moderate pervasive hematite alteration. Moderate carbonate alteration surrounding main zone.

11PUA-136A5-2a	Drill Core 10LC-15	Tuff	95.8	96.1	14N	519108	6940123	Graphite, chlorite, sulfide tuff. 5% pyrite, 3% chalcopyrite. Moderate pervasive hematite alteration. Moderate carbonate alteration surrounding main zone.
11PUA-136A5-2b	Drill Core 10LC-15	Tuff	95.8	96.1	14N	519108	6940123	Graphite, chlorite, sulfide tuff. 5% pyrite, 3% chalcopyrite. Moderate pervasive hematite alteration. Moderate carbonate alteration surrounding main zone.
11PUA-136A5-3a	Drill Core 10LC-15	Tuff	95.8	96.1	14N	519108	6940123	Graphite, chlorite, sulfide tuff. 5% pyrite, 3% chalcopyrite. Moderate pervasive hematite alteration. Moderate carbonate alteration surrounding main zone.
11PUA-136A5-3b	Drill Core 10LC-15	Tuff	95.8	96.1	14N	519108	6940123	Graphite, chlorite, sulfide tuff. 5% pyrite, 3% chalcopyrite. Moderate pervasive hematite alteration. Moderate carbonate alteration surrounding main zone.
11PUA-136A5-4	Drill Core 10LC-15	Tuff	95.8	96.1	14N	519108	6940123	Graphite, chlorite, sulfide tuff. 5% pyrite, 3% chalcopyrite. Moderate pervasive hematite alteration. Moderate carbonate alteration surrounding main zone.

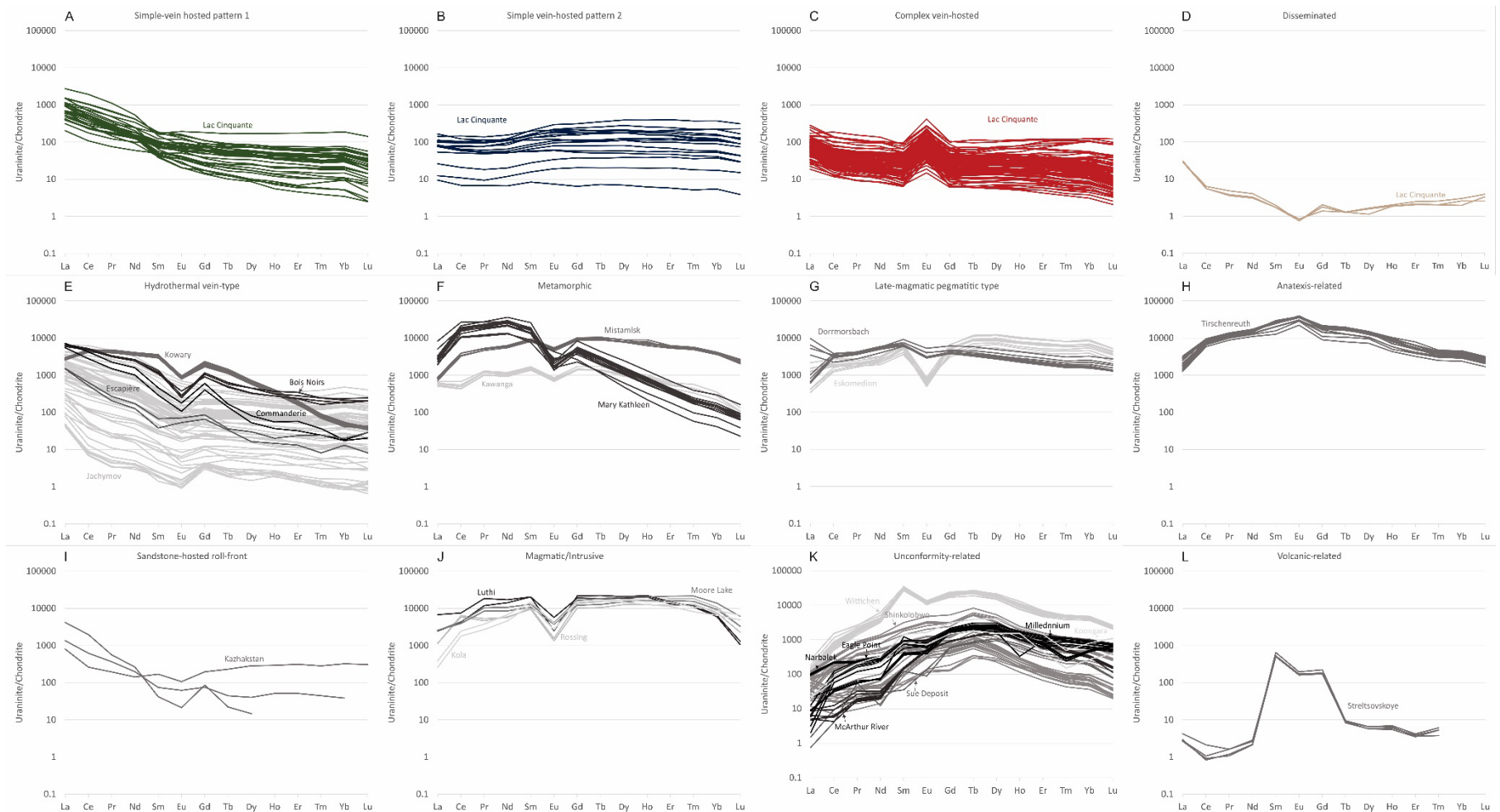
Appendix E – SEM data

<https://doi.org/10.5683/SP3/FM8WTE>

Appendix F – LA-ICP-MS data

<https://doi.org/10.5683/SP3/FM8WTE>

Appendix G – Comparison of REE profiles of various uranium deposits to REE profiles of LC uranium minerals



Appendix G, Figure 1: Comparison of REE profiles of LC and various deposit types, normalized to chondrite (McDonough & Sun, 1995). A) LC simple vein-hosted pattern 1 uraninite, from this study. B) LC simple vein-hosted pattern 2 uraninite, from this study. C) LC complex vein-hosted uraninite, from this study. D) LC simple disseminated uraninite, from this study. E) Hydrothermal vein-type uraninite, modified from Mercadier et al. (2011) and from Frimmel et al. (2013). F) Metamorphic-related uraninite, modified from Mercadier et al. (2011) and modified from Frimmel et al. (2013). G) Late-pegmatitic type uraninite, modified from Frimmel et al. (2013). H) Anatexis-related uraninite, modified from Frimmel et al. (2013). I) Sandstone-hosted roll-front, modified from Mercadier et

al. (2011). J) Magmatic/intrusive uraninite, modified from Mercadier et al. (2011). K) Unconformity-related uraninite, modified from Mercadier et al. (2011) and from Frimmel et al. (2013). L) Volcanic-hosted uraninite, modified from Mercadier et al. (2011).